Mechanisms of Homeostatic Plasticity in the Mouse Visual Cortex

Sammons, Rosanna Penelope

Awarding institution:
King's College London

Mechanisms of Homeostatic Plasticity in the Mouse Visual Cortex

Rosanna P. Sammons

MRC Centre for Developmental Neurobiology,
King's College, London

A thesis submitted to King's College London in part fulfilment for the degree of Doctor of Philosophy

September 2015

Supervisors: Dr Tara Keck and Dr Matthew Grubb
Examiners: Professor Zoltan Molnar and Professor Ole Paulsen

Statement of Declaration

I declare that the work in this thesis was performed myself with the following exceptions:

i) The macro used to measure proxies for dendritic spine size was originally obtained from Sonja Hofer, and adapted for use by Anton Gauert and Dr Samuel Barnes.

ii) GCAMP data shown in Figure 4.2 was collected by Dr Tara Keck and Dr Georg Keller, in the lab of Dr Georg Keller. Raw data was registered and individual cell regions of interest were selected by Dr Georg Keller; GCAMP signals were analysed by Dr Samuel Barnes. Reconstruction and immunohistochemistry was performed by myself with the assistance of David Elliott.

Table of Contents

List of Figures

List of Tables

Abstract

During development, newly established cortical circuits are undergoing a period of experience dependent refinement. Visual deprivation during this time leads to the induction of plasticity mechanisms, including homeostatic plasticity measures. These are a distinct set of plasticity mechanisms thought to play a role in maintaining stability within networks, and preventing large perturbations in overall activity levels. Homeostatic plasticity mechanisms can be divided into synaptic and intrinsic mechanisms. While details of individual mechanisms are reasonably well understood, details of how these different mechanisms are linked to one another are much less clear. In this thesis, I investigate the relationship between structural and functional forms of synaptic and intrinsic plasticity in layer 2/3 neurons in the monocular visual cortex, before and after induction of plasticity via monocular enucleation. I find that while axon initial segment (AIS) plasticity takes place following deprivation, in both pyramidal neurons, and a subset of inhibitory neurons, it does not correlate with functional measures of excitability. However, in control conditions, I do find a relationship between the synaptic inputs of a neuron, and its intrinsic excitability. Following deprivation, this relationship is altered. Specifically, I find that the activity status of the neuron affects the level of intrinsic excitability, and to some extent, the synaptic input to the cell. Putatively inactive neurons show increased excitability, and trend towards stronger synaptic input in comparison to their active counterparts. These differences between active and inactive cells may reflect the engagement of homeostatic mechanisms in inactive cells, in order to restore their activity levels.

Chapter 1: Introduction

One of the remarkable features of the brain is its huge capacity for plasticity. Even into adulthood, our brains are able to adapt to their surroundings and update synapses, enabling us to learn new skills and form new memories. On top of these more recognisable outcomes, plasticity is also at work maintaining stability across the central nervous system. Hebbian plasticity, thought to be the underlying basis for learning and memory (Bliss and Collingridge, 1993), involves the strengthening and weakening of individual specific synapses depending on the activity patterns of pre and postsynaptic cells. Long-term potentiation (LTP) and long-term depression (LTD) are the most studied forms of Hebbian plasticity, describing the up and down regulation of synaptic strength following periods of correlated, or decorrelated pre- and post-synaptic firing, respectively (Bliss and Lomo, 1973). Another form of Hebbian plasticity, spike timing dependent plasticity (STDP), describes plasticity that is determined by the temporal differences between pre- and post-synaptic firing (Magee and Johnston, 1997; Markram et al., 1997). Without regulatory systems in place, these forms of plasticity can rapidly destabilise network activity, however. For example, excessive positive feedback might lead to network saturation, and eventually cause pathological scenarios such as epileptiform activity or seizures (Turrigiano and Nelson, 2000). Conversely, in the opposite scenario, unconstrained depression could lead to unwanted synaptic loss (Collingridge et al., 2010), and silencing of cells and whole networks (Fig. 1.1). Homeostatic plasticity is proposed to regulate changes brought about by LTP and LTD-like plasticity, and provide a way to maintain stability within networks.

Homeostatic plasticity can be broadly separated into synaptic homeostatic plasticity and intrinsic homeostatic plasticity. Within these two classes a number of mechanisms have been identified. Often characterised by three main mechanisms, these are: changes in intrinsic excitability, altering the ratio of excitation and inhibition – known as the E/I balance – and, synaptic scaling

(Turrigiano, 2011). We are beginning to get a much clearer idea of the details of each mechanism. However, research so far has demonstrated that the engagement of homeostatic mechanisms can be dependent on a number of factors including, developmental age, cortical layer, and mode of plasticity induction (Desai et al., 2002; Maffei and Turrigiano, 2008; also see table 1.1). With varied responses reported to different activity manipulations, there is still a plethora of unanswered questions in the field. In particular, one area that remains poorly understood is how multiple homeostatic mechanisms may be engaged by neurons, and how they interact with one another.

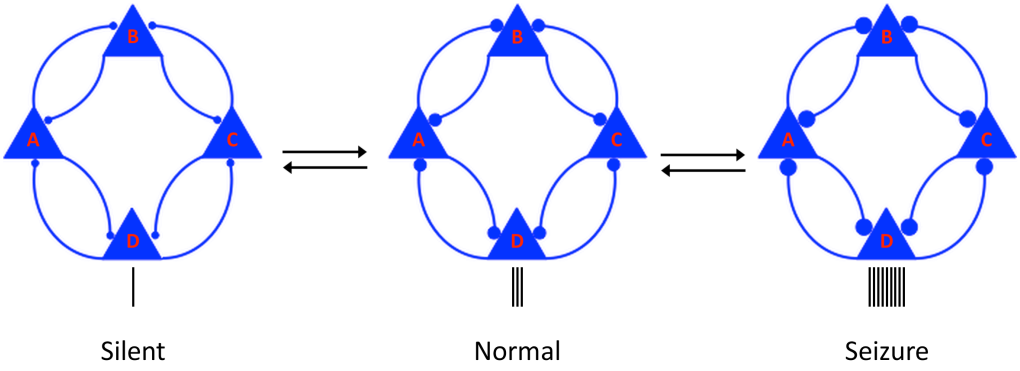

Figure 1.1 Consequences of repeated strengthening or weakening of synaptic connections without a braking system.

Schematic of a recurrent loop network containing four neurons, demonstrating the problem of destabilisation by persistent Hebbian plasticity. As each cell in the circuit fires an action potential they drive their post-synaptic partners, which then drive the next cell in the circuit as well as feeding back onto their pre-synaptic partner. Thus, increasing the output of one of the cells will drive its post-synaptic partner more strongly, and, in turn drive feedback onto itself more strongly, thus causing further strengthening. Several iterations of this strengthening will result in a network that is much more active than it started out, potentially leading to excitotoxicity. In a converse scenario, decreasing the output of a cell can lead to the whole network falling silent.

Table 1.1 Key references describing homeostatic plasticity in the cortex following different activity manipulation paradigms.

Reference	Manipulation	Cortical layer/ juvenile or adult	Observed activity changes and plasticity mechanisms
Desai et al., (2002)	Dark rearing (DR) TTX injection (TTXi)	L2/3/juvenile L4/juvenile	L2/3 – TTXi has no effect at 2 postnatal weeks but at 3 postnatal weeks increases mEPSC amplitude. L4 – TTXi increases mEPSC amplitude cf. control, when TTX applied at 2 postnatal weeks but not 3 postnatal weeks. DR prevents developmental decrease in mEPSC amplitude (i.e. mEPSC amplitude increased cf. control).
Frenkel and Bear (2004)	Lid suture (LS) TTX injection	L4/juvenile	LS – initial depression of deprived eye responses followed by potentiation of non-deprived eye responses. TTXi – no depression of deprived eye responses but immediate potentiation of non-deprived eye responses
Maffei et al., (2004)	Lid suture	L4/juvenile	Spontaneous activity increased 48 hrs post LS. Effect caused by shift in balance of E/I towards E, by increasing amplitude of E-E connections, and decreasing amplitude of I-E connections.
Goel and Lee (2007)	Dark rearing	L2/3/adult	DR for 2 days produced increase in mEPSC amplitude in mice at P21, P38 and P96. However, scaling was only multiplicative at P21 and P38. One day of light exposure reversed scaling at all ages.
Maffei and Turrigiano (2008)	Lid suture TTX injection	L2/3/juvenile	LS – decrease in mEPSC amplitude but increase in intrinsic excitability. TTXi – increase in mEPSC amplitudes (synaptic scaling). Both cause increase in spontaneous firing rates.
Keck et al., (2013)	Retinal lesion (RL)	L5/adult	Decrease in activity 6 hrs post RL, then increase over next 24-48 hrs. At 24 and 48 hrs post RL mEPSC amplitude is increased, and *in vivo* spine size is increased.
Hengen et al., (2013)	Lid suture	L2/3/juvenile	Firing rate decreased at 48 hrs post LS. Recovered by 72 hrs post LS. Decrease in FSIN firing rate at 24 hrs post LS. Recovered by 48 hrs post LS. Initial decrease (48 hrs post LS) then increase (96- 144 hrs post LS) in mEPSC amplitude onto pyramidal cells.

Lambo and Turrigiano (2013)	Lid suture	L2/3/juvenile	Initial (1-2 days post LS) decrease in mEPSC amplitude followed by later (6 days post LS) increase in mEPSC amplitude.
Barnes et al., (2015)	Enucleation (enuc.)	L2/3/adult	Decrease in activity at 24 hrs post enuc. Recovery over 48-72 hrs post enuc. Decrease in mIPSC frequency and amplitude. E/I shift towards E.

mEPSC, mini excitatory postsynaptic potential; mIPSC, mini inhibitory postsynaptic potential.

Intrinsic plasticity

Intrinsic excitability refers to how electrically excitable a neurons is. Given an injection of current into a neuron, the output of that neuron will vary according to several factors. These factors include the number and complement of ion channels expressed by the neuron, as well as their channel kinetics, and passive properties, such as membrane capacitance, that turn an incoming signal into an outgoing action potential. While synaptic plasticity has been the major focus of the homeostatic plasticity field over the last two decades, there is increasing evidence that intrinsic plasticity also has important roles in maintaining stability within networks (Desai et al., 1999; Golowasch et al., 1999a; O'Leary et al., 2010; Turrigiano et al., 1994). Furthermore, there are an abundance of targets for intrinsic plasticity mechanisms. If we consider the ultimate output of a neuron, the action potential (AP), there are 6 loci at which alterations to ion channels would change the progression of the AP, and at each locus potentially numerous distinct channels that could be modulated (Fig. 1.2). Modifications to ion channels can include altering the number or density of channels available, or altering the channel kinetics such as activation and inactivation times. These can often be regulated by the expression of different subunit isoforms, which is in turn regulated by gene transcription. Thus, there are many opportunities for fine-tuning of a neurons' intrinsic excitability.

An early modelling study proposed that the maximal conductance of ionic currents were regulated by calcium concentration, and therefore, indirectly by activity (LeMasson et al., 1993). Experimental studies then went on to show that indeed, intracellular calcium levels were capable of regulating the conductance of all three major currents, Na^+, K^+ and Ca^{2+} (Desai et al., 1999; Golowasch et al., 1999a, 1999b; Li et al., 1996; Turrigiano et al., 1994). In primary cultured neurons from the visual cortex, activity deprivation via tetradotoxin (TTX) blockade of Na^+ channels led to an increase in intrinsic excitability mediated by an increase in the amplitude of Na^+ currents (I_{Na}) and a reduction in outward hyperpolarising currents (Desai et al., 1999).

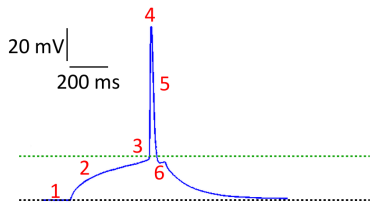

#	Phase	Channels involved
1	Resting membrane potential	Leak channels (largely K^+, some Na^+)
2	Subthreshold activation	Na_V, K_V (A-type), Ca_V (T-type)
3	Threshold activation/rising phase	Na_V, (K_V)
4	Action potential peak	Na_V, K_V, Ca_V
5	Repolarisation	Ka_V, Ca_V
6	Afterhyperpolarisation	K^+ channels

Figure 1.2 Currents and channels involved in the initiation and propagation of the action potential

In blue, the voltage trace of an AP. The black dotted line indicates resting membrane potential and the green dotted line indicates the AP threshold. For each numbered phase of the AP, the table on the right gives examples of some of the channels active at each phase. 1, At resting membrane potential (V_m), voltage-dependent channels are closed; flow of potassium and sodium channels down their concentration gradient, through leak channels, sets the V_m, along with the Na^+/K^+ ATPase pump. 2, Upon depolarisation, both voltage-gated Na^+ (Na_v) and K^+ (K_v) channels are activated, though K_v are slower to open than Na_v. If however, the depolarisation is not great enough Na_v will close and inactivate until resting membrane potential is reached, and K_v will close once depolarisation ceases. 3, If the depolarisation is large enough to reach activation threshold, this will result in AP generation. Initial influx of Na^+ through Na_vs causes further depolarisation, therefore opening yet more Na_v, resulting in the steep rising phase of the AP. 4, As the membrane potential drives towards the equilibrium potential for Na^+, Na_v begin to inactivate and the AP reaches its peak. Meanwhile, K_v have begun opening in response to the depolarisation and K^+ flows outwards. In addition, some types of voltage-gated calcium channels (Ca_vs) are activated. 5, By now the major conductance is of K^+ flowing out of the cell. The driving force on calcium is also greatest during the falling phase of the action potential. This in turn causes the activation of other types of K^+ channels that are calcium sensitive, such as BK channels. 6, The afterhyperpolarisation (AHP) is mediated by potassium channels. Several different classes of potassium channel are involved including BK channels, small-conductance calcium-

activated potassium (SK) channels and members of the K_v7 family of channels. The AHP can be divided into slow, medium and fast components, with different channels attributable to each component.

This response was considered a homeostatic response to maintain activity levels within the neuron after the activity deprivation. Meanwhile, the inverse case has been shown in hippocampal neurons, demonstrating the bidirectionality of this process. Cells treated with elevated K^+, to depolarise the neurons and increase activity, show a higher spike threshold and fire fewer spikes in response to injected current (O'Leary et al., 2010). This process is reversible, returning cells to normal levels of K^+ returns threshold and spiking response back to control levels, further highlighting its homeostatic nature.

More recently, several studies have proposed a structural correlate to changes in intrinsic excitability. The axon initial segment (AIS) is a highly specialised, protein-rich region of the proximal axon and has been shown to be a dynamic structure, modulated in an activity-dependent manner. The AIS has two important roles for the neuron. The first is to act as a barrier, preventing dendritic and somatic proteins diffusing into the axon, thereby maintaining neuronal polarity (Rasband, 2010). One of the key proteins in this function is a scaffolding protein called AnkyrinG (AnkG). Without AnkG, Na^+ channels do not cluster at the AIS (Zhou et al., 1998). Furthermore, axons lack the distinct molecular characteristics that define an axon, such as expression of sodium channels, and AIS components βIV spectrin and Neurofilament-186. Instead, processes take on dendritic characteristics, such as expression of somatodendritic protein MAP2, post-synaptic proteins such as PSD-95, and the formation of dendritic spines (Hedstrom et al., 2008). Expression of AnkG is restricted to the AIS, which has made it an attractive tool for labelling the AIS and allowing further study into both of its roles. The second function of the AIS is the initiation of APs. A very high density of ion channels is found at the AIS, in particular Na^+ density is 50 times higher in this region than in proximal dendrites (Kole et al., 2008). Early work in motoneurons suggested AP generation occurred at the initial segment or first node of Ranvier (Coombs et al., 1957; Fatt, 1957; Fuortes et al., 1957). Subsequent work corroborated with these findings demonstrating in cortical pyramidal neurons, (Palmer and Stuart, 2006; Stuart and Sakmann, 1994; Stuart et al., 1997), cerebellar purkinje cells, (Clark et al., 2005; Stuart and Häusser, 1994) and cortical interneurons (Li et al., 2014) that AP generation occurs along the axon rather than at the soma. Even

more specifically than this, several studies in cortical pyramidal neurons have identified the distal portion of the AIS to be the precise location of AP generation (Kole et al., 2007, 2008; Palmer and Stuart, 2006). However, the complement of channels found at the AIS varies among different neuronal subgroups, and is often non-uniform across the length of the AIS (Lorincz and Nusser, 2008), and so it is likely that the specific site of AP initiation varies across different cell types.

Plasticity at the AIS was first demonstrated in two parallel studies (Grubb and Burrone, 2010; Kuba et al., 2010). One of these studies showed that upon chronic depolarisation, via high K^+ treatment, cultured hippocampal neurons the AIS underwent a distal relocation (Grubb and Burrone, 2010). Furthermore, Grubb and Burrone found that returning neurons to non-depolarised conditions could reverse the relocation. Meanwhile, the second study showed that following cochlear ablation in the chick, neurons in the auditory cortex had significantly longer AISs compared to neurons in the control hemisphere (Kuba et al., 2010). In both cases, AIS changes were accompanied by a homeostatic alteration in excitability. Neurons with distally shifted AISs were less excitable than control neurons. Conversely, auditory neurons with long AISs were more excitable than their control counterparts, with shorter AISs. Combining these findings with the knowledge that AP initiation occurs along this initial portion of the axon, AIS plasticity may provide a powerful way to finely tune neuronal output. Since these original studies documenting this novel form of plasticity, several studies have reported AIS plasticity in disease models including epilepsy and traumatic brain injury (Baalman et al., 2013; Harty et al., 2013), indicating the potential therapeutic significance this newly identified form of plasticity could have.

Knowledge of the molecular pathway is crucial for advancing our understanding of a potential new therapeutic target, as well as revealing how the mechanism may potentially interact with other on-going forms of plasticity. Similar to changes described earlier in channel conductance, calcium-dependent mechanisms, rather than AP firing rates, mediate AIS plasticity (Evans et al., 2013; Grubb and Burrone, 2010). Further study into the exact mechanisms

regulating AIS plasticity have shown that, in the case of AIS relocation, this process is dependent on calcineurin signalling acting downstream of L-type Ca_v1 VGCCs (Evans et al., 2013). But, while other forms of plasticity have also been shown to be dependent on intracellular Ca^{2+} levels, the calcineurin pathway was not found to be involved in other forms of plasticity observed in cells following high K^+ treatment. Thus, although Ca^{2+} may act as an initial trigger for multiple plasticity forms, there is divergence in the precise molecular pathways regulating different mechanisms.

Synaptic scaling

Synaptic scaling, first demonstrated by Turrigiano et al., (1998), describes the mechanism by which all of a cells' synapses are scaled either up or down to counteract a large change in activity levels. This is in contrast to Hebbian long-term potentiation or long-term depression, which acts in a synapse specific manner. Instead, synaptic scaling alters the strengths of all of the neurons synapses proportionally, in such a way that any relative strengths set by Hebbian plasticity mechanisms are kept in tact. This mechanism was first shown in cortical cultured neurons, where application of tetradotoxin (TTX) to block sodium channels and abolish AP firing led to an increase in the amplitude size of mini excitatory post-synaptic currents (mEPSCs) as well as EPSCs. The measure of mEPSCs, and mini inhibitory post-synaptic currents (mIPSCs), are often used as a way to assess the synaptic inputs onto a cell; an mEPSC (or mIPSC) is defined as the post-synaptic response to the unevoked release of a single vesicle of neurotransmitter. The frequency of mEPSC/mIPSCs is used as an indication of the number of excitatory or inhibitory synapses, respectively, on a cell, while the amplitude of the events are used as a gauge of the strength of the synapses (Turrigiano et al., 1998). The increase in mEPSC amplitudes following TTX treatment is thought to maintain activity within the neurons, whose spiking activity has been lost. The amplitudes were increased in a multiplicative fashion, meaning that the distribution of amplitudes measured in TTX could be scaled by a factor and then superimposed over the distribution of amplitudes seen in control, with little deviation. The process was also shown to be bidirectional, with the application of bicuculline, to block ionotropic γ-aminobutyric acid (GABA) receptors and remove inhibition, causing a downscaling of mEPSC

amplitudes. It is largely thought that the locus of expression of synaptic scaling is the post-synapse. Synaptic scaling typically measures α-amino-3-hydroxy-5-methyl-4-isoxazolepropionic acid (AMPA) receptor mediated currents and several studies have shown that scaling is accompanied by trafficking of AMPA receptors (Lissin et al., 1998; O'Brien et al., 1998; Wierenga et al., 2005), suggesting that the post-synaptic compartment is the site of synaptic scaling. Furthermore, recent *in vivo* work provided support for this hypothesis, as well as providing a structural correlate for synaptic scaling (Keck et al., 2013). Using two-photon laser scanning microscopy, Keck et al., showed that following retinal lesions, dendritic spine size in the visual cortex scaled up in a similar manner to mEPSC amplitude. Combining this with previous work showing AMPA receptor numbers to correlate with spine size (Béïque et al., 2006; Matsuzaki et al., 2001), there is now a large body of evidence demonstrating the post-synaptic site to be the primary locus of synaptic scaling. There is however, also evidence for a presynaptic element to synaptic scaling, with TTX treatment of hippocampal cultured neurons causing an increase in vesicle release probability (Zhao et al., 2011).

For some time, it had generally been considered that the main cue for synaptic scaling was a change in overall firing rates in a neuron, in turn causing changes to intracellular calcium (Ca^{2+}) levels. In the case of synaptic scaling in the upwards direction, a drop in firing rates would cause a decrease in intracellular Ca^{2+}, which in turn results in lower levels of activated Ca^{2+}/calmodulin-dependent protein kinase IV (CamKIV), and increased transcription leading to greater AMPAR expression (Ibata et al., 2008; Thiagarajan et al., 2002). In addition, numerous other molecular factors have been implicated in synaptic scaling, including brain-derived neurotrophic factor (BDNF) (Rutherford et al., 1998), tumour necrosis factor α (TNFα) (Stellwagen and Malenka, 2006) and the early immediate gene *activity-regulated cytoskeleton-associated protein* (Arc) (Rial Verde et al., 2006; Shepherd et al., 2006). However, recent evidence suggests that, rather than spiking rates, a more subtle change in neurotransmission may be the trigger for the scaling process (Fong et al., 2015), in a similar vein to intrinsic plasticity discussed earlier. The tight relationship between neurotransmission and firing has made it difficult to distinguish

between the two as a trigger. However, studies showing the blockade of AMPA receptors (AMPARs) is sufficient to trigger scaling (Jakawich et al., 2010; O'Brien et al., 1998; Turrigiano et al., 1998) suggest that scaling may not be as reliant on firing rates as originally thought. Using optogenetic techniques to restore spiking activity in cultures treated with AMPAR/kaintate receptor antagonist 6-cyano-7-nitroquinoxaline-2,3-dione (CNQX), Fong et al., (2015) showed that scaling could be triggered in conditions where AMPAR transmission was reduced but firing rates remained unperturbed. They confirmed the necessity for altered AMPAergic transmission in triggering scaling by enhancing AMPAergic mEPSCs using a positive AMPAR modulator during TTX-induced spiking blockade and showing that this attenuated the scaling observed with TTX alone. These results find common ground with work demonstrating local-level synaptic scaling, in which scaling only occurs in those synapses whose neurotransmission have specifically been inhibited (Béïque et al., 2006; Hou et al., 2008). Thus, global and local forms of homeostatic plasticity may be more similar than originally thought since both appear to be triggered by reduced neurotransmission, rather than one being a response to reduced rates of spiking.

Synaptic scaling has been reported in neurons in a number of different CNS regions including visual cortex (Desai et al., 2002; Gainey et al., 2009; Goel and Lee, 2007; Turrigiano et al., 1998), hippocampus (Kim and Tsien, 2008; Stellwagen and Malenka, 2006), and spinal cord (Knogler et al., 2010; O'Brien et al., 1998), and thus, appears to be a relatively ubiquitous form of homeostatic plasticity. However, scaling does not occur at all developmental stages and has been shown to be layer and age dependent in the cortex. In layer 4, which receives the primary input to the cortex, synaptic scaling is observed during early development but does not occur when deprivation happens three weeks post birth (Desai et al., 2002). In contrast, layer 2/3 scaling is seen following deprivation in juvenile and adult mice but loses it multiplicative nature in adults (Goel and Lee, 2007). Furthermore, induction of scaling can depend on the mode of deprivation, with TTX injection but not eyelid suture causing synaptic scaling in layer 2/3 (Maffei and Turrigiano, 2008). Thus, in spite of its prevalence in the

literature, a specific set of conditions must be met in order to activate synaptic scaling.

E/I balance

Each neuron in the brain has several thousand synapses, formed with either pre-synaptic excitatory or inhibitory neurons (Cragg, 1967; Schüz and Palm, 1989). The balance between excitation and inhibition (E/I balance) for a neuron is crucial for maintaining stability within a neuronal network. Networks of neurons are highly complex systems containing recurrent loops, feedback and feedforward connections, meaning that small changes the ratio of incoming excitation and inhibition in a single cell can have far-reaching effects across cascades of neurons. While such a change could prove potentially damaging, it also presents an efficient way to counteract any large unwanted perturbations in activity within a given network. In addition to synaptic scaling described above, a neuron's inputs can be altered by changes to the number of both excitatory and inhibitory synapses, as well as to pre-synaptic neurotransmitter release probabilities.

Many groups have addressed individual changes to either excitatory or inhibitory synapses. While the majority of reports relating to excitatory plasticity have been related to synaptic scaling and therefore to the strength of the post-synapse, there are also reports of changes to the number of synapses indicated by altered mEPSC frequency (Goold and Nicoll, 2010). Work in the monkey showed that levels of inhibitory neurotransmitter GABA are regulated by activity (Hendry and Jones, 1986; Hendry et al., 1994), with levels of GABA immunostaining decreasing after activity deprivation. Since these early studies, altered inhibition has been shown in several cells types and to both the pre- and post-synaptic site. Similar to synaptic scaling of excitatory synapses, changes to the amplitude of mIPSCs have been reported following activity manipulations (Hartman et al., 2006; Kilman et al., 2002; Lau and Murthy, 2012; Rannals and Kapur, 2011; Swanwick et al., 2006). However, rather than scaling in a multiplicative manner such as in synaptic scaling, changes in mIPSC were often associated with altered mIPSC frequency indicating a potential change in

inhibitory synapse density as well as strength (Barnes et al., 2015a; Hartman et al., 2006; Keck et al., 2011, 2013; Kilman et al., 2002; Rannals and Kapur, 2011). Presynaptic changes to inhibition include decreased levels of the 65-kDa isoform of glutamic acid decarboxylase (GAD65), the enzyme responsible for synthesis of GABA from glutamate, leading to reduced vesicle filling following activity deprivation (Hartman et al., 2006), and the converse of this – increased GAD65 puncta – following elevated activity (Rannals and Kapur, 2011). In general, changes to inhibitory synapses oppose changes seen to excitatory synapses following the same activity manipulation (Rutherford et al., 1998), i.e. activity deprivation causes an increase in excitation, but a decrease in inhibition, and the opposite occurs for paradigms where activity is up-regulated.

A number of studies have now examined the combined changes in excitation and inhibition allowing examination of the ratio between the two (Barnes et al., 2015a; Maffei and Turrigiano, 2008; Maffei et al., 2004). Intraocular TTX injection in rats produces an increase in spontaneous firing in layer 2/3 visual cortex pyramidal neurons, caused by an increase in excitatory drive and a decrease in inhibitory drive, shifting the E/I balance in the direction of excitation (Maffei and Turrigiano, 2008). In contrast, using eyelid suture as the method of deprivation also leads to an increase in spontaneous firing, but has a profoundly different effect on the E/I ratio. Here excitatory drive is decreased, while inhibitory drive remains unchanged, creating an overall shift towards inhibition. In this case, the increase in firing is achieved by increasing the intrinsic excitability of neurons. Following monocular enucleation in the adult mouse, the E/I balance is altered yet again differently, this time via a decrease in inhibition (Barnes et al., 2015a). These three examples of activity deprivation all produce remarkably different changes to the E/I ratio of layer 2/3 neurons in the visual cortex, underlining how the employment of homeostatic mechanisms may be specifically tailored according to exactly how perturbations affect incoming levels and patterns of activity.

Global versus local homeostatic plasticity

One aspect of homeostatic plasticity that several studies have addressed is the identification of both the spatial scale of the trigger, and the spatial scale of the implementation of plasticity. For example, do local changes to levels of activity in individual neurons activate homeostatic mechanisms in that cell, or is a global change in activity required to elicit homeostatic plasticity? Moreover, does homeostatic activity restore activity of the individual neuron, or does it serve to maintain the level of the whole network? Several studies have addressed these questions. Overexpression of the potassium inward rectifier channel Kir2.1 to silence individual neurons results in a homeostatic increase in synaptic input, although by an increase in synapse number rather than synaptic scaling, in the silenced neurons restoring their activity levels (Burrone et al., 2002). This demonstrates that the local changes to activity are able to trigger homeostatic mechanisms. The cell autonomous nature of synaptic scaling induction was demonstrated in cortical cultured neurons, where TTX application at the soma to inhibit post-synaptic firing resulted in synaptic scaling, but TTX application at dendritic locations to inhibit pre-synaptic input did not induce scaling (Ibata et al., 2008). Increasing the activity of individual cells has been to shown to be sufficient to elicit a depression of excitatory synapse function (Goold and Nicoll, 2010). However, only global, and not single cell suppression of spiking is enough to elicit changes to inhibitory synapses (Hartman et al., 2006), highlighting key differences between the control of excitatory and inhibitory responses. Thus, while many studies use global activity manipulations to investigate homeostatic mechanisms (Desai et al., 2002; Gainey et al., 2009; Turrigiano et al., 1998; Wierenga et al., 2005), there is evidence that certain homeostatic mechanisms can be triggered following local activity changes.

Once activated, on what spatial scale are homeostatic mechanisms implemented? Moreover, do all neurons undergo the same uniform changes, to bring their individual activities in line with where they had previously been? Or do select neurons undergo plasticity to restore the overall network level of activity? At the most local level, suppression of individual synapses has been shown to increase AMPAR trafficking into these inhibited synapses (Hou et al.,

2008). However, another study using local synaptic blockade failed to observe changes at the post-synapse (Ibata et al., 2008). The existence of such a local level scaling is controversial, since it would appear to directly antagonise synapse-specific forms of plasticity such as LTP or LTD (Turrigiano, 2012). At the dendritic level, it has been shown that the release probability of neurotransmitter is homeostatically regulated (Branco et al., 2008). At the cell level, both global activity inhibition, and suppression of activity in individual neurons, has led to the restoration of activity levels, accompanied by synaptic homeostatic mechanisms (Burrone et al., 2002; Turrigiano et al., 1998).

In a more intact preparation however, how do different neurons respond? In organotypic hippocampal cultures, TTX induced activity-suppression leads to differential homeostatic responses in specific synapse types, in such a way that prevents overall network unbalancing (Kim and Tsien, 2008). This study described three different responses in three different synapse types within the hippocampus: mossy fibre synapses underwent an increase in mEPSC frequency, recurrent collateral synapses underwent a decrease in mEPSC frequency, and Schaffer collateral synapses showed an increase in mEPSC amplitude. Overall, these changes prevented epileptiform activity, as might have occurred if all synapses had undergone the same increase in strength or number. In contrast, *in vivo* experiments in the mouse visual cortex show that following monocular enucleation, all neurons undergo the same homeostatic reduction in inhibition, but only a subset of these neurons recover their activity (Barnes et al., 2015a). Thus, while these results are contrasting in how ubiquitous a homeostatic mechanism may be across all neurons, they both suggest that, in more intact systems, the implementation of homeostatic plasticity is employed to serve the whole network, rather than the individual activity of the neuron.

Homeostatic plasticity in the recovery of activity in vivo

Following large perturbations in activity, homeostatic plasticity is proposed as way in which to restore activity. Much of the work on homeostatic plasticity has been carried out in cultured preparations (Burrone et al., 2002; Desai et al.,

1999; Hartman et al., 2006; Ibata et al., 2008; Turrigiano et al., 1998), allowing activity manipulations to be applied on different spatial levels, as described in the previous section. However, more recently, advances in techniques have allowed activity of neurons, even at the individual cell level, to be followed chronically *in vivo* following perturbations in activity (Barnes et al., 2015a; Hengen et al., 2013; Keck et al., 2013). Recovery of activity has been demonstrated in both juvenile (Hengen et al., 2013), and adult rodents (Barnes et al., 2015a; Keck et al., 2013). Common to both adult and juvenile studies, is that following deprivation, a reduction in levels of inhibition precede changes to excitation (Barnes et al., 2015a; Hengen et al., 2013; Keck et al., 2013). These studies differ in the timing of excitatory activity reduction, however, although this may be due to different methods of deprivation used, or layer specificity. The homeostatic mechanisms accompanying activity recovery also vary across different studies. Following eyelid suture and retinal lesions, synaptic scaling occurs at the same time as activity recovery (Hengen et al., 2013; Keck et al., 2013) indicating its potential role in mediating, at least in part, recovery of activity. Meanwhile, in adult mice following monocular enucleation, synaptic scaling is not observed, but instead the E/I ratio is shifted towards excitation, due to a reduction in inhibition (Barnes et al., 2015a). However, this homeostatic plasticity could not be wholly responsible for activity recovery, since not all neurons did recover their activity. Recovery of individual neuron activity was attributed to a combination of the altered E/I ratio, and the local activity of the specific subnetwork in which the neuron resided (Barnes et al., 2015a). Thus, homeostatic mechanisms appear, at least in part, to play a role *in vivo* in the recovery of cortical activity following activity manipulations. Interestingly, only synaptic homeostatic mechanisms have been reported, although not all studies looked for changes in intrinsic excitability and so this cannot by ruled out as playing a role in recovery following certain activity deprivation scenarios.

Role of inhibition in development

As demonstrated by Desai et al., (2002), homeostatic plasticity is regulated differentially throughout life. This is not surprising given that during early post-

natal life there are still many adjustments taking place, and synaptic connections are still being formed. One of the major factors that is changing in this developmental stage is inhibition, which plays a key role in development. For a brief period in early postnatal life, GABA acts as a depolarising signal for neurons. The developmental switch in expression of co-transporters from Na+-K+-2Cl- to K+-2Cl- alters the equilibrium potential for chloride and thus renders GABA hyperpolarising (Ben-Ari, 2002; LoTurco et al., 1995; Owens et al., 1996; Rivera et al., 1999). In rodents, this switch occurs within the first two weeks of postnatal life (Ben-Ari, 2002). At two weeks post birth, in mice, eye opening occurs. Shortly after this, at around postnatal day 21 (P21) the critical period for the visual system begins. The critical period describes a window during development in which experience provides essential information for the proper development of a system. The length of the critical period is dependent on the life span of the individual species and can range from weeks to years (Hensch, 2005). However, in the visual system, consistent across species, monocular deprivation during this time causes dramatic changes to the way the eye is represented in the brain. Full visual acuity through the covered eye is lost. Consequently, there is an expansion in the representation of the non-deprived eye, in the cortex. Once the critical period has come to an end, at around P35 in mice, monocular deprivation will no longer cause such drastic altered representation of visual inputs. Inhibition is crucial for this activity-dependent plasticity seen in development. Deletion of the *Gad65* gene prevents the onset of the critical period and thus, the loss of visual acuity following monocular deprivation (Hensch et al., 1998). Conversely, enhancing GABA function with benzodiazepines just after eye opening promotes plasticity and causes an early onset of the critical period (Fagiolini and Hensch, 2000). Additionally, acceleration of GABA maturation via increased BDNF has also been demonstrated to artificially open the critical period (Hanover et al., 1999; Huang et al., 1999). Thus, GABAergic transmission is crucial for developmental plasticity, but do GABAergic neurons themselves undergo forms of homeostatic plasticity following activity deprivation? This shall be discussed in the next section.

Diversity of inhibition and its plasticity

On a gross scale, characterization of inhibitory neurons begins with where the interneurons migrate from during development. Two distinct streams of migrating interneurons have been described, with around half of inhibitory neurons migrating from the medial ganglionic eminence (MGE) and the other half arriving from the caudal ganglionic eminence (CGE) (Wonders and Anderson, 2006). Neurons derived from the MGE express either parvalbumin (PV) or somatostatin (SST), and around half of cells from the MGE are fast-spiking neurons (Butt et al., 2005). In contrast, no fast-spiking cells emerge from the CGE, with the majority of CGE-derived neurons having regular spiking firing properties. Cells originating from the CGE show a greater preference for expressing calretinin and neuropeptide Y (NPY) (Butt et al., 2005). Additionally, inhibitory neurons may express other calcium binding proteins including calbindin (Clb) and cholecystokinin (CCK), or neuropeptides including vasointestinal peptide (VIP) and reelin. The specific origins of neurons expressing these factors are less distinct, with some overlap and coexpression with other markers, though VIP expression is restricted to CGE-derived neurons (Kawaguchi and Kondo, 2002; Rudy et al., 2011; Wonders and Anderson, 2006). Thus, in some instances, inhibitory neurons are distinguished by other features including electrophysiology, firing patterns or morphology. Great efforts are being made to arrive at a general consensus for classification of inhibitory neuron subtypes (Ascoli et al., 2008; DeFelipe et al., 2013). The sheer variation across inhibitory neurons may be why knowledge of homeostatic mechanisms occurring in these cells lags far behind that of their excitatory counterparts. While limited, there are reports into the occurrence of homeostatic plasticity in some types of inhibitory neurons. In cortical slice culture, both PV and SST cells showed an increase in intrinsic excitability following 5 days of activity deprivation. Both cell types also expressed increase excitatory drive, but changes to inhibitory drive was different between PV and SST (Bartley et al., 2008). In layer 4 of the visual cortex, deprivation has also been shown to increase the strength of connections between pyramidal neurons and fast-spiking (PV) neurons (Maffei et al., 2006). Structural changes have been observed in cortical inhibitory neurons following retinal lesions (Keck et al.,

2011; Marik et al., 2014). Large-scale axonal sprouting and pruning occurs rapidly following lesions (Marik et al., 2014). Furthermore, a group of inhibitory neurons in the visual cortex were shown to carry dendritic spines, which formed functional excitatory synapses. Following retinal lesions, *in vivo* two-photon imaging showed that these neurons underwent remodelling and experienced both a loss of dendritic spines, and axonal boutons (Keck et al., 2011). These structural changes to inhibitory neurons may be contributing to a shift in the E/I balance of excitatory neurons, in turn aiding the recovery of network activity. The spine and bouton density in these inhibitory neurons remains reduced, even months after the retinal lesions. This is consistent with *in vivo* work following the activity of individual inhibitory neurons across time, where in adult mice following monocular enucleation, activity of inhibitory neurons is reduced, and does not recover to control levels, at least within several days post-enucleation (Barnes et al., 2015a). In contrast, a juvenile study has shown that the activity of fast-spiking inhibitory neurons is reduced at 24 hours after monocular deprivation, but rebounds after 48-72 hours (Hengen et al., 2013). The recovery of activity in inhibitory neurons therefore, appears to be different in the adult system compared to the juvenile, and also may vary between inhibitory neuron subtypes.

The mouse visual system as a model for homeostatic plasticity

Although a majority of the initial research into homeostatic plasticity was conducted in culture systems, as research moves towards an *in vivo* approach, the visual cortex provides a highly attractive system for continuing work. Firstly, the eye gives way to various means of manipulation, both permanent (enucleation or ablation) or temporary (eyelid suture, dark-rearing), allowing probing of different activity patterns on the outcome of plasticity and potential reversal. Secondly, the upper layers of the cortex lie superficial enough to enable *in vivo* experimentation without the need to be too invasive and disturb other brain regions. Finally, the gross architecture of the visual system and the pathways linking information from the retina to the cortex are now well established, giving us the potential to examine effects at each step in the

pathway and determine whether changes occurring may be a direct consequence of upstream alterations or intrinsically generated.

Aims and motivation

We now have substantial knowledge of the individual mechanisms of homeostatic plasticity, and have observed them corresponding with *in vivo* recovery of activity in both adult and juvenile animals (Barnes et al., 2015a; Hengen et al., 2013; Keck et al., 2013). However, one aspect that remains less well understood is whether individual cells employ multiple homeostatic mechanisms, and how these might interact with one another if they do. In adults, synaptic mechanisms involving changes to both excitation (Keck et al., 2013), and inhibition (Barnes et al., 2015a) have been demonstrated following different deprivation paradigms, and are implemented ubiquitously across all cells. No changes to the intrinsic excitability of neurons have been shown in the adult. In contrast, while *in vivo* study in juveniles reports only synaptic changes following activity deprivation (Hengen et al., 2013), other studies have reported changes to intrinsic excitability in juvenile preparations, alongside changes to synaptic input (Lambo and Turrigiano, 2013; Maffei and Turrigiano, 2008). However, often synaptic and intrinsic changes are studied in separate populations of neurons, and thus, the contributions of each mechanism to an individual cell are unknown. Furthermore, a recently identified form of structural plasticity, AIS plasticity, has been shown to correlate with the excitability of a neuron (Grubb and Burrone, 2010; Kuba et al., 2010). This form of plasticity has not yet been studied in the visual cortex, in the context of homeostatic plasticity. It may provide a useful approach for the study of multiple homeostatic mechanisms in individual neurons, allowing for post-hoc labelling which may provide information on the intrinsic excitability properties of a neuron, after functional measures of synaptic input and output activity have been collected.

Thus, the aims for this thesis are twofold. First, I shall investigate a recently reported new form of homeostatic plasticity – AIS plasticity – within the visual cortex, where it has not yet been explored in an activity-dependent manner.

Moreover, I shall examine both inhibitory and excitatory neurons to see if either cell type exhibit plasticity at the AIS. The AIS is proposed to be a potential homeostatic mechanism for adjusting excitability of neurons. Thus, I shall look at how changes to the AIS correlate with changes to functional firing properties of neurons. The second aim of this thesis is to examine how individual cells respond to deprivation both in terms of their intrinsic properties and also their synaptic inputs. Thus, I intend to address how multiple mechanisms may be employed simultaneously in individual neurons. I shall perform these experiments in the juvenile mouse, during the critical period, where all three forms of homeostatic plasticity have been previously reported to occur in rodents.

The key questions I wish to address in this thesis are:

1. Do neurons in the mouse visual cortex undergo AIS plasticity following activity deprivation?

2. Do individual cells in the mouse visual cortex undergo multiple forms of plasticity following activity deprivation?

3. How do different mechanisms of homeostatic plasticity interact with each other within single cells?

Chapter 2: Materials and methods

Surgical Procedures

Enucleation

All procedures were carried out in accordance with the Home Office Animals (Scientific Procedures) Act 1986. Sensory deprivation was achieved by monocular enucleation of the left eye. Mice were anaesthetised with an i.p. injection of ketamine (0.15 mg/g) and xylazine (0.015 mg/g) and surgery commenced when the toe pinch reflex was no longer present. Lidocaine was topically applied to the area around the eye to be removed. The eyeball was then surgically removed and the eyelids closed and glued shut. Mice were then returned to their cages to recover, where their breathing rate was monitored and body temperature maintained using a heat mat. Control mice underwent the same anaesthesia procedure, without the removal of the eye. Maxitrol eye ointment (Alcon) was applied to non-enucleated eyes during anaesthesia to prevent drying out of the eye. All enucleations or anaesthetic controls were carried out at postnatal day 23.

Immunohistochemistry

Immunostaining for the axon initial segment in inhibitory and excitatory neurons

To examine plasticity of the axon initial segment in GABAergic inhibitory neurons, a transgenic mouse line expressing GFP under the GAD65 promoter (López-Bendito et al., 2004) was used. Mice were deeply anaesthetized (ketamine, 0.3 mg/g, xylazine, 0.03 mg/g) and perfused with 10ml phosphate buffered saline (PBS; pH7.4) followed by 10ml 1% paraformaldehyde (PFA). Brains were removed and post-fixed overnight in 1% PFA containing 2.7% sucrose. The next day brains were sectioned using a vibratome (Leica,

Germany). Coronal sections through the monocular visual cortex were cut at a thickness of 50μm. Following sectioning, slices were rinsed three times in PBS, each time for 5 mins before being incubated for 2 hours in blocking solution (10% normal goat serum (NGS, Bethyl labs), 0.25% PBS-Triton-X (PBS-T) and PBS), at room temperature. Blocking solution was then replaced by primary antibody in blocking solution and incubated for 72 hours at 4˚C. To label the axon initial segment, a mouse-2α anti-AnkyrinG (1:500, Neuromab) antibody was used. In a subset of experiments slices were also incubated with rabbit anti-NPY (1:500, RayBiotech) to label the specific NPY expressing subset of inhibitory neurons. After incubation with primary antibody, slices were washed three times (20 mins each) in 0.25% PBS-T. Next slices were incubated with secondary antibody for 2 hours at room temperature (anti-mouse-2α AlexaFluor (AF) 546, and in the NPY subset anti-rabbit AF 633, both at 1:500, Invitrogen). Following incubation with secondary antibody, slices were washed three times (15 mins each) in PBS. Slices were then mounted onto glass slides with Mowiol (Calbiochem).

To label the axon initial segment in excitatory neurons, slices were prepared from wild type C57/BL6 mice. Slices were prepared as above, with the addition of neurofilament-labelling antibody (mouse anti-NF-H, 1:1000, Calbiochem) to label neurons and allow tracing of AISs back to their cell soma. The secondary antibody used was goat anti-mouse AF 633 (1:500, Invitrogen).

Immunostaining for the axon initial segment in slices used for electrophysiology recordings

At the end of patch-clamp recordings, pipettes were carefully reversed out from the recorded cell. The slice was then transferred into a well-plate containing 1% PFA (+ 2.7% sucrose) and fixed overnight. Following fixation, slices were washed three times (5 mins each) in PBS. To enhance antibody penetration in these thicker slices (300μm), additional steps were included in the immunostaining protocol. First, once slices had been rinsed they were transferred to individual tubes (Eppendorf) containing a 30% sucrose solution (sucrose suspended in PBS) and put on a rocker at room temperature for two

hours, or until the slice had sunk to the bottom of the sucrose solution. Next, slices were frozen over dry ice and subsequently thawed in PBS. Slices were then incubated in blocking solution for 2 hours (room temperature, 10% NGS) before primary antibody was added. Primary antibody (mouse-2α anti-Ankyrin-G; Neuromab and rabbit anti-cFos; Santa Cruz; both at 1:500) was diluted in blocking solution and added to the slices, which were then incubated overnight at 4˚C. After primary incubation, slices were washed three times (20 mins each) in PBS-T, and then, treated with secondary antibody (anti-mouse-2α AF 546 and anti-rabbit AF 633, Invitrogen). Secondary antibody incubation was carried out as described above (i.e. diluted 1:500 in blocking solution, incubated for 2 hours at room temperature). After secondary incubation, slices were washed three times (15 mins each) in PBS and then mounted in Mowiol (Calbiochem).

Immunostaining for c-Fos

To investigate levels of neuronal activity following deprivation, presence of c-Fos immunoreactivity was used to identify putative active and inactive neurons. This protocol is taken from Barnes et al., (2015a), where in adult animals the detection of c-Fos immunostaining in neurons is shown to be an accurate indicator of previous *in vivo* activity. Animals were deeply anaesthetized (ketamine, 0.3 mg/g, xylazine, 0.03 mg/g) and perfused with 10ml ice-cold artificial cerebrospinal fluid (ACSF). Brains were quickly removed and cut using a vibrating microtome (Leica) at a thickness of 300μm. Slices were transferred from the slicing chamber to oxygenated artificial cerebral spinal fluid (ACSF), using wide-ended Pasteur pipette, at room temperature. Slices were left to recover for 4 hours, before being fixed in 1% PFA overnight at 4˚C. The next day slices were rinsed 3 times (5 mins each) in PBS and then transferred to 10% NGS blocking solution. Slices were incubated in blocking solution for 2 hours at room temperature before being incubated with rabbit anti-c-Fos (1:500, SantaCruz) overnight. Following incubation with primary antibody, slices were washed three times (20 mins each) with PBS-T before incubation with secondary antibody at room temperature for 2 hours (goat anti-rabbit AF 633). After secondary incubation slices were washed three times (15 mins each) in PBS and mounted in Mowiol onto glass slides.

Microscopy

Imaging of inhibitory and excitatory axon initial segments

All images were acquired using a Nikon A1R Inverted confocal microscope (Nikon, Japan) equipped with GaAsP detectors. Monocular visual cortex was identified using stereotaxic coordinates, through the eyepieces with a low magnification objective (10x air objective, 0.3 NA, Nikon, Japan). To acquire images the objective was switched to a 60x oil immersion objective (1.4 NA, Nikon). Inhibitory and excitatory neurons in layers 2/3 with whole, uncut AISs were imaged with a 488nm Argon and 561 nm and 642 nm diode lasers. Images were acquired at a resolution of 1024x1024 pixels, with a pixel size of 0.21µm x 0.21µm and z step size of 0.2µm. Laser power and gain was kept constant for all images. All images were acquired blind to experimental condition.

Imaging of recorded neurons

Neurons that had been recorded from in patch-clamp recordings were identified by the green AlexaFluor 488 dye that had been in the recording pipette. The AISs of these cells was imaged using the parameters described above. A second image was taken of the cell soma with the 642 nm laser switched on to determine if the cell was c-Fos positive or not. These images had a step size of 0.5 µm. Finally the apical dendrites were imaged at a zoom of 2 and a pixel size of 0.1 x 0.1 µm and a step size of 0.5 µm.

Image Analysis

Measuring inhibitory and excitatory AIS lengths

Confocal z-stacks of cells with immunolabelled axon initial segments were analysed using the Fiji (Schindlin et al., 2012) View5D plugin (Heintzmann, KCL). Images were loaded into Fiji and then opened in View5D (Fig. 2.1). AISs from excitatory neurons were selected for analysis based on their characteristic

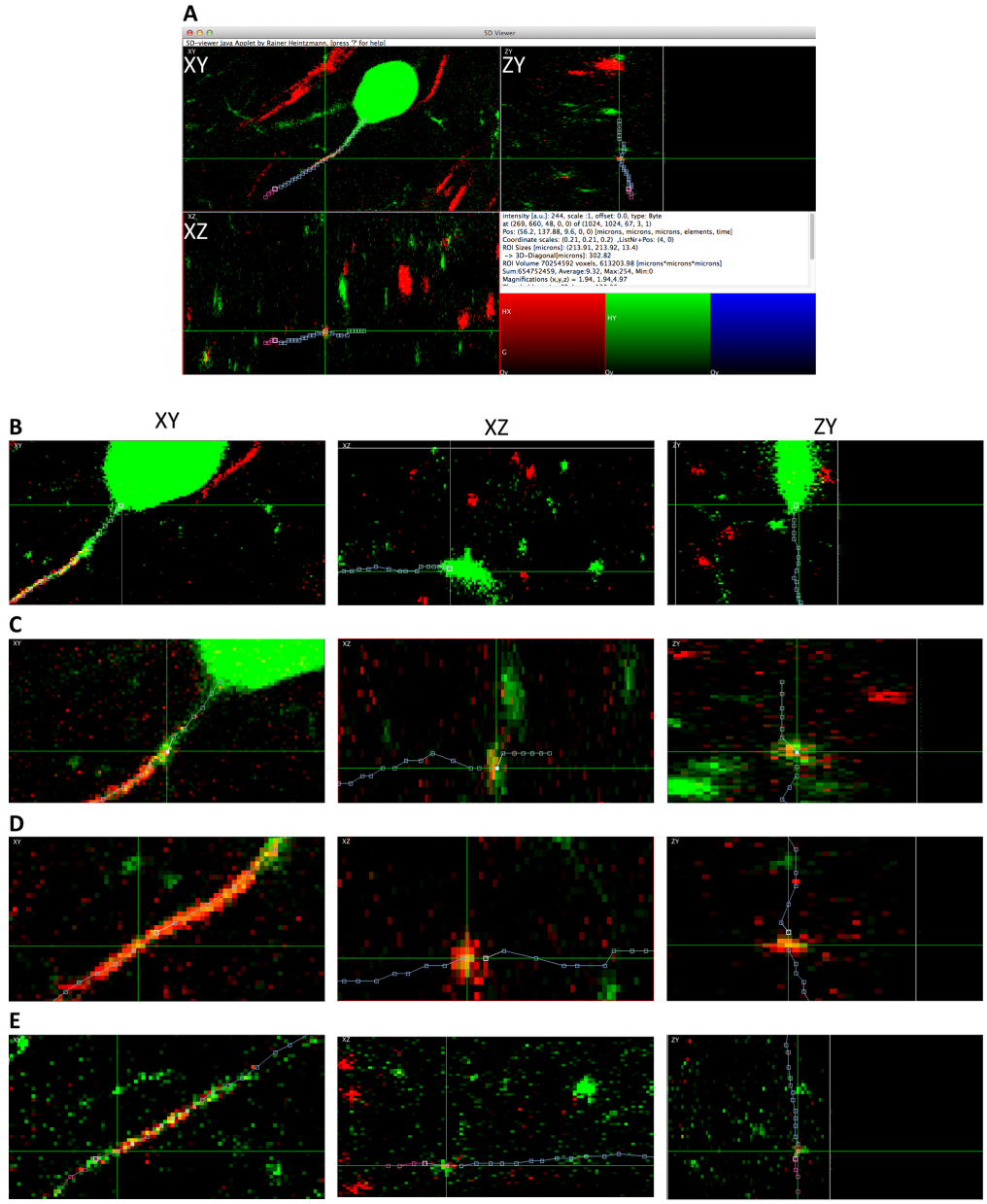

Figure 2.1 Measuring AIS parameters using 5D Viewer.

A. Example screen showing an image of a GAD65-GFP neuron stained with AnkG loaded into the 5D viewer plugin in FIJI. The measuring track used to calculate AIS position and length is shown in three colours, indicating the three segments: in green, soma to AIS start; in blue, AIS start to AIS end; in magenta, continuing axon path. **B.** Three viewing angles showing the start point selection – cross hair (in green) indicates the point where the soma ends and the axon starts. This is

taken as the last point where the cross section of the axon can be distinguished before it merges with the soma in any of the viewing planes (XZ in this example). **C.** Three viewing angles showing the selection of the start point of the AIS – this is taken as the first point of colocalisation between GFP (or NF-H for excitatory neurons) and AnkG. **D.** Example images of the three viewing angles showing the continued tracking of the AIS/axon through the centre of axon's cross section. The centre of the axon was determined, by eye, at all stages of the tracking process by using the three images to continually follow the axon in all 3 dimensions. This prevented errors in measurement caused by the axon moving in depth, that may otherwise have occurred if tracking were performed in two-dimensions. **E.** When AnkG labelling no longer colocalised with GFP (or NF-H) the second segment of the track was ended and a third segment initiated to indicate the end of the AIS and the continued path of the axon.

tapered shape and by the direction of their alignment (running from the pial surface towards to mid-brain). The measuring tool was used to trace from the edge of the soma to where the AIS began, judged manually by the colocalisation of AnkG staining and either GFP (inhibitory neurons) or NF-H staining (excitatory neurons). The start point of the AIS was then labelled by beginning a new segment on the measuring track. Points were selected along the length of the AIS, using the 3 different views (XY, XZ, YZ) to ensure points were placed in the centre of the AIS, thus tracking any depth movement that may occur. The end of the AIS was judged manually, when AnkG staining was no longer present, or distinguishable from background noise. The coordinates of the track were then saved and loaded into Matlab (Mathworks; Fig. 2.2) where a custom written script applied the distance formula shown below (F1) to the two segments of the measurement track, corresponding to the start position and AIS length. All images were analysed blind to their experimental condition.

(F1): $\sum \sqrt{[(x^{n}-x^{n+1})^{\wedge}2+(y^{n}-y^{n+1})^{\wedge}2+(z^{n}-z^{n+1})^{\wedge}2]}$

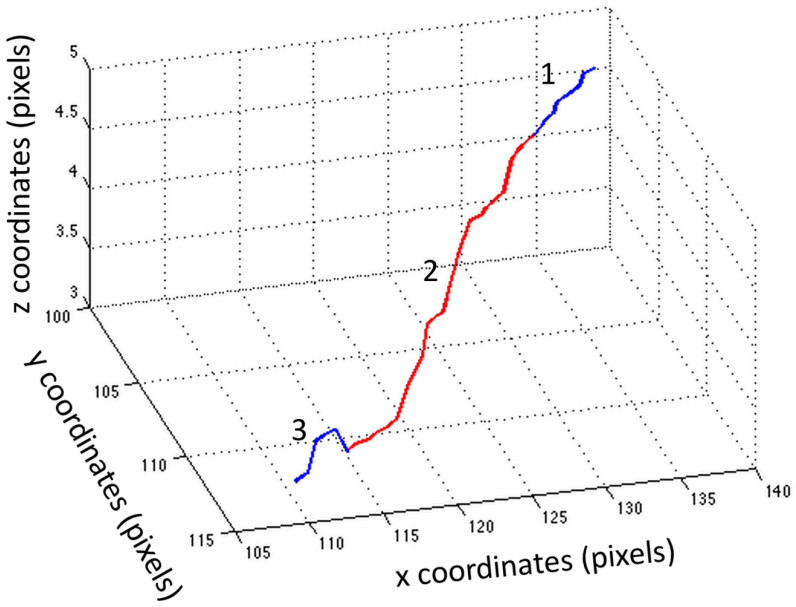

Figure 2.2 Plot of 3D track created in 5D viewer.

3D plot of coordinates from a 5D viewer track, loaded into Matlab for distance calculation. The length calculation was applied separately to the first two segments of the track, corresponding to the start distance measurement (blue, labelled 1) and the AIS length measurement (red, labelled 2). The segment labelled 3 shows the continued path of the axon.

Measuring density of c-Fos

Images of slices labelled with c-Fos were overlaid with a 600μm^2 grid and the number of c-Fos positive cells, determined by eye, was counted in each grid segment using the cell counter plugin in Fiji. Cells were counted if they were wholly inside the grid area in the xy directions and were visible for at least 1μm in the image stack (i.e. two consecutive slices in stack with 0.5 μm z-step). For each imaged slice, the same volume grid (4800 μm^3) was used to count c-Fos positive cells. The total density of c-Fos positive cells in each condition was then calculated using density measures from several different slices for that particular condition. Cells that had been labelled with c-Fos after recordings were regarded as c-Fos positive if c-Fos labelling in the cell soma was 20% greater than background levels of stain (Fig. 2.3b,c). Images were analysed blind to experimental condition.

Measuring expression of NPY in GAD65-GFP neurons

Images of GAD65-GFP neurons labelled with NPY were analysed in Fiji. Expression of NPY was quantified by drawing a region of interest (ROI) around the cell body of GAD65-GFP neurons, and then taking the mean pixel intensity value for the NPY channel at this position. The ROI was then moved to a neighbouring region of background and the mean pixel intensity again taken for each channel. Cells were considered positive for NPY if somatic labelling was 20 % greater than background levels of stain. All images were analysed blind to experimental condition.

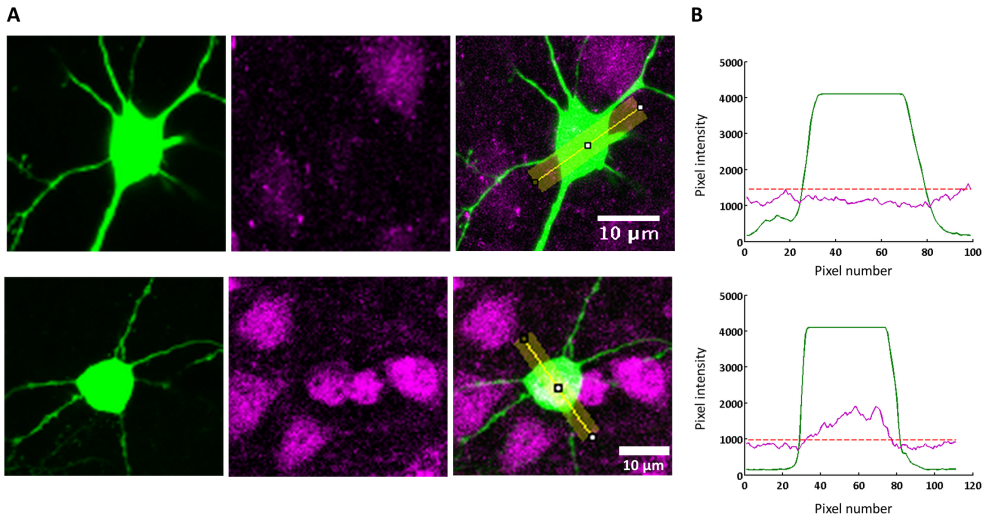

Figure 2.3 Measuring c-Fos immunolabelling intensity.

A, Example images of AF 488 filled neurons (left), c-Fos immunostain (centre) and merge (right) in a neuron classified as c-Fos negative (top row) and c-Fos positive (bottom row). In the merge image the line used to generate pixel intensity line profile in (b) is shown in yellow. **B,** Plot showing pixel intensity along line profiles across cells in (a), for the AF 488 channel (green) and c-Fos label channel (magenta). The red dashed line indicates 20 % above mean background labelling in c-Fos channel. A peak in the c-Fos intensity above this line can clearly be seen in the bottom cell, occurring alongside the peak in the green channel corresponding to the cell soma. In contrast, in the top, negative cell the pixel intensity in the c-Fos channel does not exceed the dashed line at any point over the cell soma (indicated by broad peak in green channel). A cell was considered positive for c-Fos if the mean pixel intensity of c-Fos over the soma was 20 % greater than the mean background pixel intensity.

Measuring spine density

Spine density was measured in a subset of neurons that had been recorded from using electrophysiology and filled with an AF 488 dye. Images were loaded into Fiji and the cell counter used to mark spines along a clear, non-obscured secondary apical dendrite. For each cell, the first non-obscured secondary dendrite branching off from the main apical dendrite was chosen for analysis. All spines were counted, including those projecting in the z dimension. The length of the dendrite was then measured using the simple measuring tool in Fiji, placing points along the length of the dendrite and then using these coordinates to calculate length. The density was calculated by dividing the number of spines counted on the dendrite by the length of the dendrite. All images were analysed blind to experimental condition.

Measuring a proxy for spine size

A proxy for spine size was also measured in cells filled with AF 488 dye. Images were loaded into Fiji and a custom written macro (originally obtained from Prof. Sonja Hofer and optimised for use by Dr. Samuel Barnes and Anton Gauert) was used to estimate a proxy for spine volume based on the integrated brightness of the spine, as in Keck et al., (2013). Images were analysed blind to experimental condition. The macro used three measurements to calculate an estimate for the spine volume. First an area of background (BG) was selected, secondly a region of dendrite adjacent to the measured spine, and finally the area around the spine (including spine neck but excluding any dendrite; Fig 2.4). For each selection the area and the mean pixel intensity was stored and used to calculate the integrated brightness density of the spine (F2a,b). Specifically, the mean background value was subtracted from both the mean dendrite and spine values, and the spine mean was then normalised to the dendrite, to account for differences in the level of fluorescent fill between cells. This normalised spine mean was then multiplied by spine area to give the estimate of spine volume.

(F2a): SpineNormMean = SpineMean-BGmean/DendriteMean-BGmean

(F2b): IntegratedBrightnessDensity = SpineNormMean x SpineArea

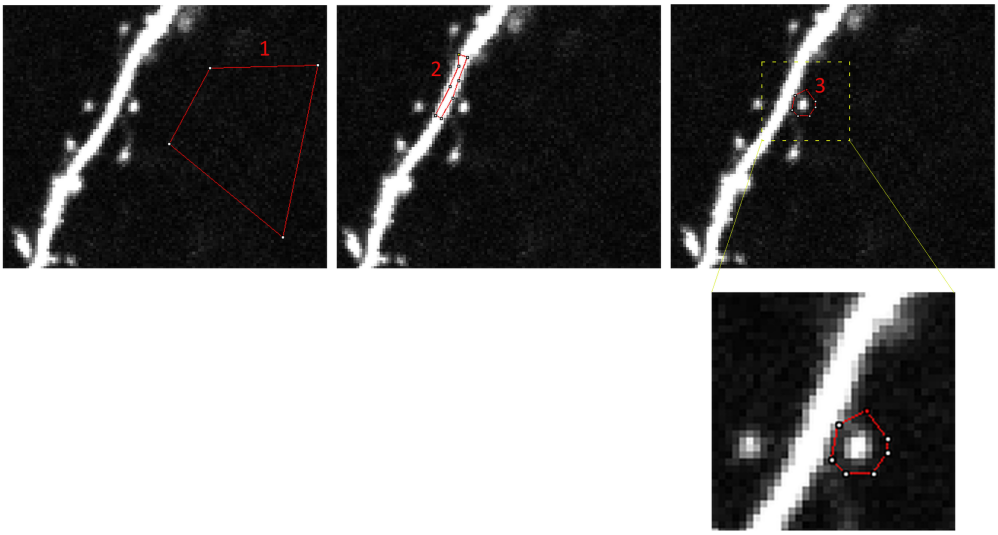

Figure 2.4 Measuring spine volume as proxy for spine size.

To get a proxy for spine size, spine volumes were estimated using a macro that required three measurements. First an area of background was selected (1, left panel). Next, an area of dendrite adjacent to the measured spine was selected (2, centre panel). Finally, the area around the spine, including spine neck was selected (3, right panel). Below, zoom in of yellow boxed area showing selection around spine. The macro then used the area and mean pixel intensity values of these three selected regions to estimate the spine volume (see F2a,b).

Electrophysiology

Preparation and Solutions

Mice were deeply anaesthetized and then transcardially perfused with 10 ml of 4°C dissection ASCF (in mM 108 choline-chloride, 3 KCL, 26 $NaHCO_3$, 25 D-glucose, 3 Na pyruvate, 2 $CaCl_2$ and 1 $MgSO_4$, saturated with 95% O_2 / 5% CO_2). The brain was removed and coronal slices containing visual cortex (300 μm) were cut using a Vibratome 3000 (Leica, Germany). Slices were transferred to a holding chamber, containing recording ACSF (in mM, 120 NaCl, 3 KCl, 23 $NaHCO_3$, 1.25 $NaHPO_4$, 10 D-glucose, 2 $CaCl_2$ and 1 $MgSO_4$ saturated with 95% O_2 / 5% CO_2) and incubated for at least 60 minutes. Individual slices for recording were transferred to the recording chamber, which was continually perfused with fresh recording ACSF. All recordings were made at room temperature. Glass recording pipettes were pulled from Borosilicate glass (Harvard Apparatus) using a micropipette puller (Sutter Instruments), with a resistance of 4 – 7 MΩ. Recording pipettes were filled with an internal solution containing the following, in mM: 130$KMeSO_4$, 8 NaCl, 2 KH_2PO_4, 2 D-glucose and 10 HEPES. In a subset of recordings the internal solution also contained AlexaFluor-488 (1mM).

Stereotaxic coordinates were used to target recordings to the monocular visual cortex. Cells were visualised on a custom-built microscope under infrared differential interference contrast microscopy. Layer 2/3 pyramidal neurons were identified based on morphology (pyramidal shaped soma) and spiking properties. Layer 2/3 GAD65-GFP inhibitory neurons were identified using epifluorescence detection via a CoolLED pE-100. Presence of GFP in the pipette at the end of recording confirmed that a GAD65-GFP neuron had been recorded. Recordings were made in either current- or voltage-clamp mode according to experimental design (Multiclamp 700B, Molecular Devices), and data acquired using Ephus freeware (VidrioTech). Liquid junction potential was not corrected for. Series resistance was monitored throughout recordings. In the majority of

recordings, series resistance remained stable throughout the recording session. However, if series resistance was seen to increase by more than 15% of the original value – usually caused by the seal between membrane and pipette closing up – an attempt to reopen the seal was made. If successfully reopened, recording continued as long as series resistance did not deviate from the original value by more than 15% in either direction. If series resistance was altered by more than 15% either way following reopening, or a stable seal was not maintained after one attempt to reopen the seal, recordings were discarded. Recordings were also discarded if the resting membrane potential or input resistance varied by greater than 10% across the duration of the recording. While recordings were not performed blind, all subsequent offline analysis described below was performed blind to experimental condition.

Measuring excitability

Excitability was measured in current clamp mode. Somatic current injections (500ms) were applied in increasing steps until the recorded neuron fired a single action potential. This current value was defined as the rheobase. For c-Fos experiments, once the rheobase had been determined, no additional positive current injections were made to the cell. For other experiments further somatic current injections were made, of increasing 10 pA steps until either 250 pA or until the AP trace became saturated (i.e channel inactivation was seen and fewer APs were fired than previous current injection steps; Fig. 2.5a). The number of APs that fired at each current step was counted and used to make an input-output function for the cell. A line was fitted to the linear portion of this function and the intercept and slope values were calculated. These values were used to test differences between the input-output functions of control and deprived groups of neurons. Passive membrane properties were calculated from -100 pA current injection. Input resistance was calculated using the following formula (F3):

(F3): Resistance(R) = Voltage(V)/Current(I)

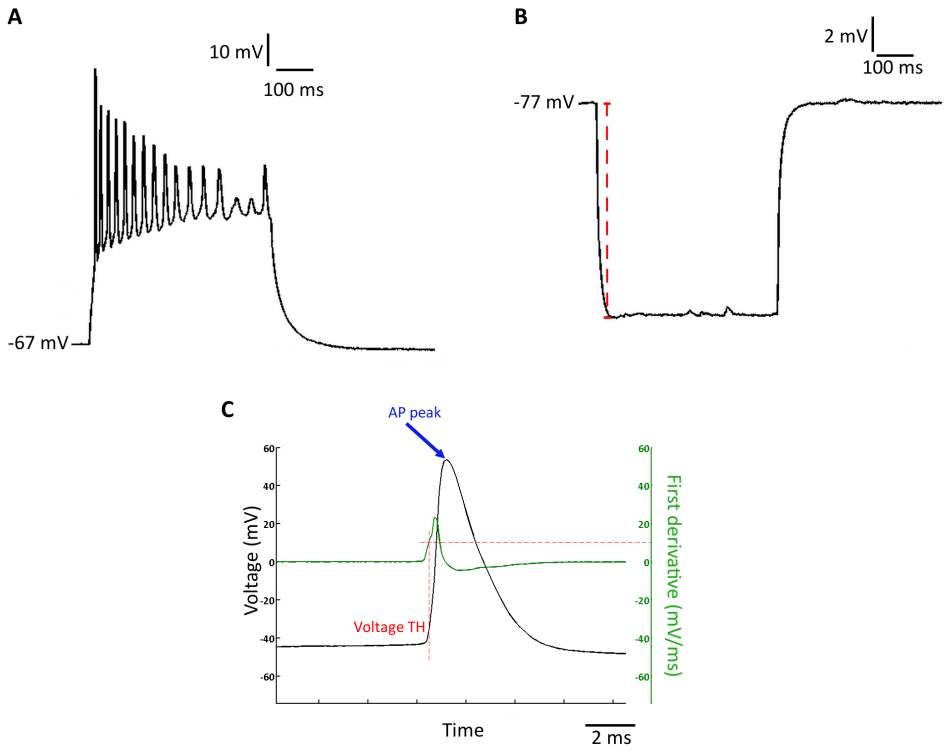

Figure 2.5 Electrophysiology methods.

A, Example trace demonstrating channel inactivation. **B,** Voltage response trace from a -100 pA current injection used to calculate passive membrane properties. Red dashed line indicates the voltage response measured that is used to calculate input resistance using formula F3. **C,** Action potential trace (black) overlaid with dV/dt trace (green), showing how action potential voltage threshold is determined. Horizontal red dashed line indicates where dV/dt reaches 10 V/s and vertical dashed red line indicates the point on the raw AP trace where this voltage potential change is reached. Action potential height was calculated as the difference between this point and the peak of the AP (blue arrow).

taking the voltage (V) as the maximum voltage deflection produced from the -100 pA current injection (I) (Fig. 2.5b). Membrane time constants were obtained using MiniAnalysis, taking the 10-90 slope value produced from the maximal voltage deflection of the same -100 pA current injection trace. Cell capacitance was calculated by the formula in F4, using the above two variables.

(F4): Capacitance = Membrane time constant / Input resistance

All measures were calculated using variables in standard unit form and then subsequently converted into appropriate units.

Voltage AP threshold was defined as the voltage potential at which dV/dt exceeded 10 V/s. Action potential height was measured as the difference between action potential threshold and the maximal voltage potential reached at the peak of the action potential (Fig 2.5c).

In a subset of neurons, the above described experiments were carried out in the presence of synaptic blockers: APV (25 μM), CNQX (20 μM), Gabazine (10 mM). This was to check for the true intrinsic nature of the observed excitability plasticity.

Ih currents were estimated using negative current injections (-100pA, 500 ms) and calculated as the difference between the maximum deflection immediately following stimulus onset (within 100ms) and the steady state voltage potential reach by the end of the stimulus. For AP waveform analysis, first and second derivatives of traces were calculated in Matlab (Mathworks), using the built-in 'diff' function. A custom-written script was used to identify axonal and somatic peaks in these traces. This script searched a 300 ms window in the first or second derivative trace, around where an AP was fired in the raw trace, and picked out the number and size of any peaks that were 50 % greater than the mean noise of baseline trace (Fig. 2.6).

Latency was calculated as the time between stimulus onset and the point when AP threshold was reached (Fig. 2.7a). Jitter was calculated as the standard

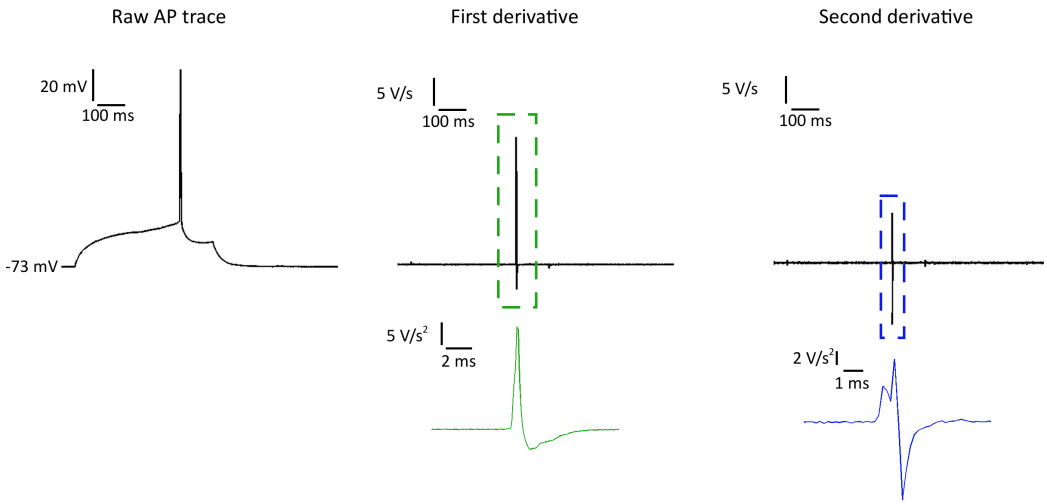

Figure 2.6 Action potential waveform analysis.

A raw action potential trace (left) and its resulting first (centre) and second (right) derivative traces, used to examine action potential waveforms. A script that searched the first and second derivative traces for peaks exceeding 1.5x the average baseline value was used to identify the axonal and somatic components of the AP trace. In most cases the first derivative trace resulted in a single peak (zoom shown in green). However, taking the second derivative resulted in many cases in the observation of two distinct peaks (zoom shown in blue), corresponding to the axonal (first peak) and somatic (second peak) components of the AP.

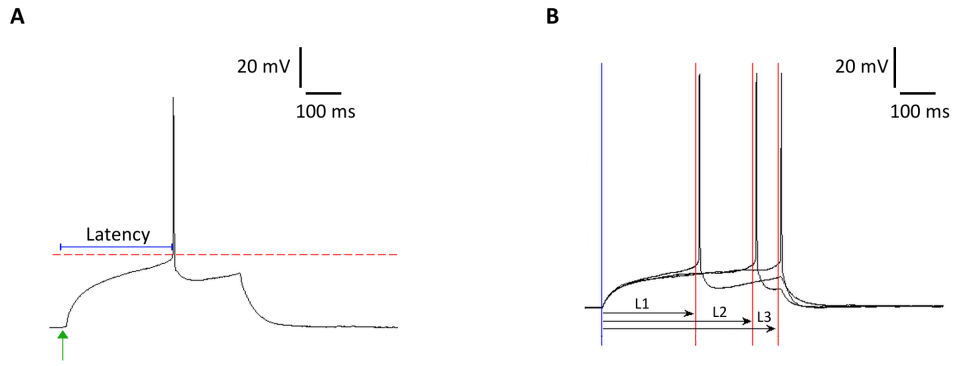

Figure 2.7 Measuring latency and jitter.

A, AP trace demonstrating how latency is measured. Green arrow indicates stimulus onset, red dashed line indicates AP threshold. Latency, indicated by blue line, is taken as the time between stimulus onset and AP threshold. **B,** Three single AP traces from the same neuron, demonstrating how jitter is measured. The amplitude of the current injection is the same for the three AP traces. Blue line indicates stimulus onset and red lines indicate AP threshold in each trace. The latency is calculated for each trace (indicated by arrows, L1, L2 and L3). Jitter is then calculated as the standard deviation of the three latency values.

deviation of multiple latency values at the same magnitude of current injection (Fig 2.7b). Latency and jitter was calculated using single AP (rheobase) traces. In a subset of cells, ten trials of 500ms current injections were made between 100 and 200pA, in 10pA steps. These ten trials were used to calculate latency and jitter at different current injection values. In these instances where a train of APs may be evoked, latency and jitter was calculated using only the first AP in a train.

Recording mini postsynaptic currents (mPSCs)

mPSCs were recorded in voltage-clamp, at -65mV holding potential, in the presence of TTX (1 μM). mPSC recordings were filtered at 3kHz and digitized at 20kHz. mPSC traces were analysed blind to experimental condition using MiniAnalysis (Synaptosoft).

Statistics

All statistical tests were carried out in SigmaPlot v.12 (Systat Software Inc.) or Matlab (Mathworks). Comparisons were made using parametric (t-test, ANOVA with Bonferroni post-hoc test, unless otherwise stated) or non-parametric (Mann-Whitney rank sum, Kruskal-Wallis ANOVA on ranks) as appropriate. To determine which test should be used a Kolmogorov-Smirnov test was run to check for normality. If data failed the normality test, data was first transformed (by taking the reciprocal) and retested for normality. If the transformed data was now normally distributed parametric tests were run using the transformed data. If following transformation, data still did not show normality non-parametric test were run on the raw, non-transformed data. Correlations coefficients were calculated with a Pearson Product Moment correlation if both variables' data passed the normality test, or Spearman's rank correlation if data from one or both variables failed the normality test. For all tests significance levels (α) were set to 0.05, except where a Bonferroni correction was carried out for multiple comparisons. In this case α was determined through dividing 0.05 by the total number of possible comparisons (stated where performed).

Chapter 3: Intrinsic plasticity in layer 2/3 pyramidal neurons of the mouse visual cortex following monocular enucleation

Introduction

Homeostatic plasticity research in the rodent visual system has revealed that several of the key mechanisms thought to prevent large perturbations in activity are employed in the visual cortex in response to altered activity input. The exact response is highly dependent on layer, activity manipulation, and age of the animal. For example, Desai et al., (2002) show that layer 4 pyramidal neurons were able to undergo synaptic scaling if activity deprivation occurred at two weeks post birth, but not at three weeks post birth. In contrast, they found that these effects were delayed in layer 2/3 where activity deprivation caused synaptic scaling if it was carried out at three weeks, but not two weeks, post birth. Similarly, intrinsic plasticity has been reported in layer 2/3 neurons of juvenile rats undergoing activity deprivation via eyelid suture (Maffei and Turrigiano, 2008), but following monocular enucleation in the adult mice, no change in intrinsic excitability of layer 2/3 neurons is observed (Barnes et al., 2015a). Instead, in the adult animal there is a shift in the E/I balance occurring alongside local subnetwork interactions. Thus, both synaptic and intrinsic forms of plasticity are undergone by neurons in the visual cortex following reductions in activity.

One form of plasticity that has yet to be explored in the visual cortex is AIS plasticity, a recently proposed structural correlate of excitability. This comparably new form of plasticity was observed simultaneously and independently in rodent hippocampal cultures and the chick auditory cortex, following elevated activity and activity deprivation, respectively (Grubb and Burrone, 2010; Kuba et al., 2010). Since these first reports there have been only a handful of subsequent reports demonstrating activity-dependent plasticity of the AIS in the cortex (Baalman et al., 2013), hippocampus (Baalman et al., 2013;

Harty et al., 2013) and olfactory bulb (Chand et al., 2015). However, with the exception of one study investigating the development of the AIS (Gutzmann et al., 2014) there has been no exploration of AIS plasticity in the visual cortex following activity manipulations. Given that intrinsic plasticity has been reported to occur in the visual cortex following activity deprivation, it is reasonable to expect that there might also be AIS plasticity present too. Thus, in this chapter I shall determine whether pyramidal neurons in layer 2/3 of the monocular visual cortex undergo AIS plasticity following monocular enucleation. I shall also measure the excitability of these neurons to examine how any potential AIS plasticity might be reflected in the functional output of the neurons.

Results

Layer 2/3 pyramidal neurons shorten their AIS following sensory deprivation

Coronal slices containing the monocular visual cortex were taken from juvenile mice sacrificed at 24, 48 or 72 hours after monocular enucleation (or control anaesthesia). Slices were stained for the AnkG and NF-H to label the AIS and neuronal cytoskeleton respectively, and AISs from layer 2/3 pyramidal neurons were measured. All controls were age-matched, and, although at 72 hours the mean AIS start position was more proximal to the soma compared to the previous two time points, this did not cause a significant change in length (Fig. 3.1). However, to ensure age-variability did not affect results, all deprived time points were compared to their age-matched controls. At 24 hours post deprivation mean AIS length was not different from control. However, at 48 and 72 hours post deprivation, AIS measurements from slices of deprived animals were now significantly shorter than their age-matched controls (Fig. 3.2). The starting location of the AIS in relation to the soma was not significantly different at any time point, suggesting that the decrease in length is occurring at the distal end of the AIS. Thus, layer 2/3 neurons in the visual cortex do show AIS plasticity, in the form of a change in length, following monocular enucleation.

Following deprivation Layer 2/3 pyramidal neurons are more excitable

To see if the observed decrease in AIS length had any functional consequences for the neurons, I performed whole-cell patch clamp recordings from layer 2/3 pyramidal neurons in the monocular visual cortex. I chose to focus on the first time point at which the length change became significant, thus, the following recordings were performed at 48 hours post deprivation in either enucleated or age- and anaesthetic-matched control animals. Previously, AIS plasticity has been shown to occur alongside changes to the intrinsic excitability of neurons (Grubb and Burrone, 2010; Kuba et al., 2010). I therefore performed current-clamp recordings to determine the action potential threshold and input-output function of neurons in control and deprived conditions.

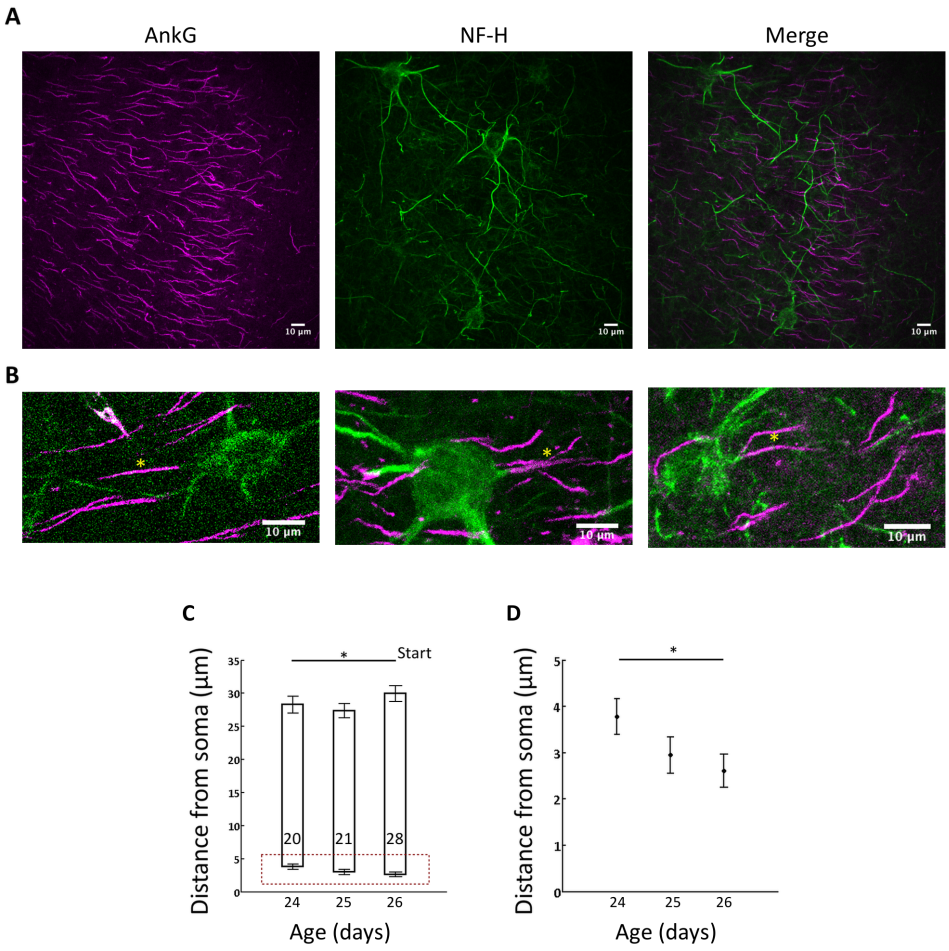

Figure 3.1 AIS position but not length varies across developmental age window.

A, Example image of a region of the monocular visual cortex in a coronal slice stained for AnkG (magenta, left) and NF-H (green, centre). On the right the merge of the two channels is shown. **B,** example images of three neurons from the different control time points, and their AISs, indicated by yellow asterisks. **C,** AIS length and position in control groups at three different ages following control anaesthesia. Bottom and top edges of bar indicate mean start and end position respectively, in relation to the cell soma. The number of AISs measured is indicated within the bar. Mean length: p24, 24.5 ± 1.5 µm; p25, 24.4 ± 1.2 µm; p26, 27.3 ± 1.1 µm, p = 0.142, one way ANOVA. **D,** Enlargement of area in dotted box of (**a**) showing start position of AIS across the three time points. Mean start position: p24, 3.8 ± 0.4 µm; p25, 3.0 ± 0.4 µm; p26, 2.6 ± 0.4 µm, p = 0.032, Kruskal-Wallis one way ANOVA with Dunn's post hoc test. *p < 0.05. Error bars indicate s.e.m.

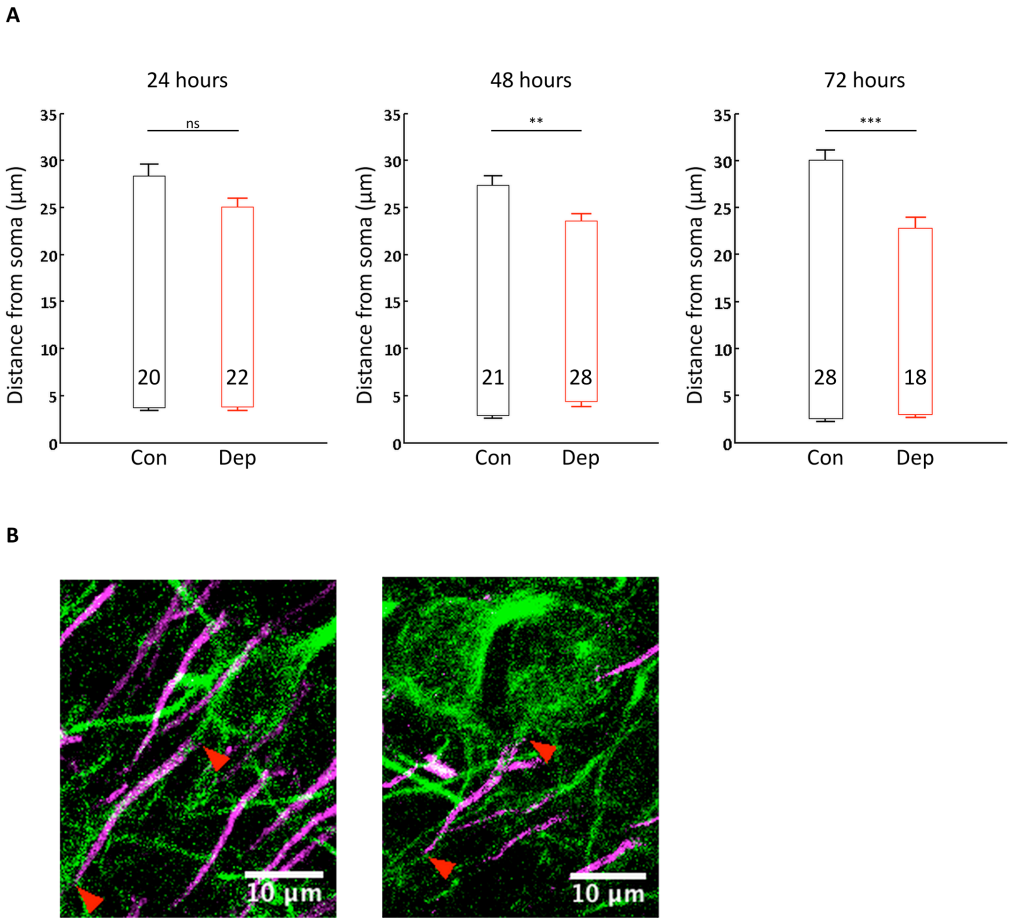

Figure 3.2 AIS length decreases following activity deprivation.

A, AIS length and position in control (black) and deprived (red) at 24, 48 and 72 hours post deprivation. Bottom and top edges of bars indicate mean start and end position respectively, with length of bar representing mean length. Numbers within bars indicates the number of AISs measured. Mean start positions: (24 hr) control, 3.8 ± 0.4 µm; deprived, 3.9 ± 0.5 µm, $p = 0.999$, (48 hr) control, 3.0 ± 0.4 µm; deprived, 4.4 ± 0.6 µm, $p = 0.05$, (72 hr) control, 2.6 ± 0.4 µm; deprived, 3.0 ± 0.3 µm, $p = 0.159$. Mean length: (24 hr) control, 24.5 ± 1.5 µm; deprived, 21.1 ± 0.8 µm, $p = 0.072$, (48 hr) control, 24.4 ± 1.2 µm; deprived, 19.1 ± 0.7 µm, $p = 0.001$, (72 hr) control, 27.3 ± 1.1 µm; deprived, 19.7 ± 1.1 µm, $p < 0.001$. **B,** Example of a control (left) and deprived (right) neuron, labelled with SMI-32 in green, and AnkG in magenta. Red arrows indicate start and end of AIS. **$p < 0.01$, ***$p < 0.001$. ns, not significant. Error bars indicate s.e.m.

To measure these, somatic current injections (500ms) were applied to neurons and the resulting voltage responses recorded. First, to determine the rheobase, or current action potential threshold, i.e. amount of current needed to elicit a single action potential, current pulses were slowly increased in amplitude until the cell fired a single action potential. Following this, current pulses of increasing 10pA steps were applied, until 200pA or saturation was reached. The number of spikes fired at each current step were then counted and used to plot input-output (I/O) functions for individual neurons. To get an overall I/O function for each condition, the mean number of APs fired across all cells from either the control or deprived condition was calculated for each current step. To compare the two conditions, the individual I/O function of each neuron was fitted with a line in the linear portion of the curve, and the equation of this line used to calculate a slope and intercept value for each cell. These values were then compared across control and deprived animals.

In contrast to what might be expected given a decrease in AIS length, neurons in the deprived condition exhibited an increase in excitability demonstrated through a reduction in rheobase value and an upwards shift in the I/O function (Fig. 3.3a-c). Thus, deprived neurons needed less current to elicit an AP, and at a given current injection would fire more APs than control cells. These neurons also tended to have higher input resistance, though the two groups were not significantly different from each other (Fig. 3.3d). However, when looking at the relationship between rheobase and input resistance there was a strong inverse relationship between the two factors (Fig. 3.3e). This is expected, since input resistance is defined as the voltage change produced by a current injection, divided by the amount of current injection. Therefore, the greater the voltage change across a membrane, the more excitable the cell, and thus, lower the rheobase will be. No difference was seen in any other passive membrane property (Table 3.1). Despite the observed increase in excitability there was no difference in action potential voltage threshold (measured by the voltage at which dV/dt first passed 10V/S), and only a trend towards decreased current density in deprived neurons was observed (Fig. 3.3f-g). The current density measure describes how much current is needed per unit area of cell to excite the

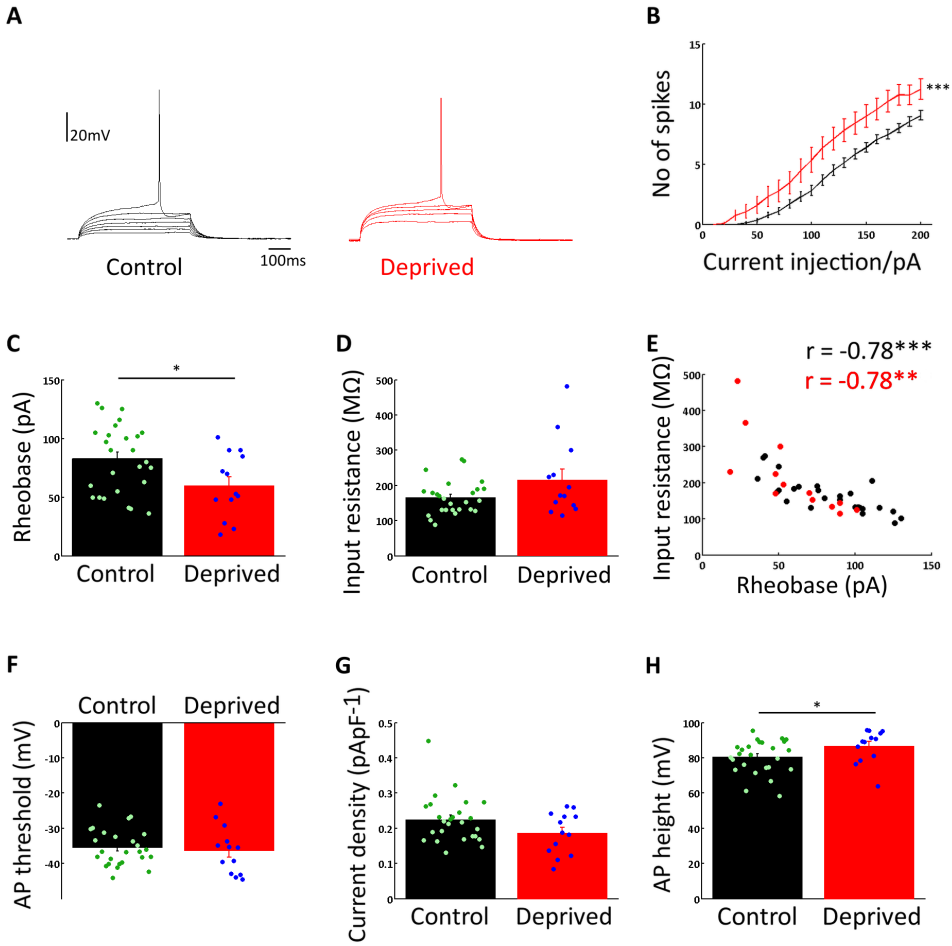

Figure 3.3 Layer 2/3 pyramidal neurons are more excitable after activity deprivation.

A, Example traces of voltage deflections following somatic current injection (0-50 pA) in a control (black) and deprived (red) neuron. **B,** Input-output function: current injection and mean number of resultant spikes for control (black) and deprived (red) neurons. Mann-Whitney rank sum on gradient values ($p = 0.014$) and t-test on y-intercept values ($p < 0.001$) of slopes fitted to the linear portion of individual control and deprived neurons I/O function. **C,** Rheobase – injected current (in pA) needed to elicit a single action potential in control (black), and deprived (red) neurons. Mean rheobase in control, 83 ± 6 pA, and deprived, 60 ± 8 pA; $p = 0.024$, t-test. **D,** Mean input resistance in control, 166 ± 9 MΩ, and deprived, 216 ± 30 MΩ; $p = 0.211$, Mann-Whitney rank sum. **E,** Scatter plot of

rheobase against input resistance showing the inverse relationship between the two factors in both control (black; r = -0.78, p < 0.001) and deprived (red; r = -0.78, p = 0.002) neurons; rho and p values were calculated using Pearson's Product Moment Correlation **F,** Mean action potential voltage threshold in control, -35 ± 1 mV, and deprived, -36 ± 2 mV; p = 0.682, t-test. **G,** Mean current density in control, 0.22 ± 0.03 pA/pF, and deprived, 0.19 ± 0.04 pA/pF; p = 0.185, Mann-Whitney rank sum. **H,** Mean action potential height in control, 81 ± 2 mV, and deprived, 87 ± 3 mV; p = 0.029, Mann-Whitney rank sum. All bar plots show mean ± s.e.m., with green and blue points representing individual cell values for control and deprived neurons respectively. N = 26 control cells and 13 deprived cells. *p < 0.05, ***p < 0.001.

Table 3.1 Deprivation does not alter resting membrane potential properties

	Control (n = 26)	Deprived (n = 13)	P-value
Vm (mV)	-72 (-75– -68)	-71 (-72 – -67)	0.309
Membrane time constant (ms)	57 (49 – 70)	55 (49 – 74)	0.818
Membrane capacitance (pF)	376 ± 23	324 ± 31	0.200

Reported values are median with interquartile range in parentheses where a Mann-Whitney Ranksum Test was used to compare groups, and mean ± s.e.m. where a t-test was used for comparisons.

cell. Thus, while not significant, the current density trends in a direction that is consistent with the change in rheobase and I/O function. Maximum firing frequency was measured in current clamp by applying a prolonged (10 sec) injection of current to maintain a holding potential close to AP voltage threshold. This was tested at three different holding potentials (-40, -35 and -30 mV) and repeated 10 times per cell at each holding potential. A mean firing frequency for each cell at the three holding potentials was then calculated (Fig. 3.4a,b). Firing frequency was consistently higher in deprived neurons than control, at each holding potential. Thus, these results agree with previous studies reporting an increase in intrinsic excitability following deprivation (Desai et al., 1999; Maffei and Turrigiano, 2008; O'Leary et al., 2010). However, combining these functional results with the earlier structural findings this now conflicts with previous evidence that reduced AIS length should result in a reduced firing frequency (Kuba et al., 2010). The above recordings were carried out in conditions where synaptic activity was freely able to take place, and thus, it is possible that there could be an interaction from any arising synaptic activity that may mask changes to excitability that a shortened AIS might cause. To test this, experiments were next performed in the presence of drugs to block synaptic activity.

Increase in excitability following deprivation is not synaptically mediated

To examine whether the increase in excitability might be mediated by synaptic activity, I repeated the same measures of excitability in a separate set of control and deprived neurons, this time in the presence of antagonists for both excitatory (CNQX and APV) and inhibitory (gabazine) synapses, thus blocking any potentially synaptically mediated mechanism. Here I find that, as before, the I/O function is again shifted so that deprived neurons produce more spikes at a given current injection (Fig. 3.5a). Furthermore, rheobase values are reduced in deprived neurons, compared to control (Fig. 3.5b). Similarly to what was seen in the absence of synaptic antagonists, there is no statistical difference between input resistance or current density in control and deprived neurons; however, there is a trend towards decrease current density values in deprived animals,

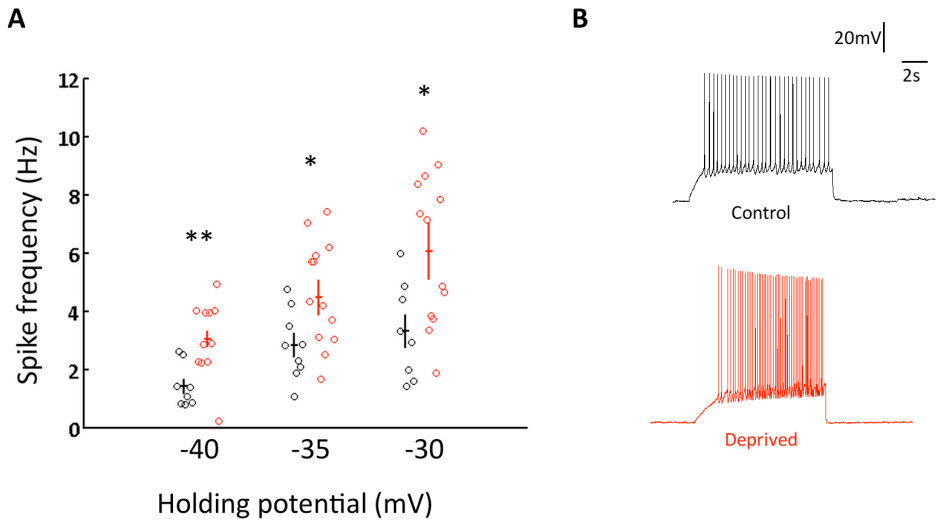

Figure 3.4 Maximum AP frequency is increased following deprivation.

A, Maximum AP frequency at three different holding potentials. Each point represents one control (black) or deprived (red) cell, with mean ± s.e.m. error bars for overall control and deprived conditions in bold. Mean AP frequencies: (-40 mv) control, 1.4 ± 0.3 Hz; deprived, 3.1 ± 0.4 Hz; p = 0.006, t-test; (-35 mv) control, 2.8 ± 0.4 Hz; deprived, 4.7 ± 0.5 Hz; p = 0.015, t-test (-30 mV) control, 3.3 ± 0.6 Hz; deprived, 6.2 ± 0.7 Hz; p = 0.011, t-test. **B,** Example traces of control (top, black) and deprived (bottom, red) voltage responses when current was injected to maintain a holding potential of -40 mV. *p < 0.05, **p < 0.01.

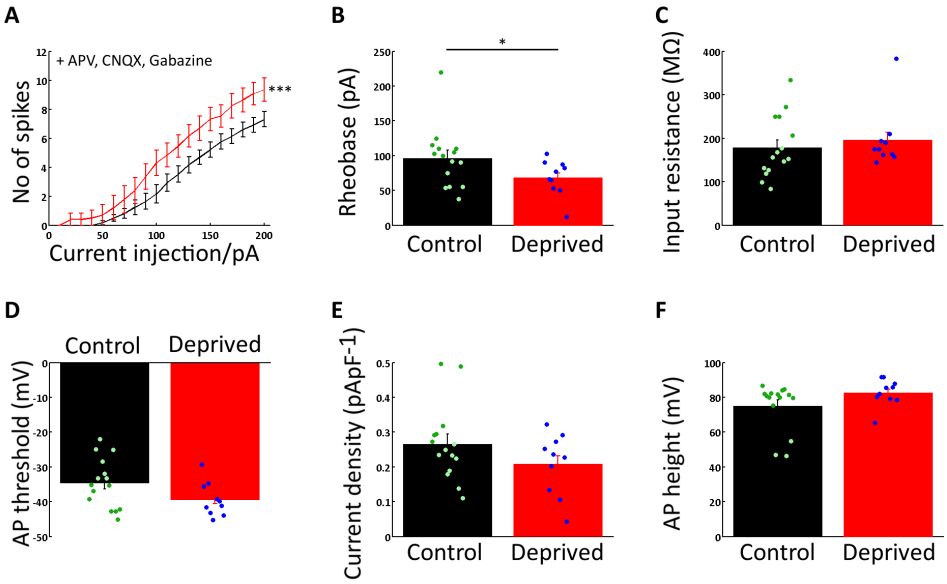

Figure 3.5 Increased excitability after deprivation is not synaptically mediated.

A, Input-output function: injected current and resultant mean (± s.e.m.) number of action potentials for control (black) and deprived (red); t-test on gradient values of individual control and deprived neurons' slopes ($p = 0.320$) and y-intercept ($p < 0.001$). **B,** Mean rheobase in control, 96 ± 11 pA, and deprived, 69 ± 8 pA; $p = 0.049$, Mann-Whitney rank sum. **C,** Mean input resistance in control, 178 ± 18 MΩ, and deprived, 195 ± 22 MΩ; $p = 0.332$, Mann-Whitney rank sum. **D,** Mean action potential threshold in control, -35 ± 2 mV, and deprived, -39 ± 2 mV; $p = 0.076$, t-test. **E,** Mean current density in control, 0.27 ± 0.03 pA/pF, and deprived, 0.21 ± 0.03 pA/pF; $p = 0.180$, t-test. **F,** Mean action potential height in control, 75 ± 4 mV, and deprived, 83 ± 2 mV; $p = 0.157$, Mann-Whitney rank sum. Error bars indicate s.e.m. N = 15 control cells and 10 deprived cells. *$p < 0.05$, ***$p < 0.001$.

further suggesting that these cells are more excitable (Fig. 3.5c,e). Additionally, there is no difference between AP threshold in control and deprived neurons (Fig. 3.5d). Action potential height, which was increased after deprivation when synaptic transmission was not antagonised, is now not different in control and deprived conditions (Fig. 3.5f). Thus, while there are some minor differences (no change in AP height) between these results and the previous findings measured without synaptic antagonists, the overall outcome reflects the same conclusion – following deprivation, neurons have increased excitability. These results indicate that this increase in excitability following deprivation is intrinsic and is not caused by a synaptic effect.

Decrease in AIS length is not associated with changes to spike waveform

Thus far, the structural data showing a decrease in AIS length and the functional data revealing an increase in excitability are not consistent with the previous work on AIS plasticity. In the auditory cortex, a longer AIS is associated with an increase in excitability (Kuba et al., 2010). The present work in the visual cortex appears to be in contrast to these findings. However, there are more subtle features of neuronal excitability that may arise from AIS structural changes. The AIS is the initiation zone for APs (Kole et al., 2007, 2007; Palmer and Stuart, 2006), and examination of spike waveforms have shown features of the waveform that can be attributed to the axonal generation of spikes (Bean, 2007; Meeks and Mennerick, 2007). One way to examine the spike waveform of an AP is to make a phase-plane plot. Here, the time derivative (dV/dt), i.e. change in voltage across time, is plotted against voltage. This gives an informative visualisation of different components, or phases, of AP generation. In a phase plot, a commonly detected 'double hump' is thought to reflect the distinct axonal and somatic compartments of the AP generation (Bean, 2007; Fig. 3.6b). The first hump, occurring before the peak rate of rise, is thought to be attributable to axonal generation of the AP. The second hump, or peak of the phase plot reflects the somatic spike. Previous work has shown that application of TTX locally to the axon significantly reduces the first, axonal component of the waveform derivative (Meeks and Mennerick, 2007). Thus, I hypothesised that with a

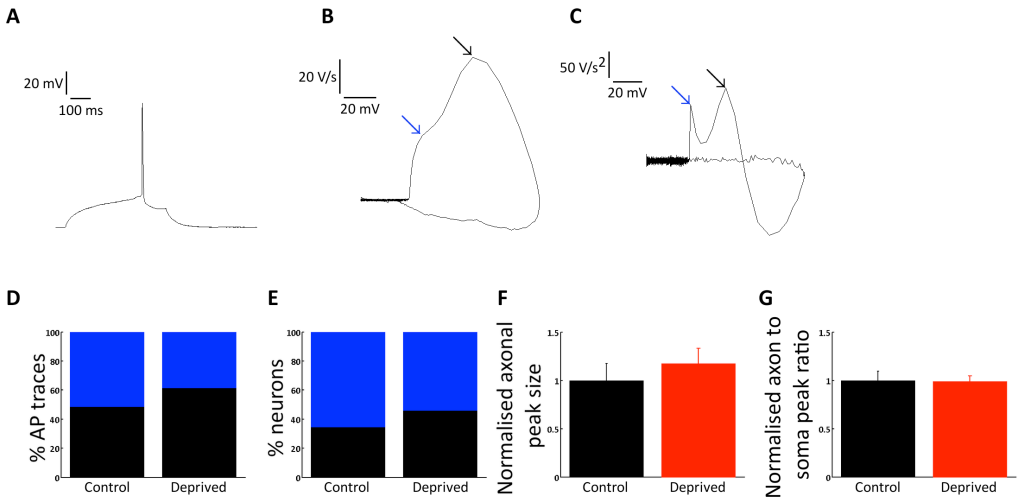

Figure 3.6 Deprivation does not alter the waveform of action potentials.

Example traces of **A,** A single action potential, **B,** The first derivative plotted against voltage (i.e. a phase-plane plot), and **C,** The second derivative plotted against voltage. Blue arrows indicate the axonal component of the waveforms and black arrows indicate the somatic component in the first and second derivative traces. **D,** Percentage of action potential traces that exhibit a single (black) or double (blue) peak in their second derivative trace. Percentages for control: 49 % single peak, 51 % double peak; deprived: 58% single peak, 42 % double peak; p = 0.266, Chi-square test; n = 78 control trials and 39 control trials. **E,** Percentage of neurons that exhibit no double peaks (black) or at least one double peak (blue) across three trials. Percentages for control: 35 % never exhibiting double peak, 65 % exhibiting double peak at least once; deprived: 46 % never exhibiting double peak, 54 % exhibiting at least one double peak; p = 0.727, Chi-square test; n = 26 control cells and 13 deprived cells. **F,** Size of axonal peak, normalised to mean of control values. Normalised mean in control, 1 ± 0.2; deprived, 1.2 ± 0.2; p = 0.260, Mann-Whitney rank sum. **G,** Ratio of axonal to somatic peak normalised to mean control value. Normalised mean in control, 1 ± 0.09; deprived, 1 ± 0.05; p = 0.925, t-test. Error bars indicate s.e.m.

shorter AIS, and, particularly with the shortening occurring at the distal end where the APs are thought to be generated, there may be detectable changes in the phase plots of APs from control and deprived neurons. Although I have no direct evidence for reduced sodium channel density following deprivation, it has been shown previously that changes to the AIS have occurred alongside changes to sodium channel density (Grubb and Burrone, 2010; Kuba et al., 2010). Thus, if the observed shortening of the AIS is accompanied by a reduction in sodium channels at this initial section of the axon then one might predict that the size of the first peak, the axonal component, would be reduced or even possibly absent. Upon examination of the first derivative phase plots of single APs, in both control and deprived conditions, very few neurons exhibited two peaks in their phase-plane plot. This lack of a double peak may be caused by the sampling rate of recordings not being sensitive enough to pick up the rapid change in voltage associated with the axonal component. One way to overcome this is to take the second derivative of the trace, thus, now looking at the acceleration rate of voltage change. By taking the second derivative of the action potential trace in the present data, double peaks were reliably detected in a sufficient number of traces for analysis (Fig. 3.6a-c). For each cell, three trials in which a single AP was elicited by somatic current injection were collected and analysed. In control neurons just under half of all APs (49%) showed a double peak in their second derivative trace. This was reduced to 42% in deprived neurons, though this result was not statistically significant (Fig. 3.6d). Additionally, the proportion of neurons that showed at least one second derivative trace containing a double peak, across the three trials was 65 % in control, and 54% in deprived conditions (Fig. 3.6e). However, again this result was not significant. The magnitude of the axonal peak was not different in control and deprived neurons (Fig. 3.6f). Additionally, the size of the axonal peak relative to the somatic peak did not differ between control and deprived conditions (Fig. 3.6g). Thus, there were no apparent differences in the waveforms of control and deprived neurons, suggesting that the sodium driving force is not different in the two conditions. This suggests that despite the observed shortening of the AIS, there are no functional indications that there has been a loss of sodium channels from this region.

Direct comparisons of AIS length and excitability

While the findings that neurons are more intrinsically excitable following deprivation agrees with several other studies in the literature (Desai et al., 1999; Maffei and Turrigiano, 2008; O'Leary et al., 2010), the original finding of a reduced AIS length is not consistent with this functional change in excitability given previous work (Grubb and Burrone, 2010; Kuba et al., 2010). Furthermore, examination of AP waveforms did not reveal any differences between the driving force of control and deprived neurons. In attempt to address this mismatch between structural and functional observations, I decided to look directly at AIS length and functional excitability measures in the same cell, by filling recorded neurons with a fluorescent dye (AF 488) and staining the slice to label for AnkG after recording. At the end of a recording experiment, the recording electrode was carefully removed and slices were fixed overnight in 1% PFA. The following day, slices were immunostained with an antibody against AnkG to label the AIS and subsequently imaged using the fluorescent dye to identify the functionally recorded cell (Fig. 3.7a). Each slice contained a single recorded cell. This approach allowed me to directly compare excitability recordings with the AIS length and position in an individual cell. I correlated AIS length with a number of excitability measures and passive membrane properties. Cells were recorded at 24, 48 and 72 hours post deprivation (or age-matched, anaesthetic control) but to achieve reasonable numbers of cells for correlations, data from these different time points were pooled together.

Under control conditions, I found no correlation between AIS length and any excitability measure, or membrane property (Fig. 3.7b-g). Equally, AIS position did not significantly correlate with any of the excitability or membrane property measures examined (Fig. 3.8a-f). Furthermore, following deprivation, there were also no significant correlations between either AIS length or position and any other measure of excitability or passive membrane property (Fig. 3.9a-f, Fig. 3.10a-f). In control animals, there was a weak negative correlation between AIS

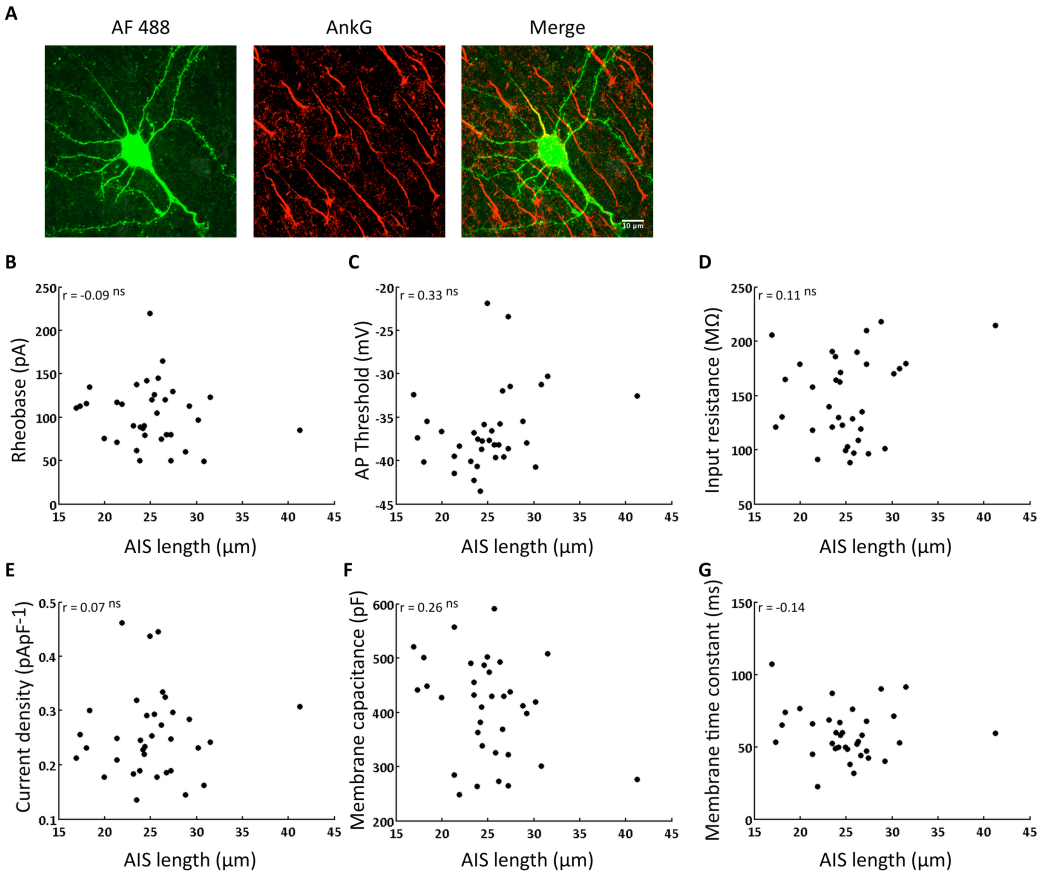

Figure 3.7 AIS length does not correlate with functional output measures or passive cell measures under control conditions.

A, Example of a neuron filled with AF 488 during recording and then post-hoc immunostained with antibodies against AnkG to label for the AIS. Left, AF 488 filled cell, centre, AnkG and right, merge. **B,** Scatter plot between AIS length and rheobase value, p = 0.623. **C,** Scatter plot of AIS length and voltage AP threshold, p = 0.053. **D,** Scatter plot of AIS length and input resistance, p = 0.541. **E,** Scatter plot of AIS length and current density, p = 0.677. **F,** Scatter plot of AIS length and membrane capacitance, p = 0.127. **G,** Scatter plot of AIS length and membrane time constant, p = 0.407. All rho and p values were calculated using Spearman's rank order correlation. Each point represents a single control neuron, n = 35 cells.

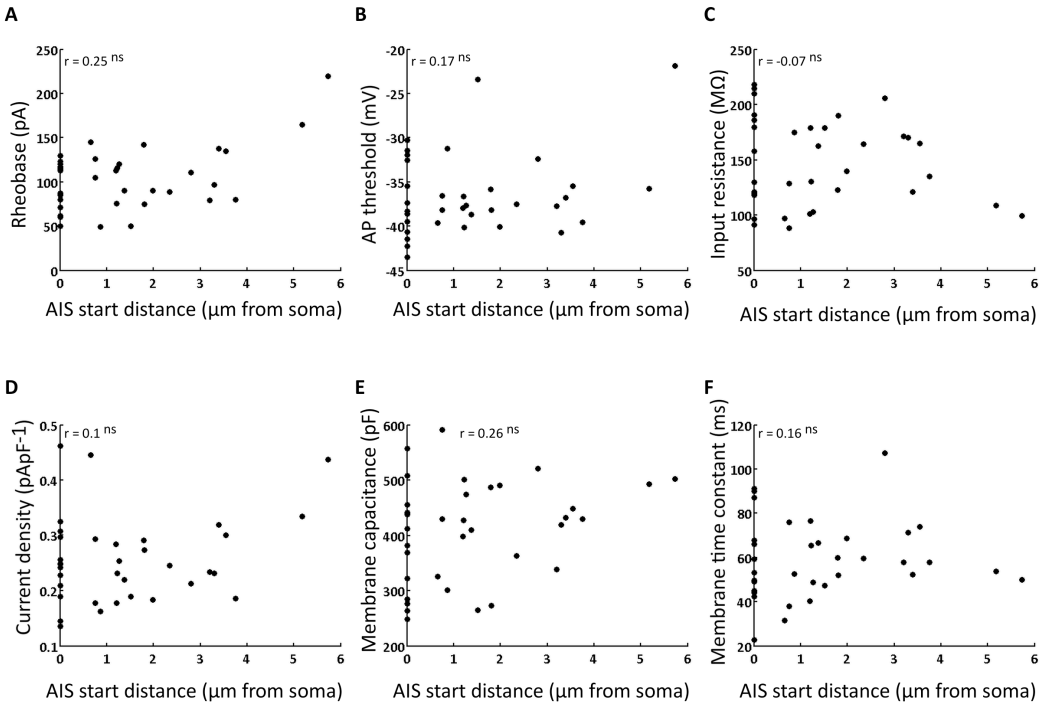

Figure 3.8 AIS position does not correlate with functional output measures or passive cell properties under control conditions.

A, Scatter plot of AIS position and rheobase value, p = 0.154. **B,** Scatter plot of AIS position and voltage AP threshold, p = 0.338. **C,** Scatter plot of AIS position and input resistance, p = 0.703. **D,** Scatter plot of AIS position and current density, p = 0.571. **E,** Scatter plot of AIS position and membrane capacitance, p = 0.127. **F,** Scatter plot of AIS position and membrane time constant, p = 0.398. All rho and p values were calculated using Spearman's rank order correlation.

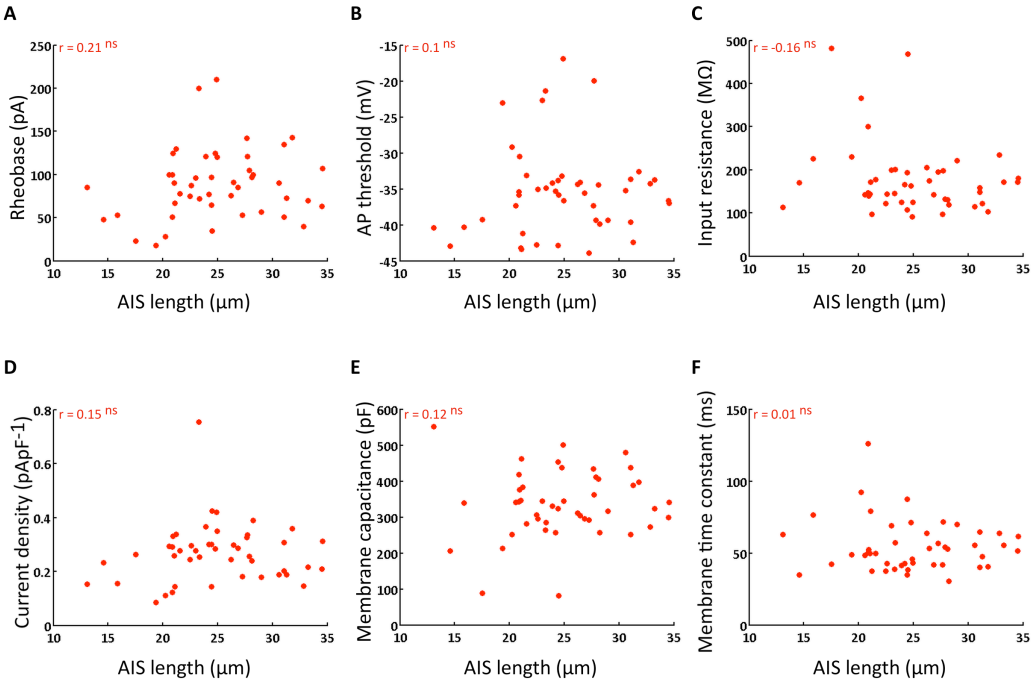

Figure 3.9 Following deprivation AIS length does not correlate with functional output measures or passive cell properties.

A, Scatter plot of AIS length and rheobase value, p = 0.162. **B,** Scatter plot of AIS length and voltage AP threshold, p = 0.507. **C,** Scatter plot of AIS length and input resistance, p = 0.281. **D,** Scatter plot of AIS length and current density, p = 0.316. **E,** Scatter plot of AIS length and membrane capacitance, p = 0.435. **F,** Scatter plot of AIS length and membrane time constant, p = 0.936. Each red point represents a single neuron after deprivation, n = 46 cells. All rho and p values were calculated using Spearman's rank order correlation.

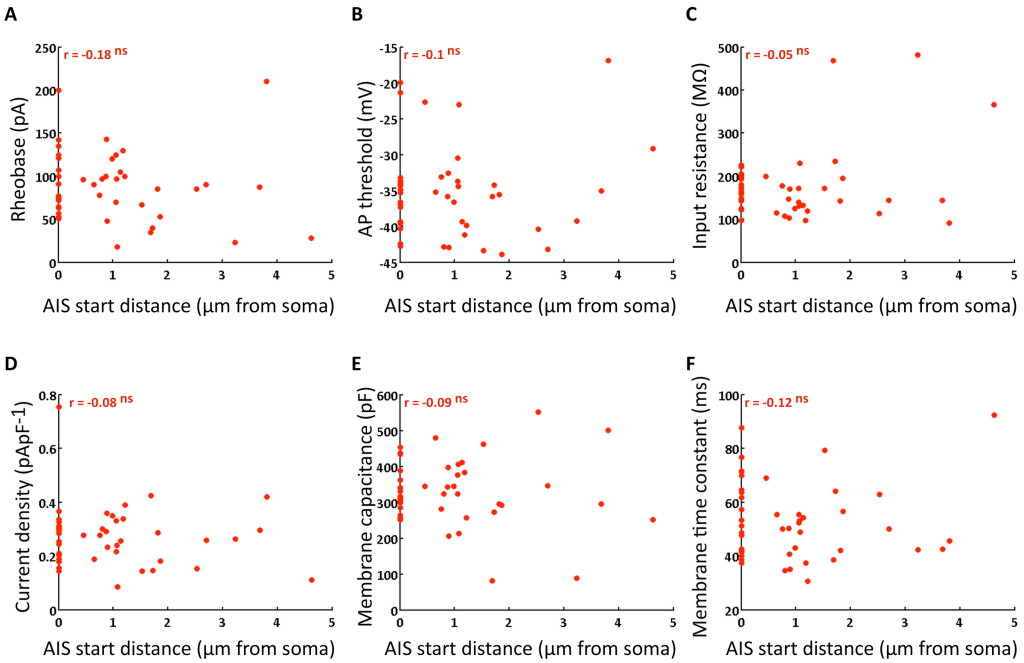

Figure 3.10 AIS position does not correlation with functional output measures or passive cell properties following deprivation.

A, Scatter plot of AIS position and rheobase value, p = 0.238. **B,** Scatter plot of AIS position and voltage AP threshold, p = 0.518. **C,** Scatter plot of AIS position and input resistance, p = 0.748. **D,** Scatter plot of AIS position and current density, p = 0.611. **E,** Scatter plot of AIS position and membrane capacitance, p = 0.564. **F,** Scatter plot of AIS position and membrane time constant, p = 0.450. All rho and p values were calculated using Spearman's rank order correlation.

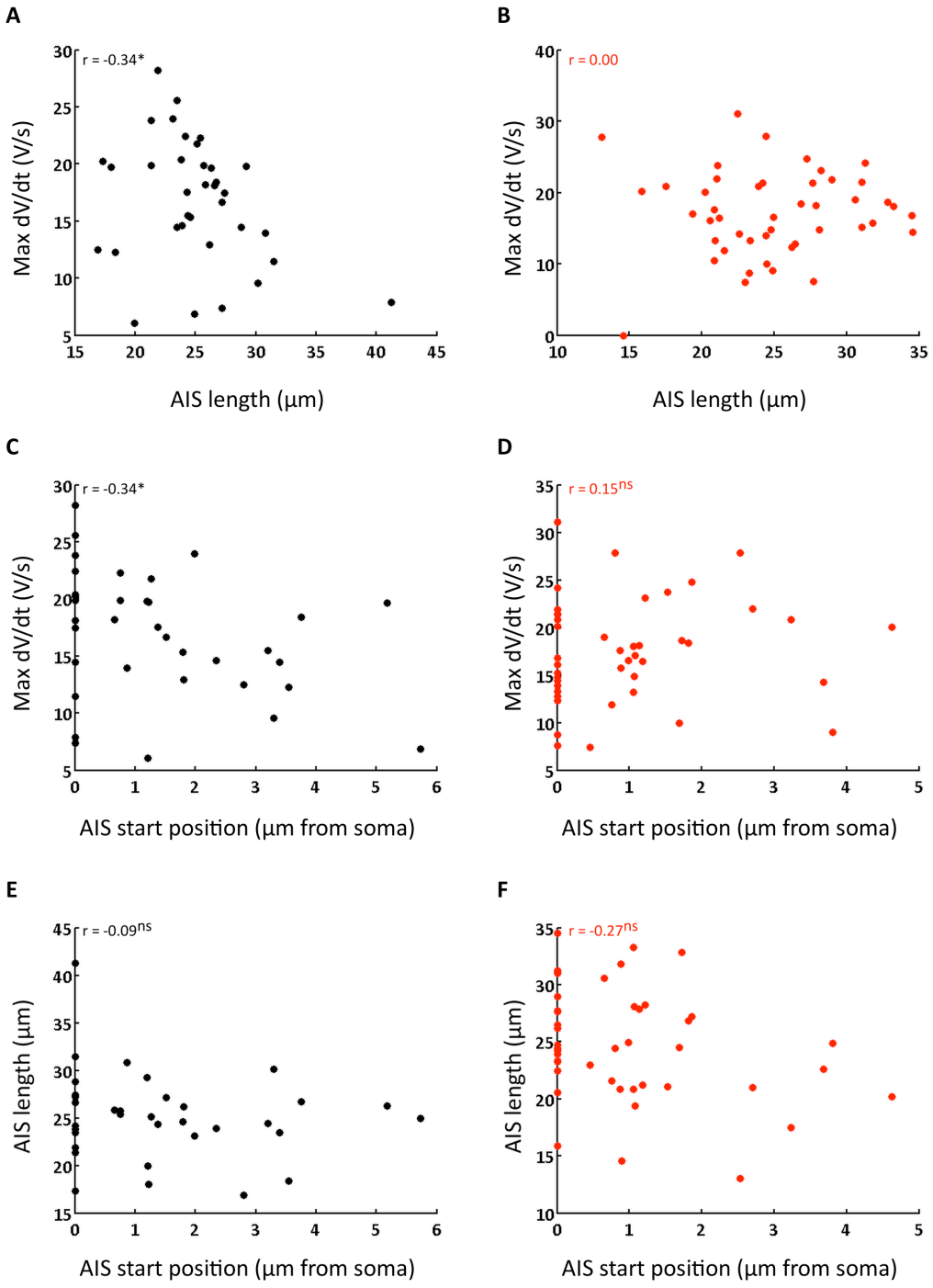

Figure 3.11 AIS length does not correlate with position.

A, Scatter plot of AIS length and maximum differential in control, p = 0.0487. **B,** Scatter of AIS length and maximum differential in deprived, p = 0.983. **C,** Scatter plot of AIS position and maximum differential in control, p = 0.0482. **D,** Scatter

plot of AIS position and maximum differential in deprived, p = 0.344. **E,** Scatter plot of AIS length and AIS position in control, p = 0.622. **F,** Scatter plot of AIS length and position in deprived, p = 0.077. All rho and p values were calculated using a Spearman's rank order correlation.

length and the maximum differential (Fig. 3.11a), suggesting counter-intuitively that cells with a shorter AIS have a faster rate of depolarisation. However, counteracting this correlation was another weak correlation between AIS position and maximum differential (Fig. 3.11c), such that a more proximal AIS would result in a higher rate of depolarisation. These weak correlations were not observed in deprived animals (Fig. 3.11b,d). There was no correlation between AIS length and AIS position in either control (Fig. 3.11e) or deprived conditions (Fig. 3.11f). Thus, in the present preparation AIS length and position does not correlate with either neuronal membrane properties, or intrinsic excitability measures in layer 2/3 pyramidal neurons.

Potential causes for increased excitability following deprivation

Since synaptic modifications have been ruled out in playing a part in the increased intrinsic excitability, and AIS measurements are not consistent with the measured excitability changes, this means there must be an alternate mechanism that is causing increased output of neurons following deprivation. Thus, using the excitability data already collected and described I looked for indications of what might be causing the increase in excitability following deprivation. Increases in excitability have previously been shown to be caused by altered regulation of potassium channels (Breton and Stuart, 2009; Jung and Hoffman, 2009). Since potassium channels are known to be involved in both the after hyperpolarisation (AHP) and hyperpolarisation-activated currents (Ih), I looked for differences in either of these properties in the data from control and deprived neurons. I found no difference in AHP measured from single action potential traces (Fig. 3.12a,b), or, in the amplitude of Ih currents measured from hyperpolarising somatic current injections (Fig. 3.12c,d). Though no difference was seen here, this does not rule out the possibility of potassium channels being involved in the increased excitability observed following deprivation. In these experiments I have only examined the fast AHP, while K^+ channels are also linked to the medium and slow AHPs, and additionally calcium channels mediating the after-depolarisation (ADP) may be altered by activity deprivation.

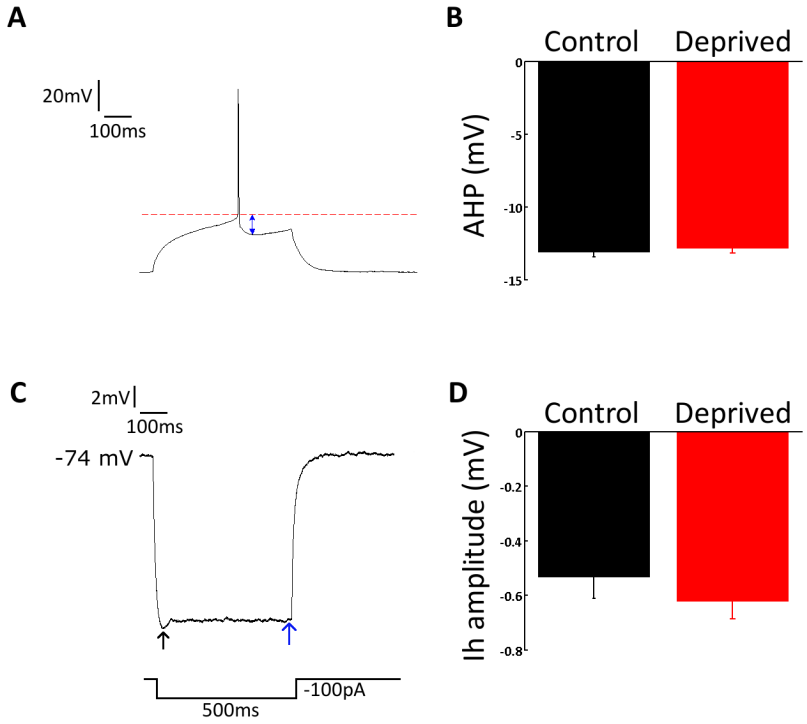

Figure 3.12 Deprivation does not alter the AHP or Ih.

A, AHP was measured in single AP traces by calculating the difference between AP threshold, indicated by dashed red line, and minimum voltage immediately following AP peak. Blue arrowhead indicates AHP. **B,** AHP did not differ between control and deprived neurons. Mean AHP in control, -13 ± 2 mV, and deprived, -13 ± 2 mV; p = 0.629, t-test. **C,** Ih amplitude was measured by taking the difference between the minimum voltage recorded directly after a hyperpolarising pulse was delivered (black arrow) and the steady state voltage reached before the offset of the pulse (blue arrow). Top, example trace of hyperpolarising current injected at the soma; bottom, schematic of current injection. Mean Ih amplitude in control, -0.5 ± 0.1 mV, and deprived, -0.6 ± 0.1 mV; p = 0.318, Mann-Whitney rank sum. Error bars indicate s.e.m.

Deprivation does not affect timing or precision of spiking in layer 2/3

In the cortex, the timing of spikes is an important aspect of synaptic transmission. Spike timing dependent plasticity occurs across many connections in the cortex, and as its name suggests, is heavily dependent on the precise timing of pre- and postsynaptic cell spikes. Changes in latency and precision of spiking have been shown to occur during reorganisation in the cortex (Barnes et al., 2015b). Thus, I hypothesised that given that the AIS is the site of spike initiation perhaps changes to the AIS following deprivation cause alterations to the timing or precision of AP firing. Therefore, I looked at the latency and jitter of APs in control and deprived conditions to see if this was altered by deprivation. Latency was defined as the time between stimulus onset and AP threshold being reached. I first examined the latency of APs in trials where single action potentials were elicited. Here I found no difference in latency between control and deprived conditions (Fig. 3.13a,b). I next looked at latency across a range (100-200pA) of current injections to determine if this may better resolve any differences in spike timing. Here, latency was defined as the time between the start of the current pulse and onset of the first action potential of a train. A clear relationship between current injection and latency can be seen (Fig. 3.13d), such that latency decreases with larger current injections. This relationship was observed in both control and deprived conditions. Thus, I examined latency values at two specific current injections, one where minimal current was injected to elicit APs in a sufficient number of cells (100 pA) and one where cells had reached almost maximum firing rate (200 pA). At both current injections, no difference in latency values was observed between control and deprived neurons (Fig. 3.13c). Thus, deprivation does not appear to affect the onset timing of APs.

I next examined whether the precision of spike timing was affected by activity deprivation. I first examined the jitter in single AP trials (3 trials per cell) and found that although this was increased in deprived neurons, this increase was not significant (Fig. 3.14a,b). I next looked at jitter across different current injections to again to see if this might reveal more conclusive evidence of

increased jitter. In a subset of cells, I recorded ten trials of increasing steps of somatic current injection. I examined jitter in the first spike of each train at these different current injections. Again, as with latency, jitter was reduced as a function of current injection (Fig. 3.14c). Thus, I again compared jitter values at two different current injections, one high and one low. Converse to the trend observed in single AP trials, at both the low and high current step jitter tended to be lower in deprived cells compared to control. However, there was considerable variability within the control group and these trends were not statistically significant. Therefore, deprivation does not appear to alter the precision timing of APs either.

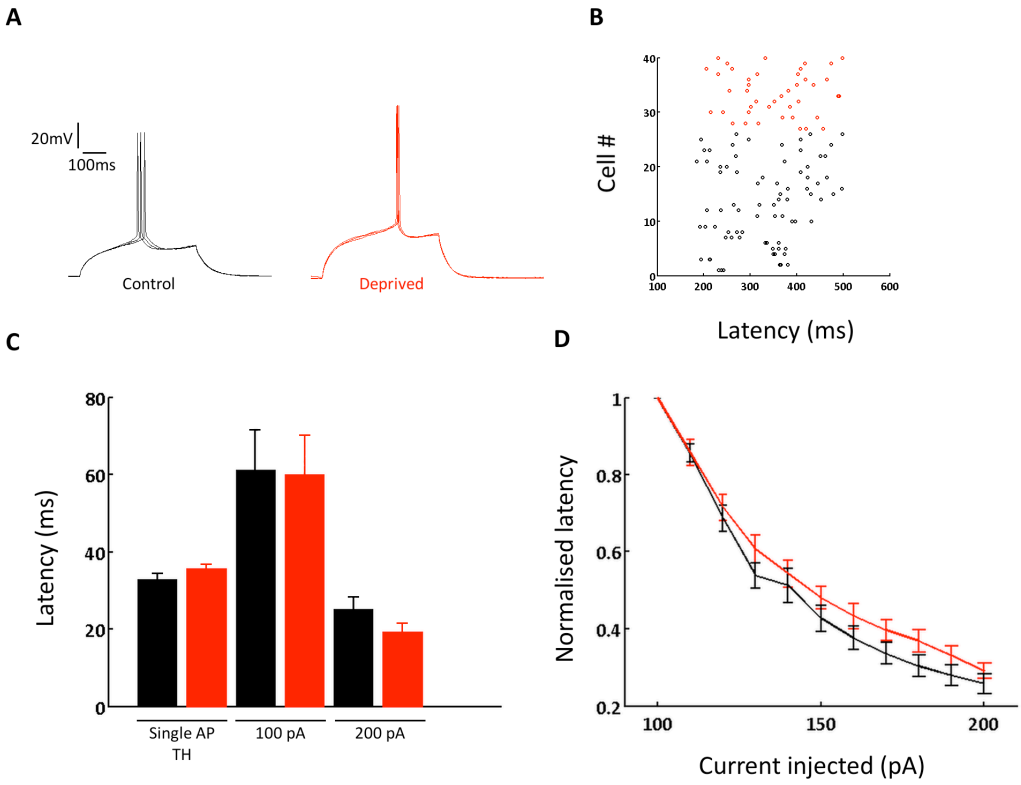

Figure 3.13 Deprivation does not alter latency of action potentials.

A, Example traces of three trials eliciting single action potentials used to calculate mean latency within a cell, in control (left, black) and deprived (right, red). **B,** Scatter plot of three latency times for control (black, n = 27) and deprived (red, n = 14) cells. Each row shows three trials for one cell. **C,** Mean latency at different current injections in control (black) and deprived (red) neurons. Latency ± s.e.m. for single AP at threshold: control, 33 ± 1 ms; deprived, 35 ± 2 ms, p = 0.267, t-test; at 100 pA: control, 61 ± 12 ms; deprived, 60 ± 11 ms, p = 0.724, Mann-Whitney rank sum (n = 12 control cells, 13 deprived cells); at 200 pA: control, 25 ± 3 ms; deprived, 19 ± 2 ms, p = 0.172 , t-test (n = 14 control cells, 12 deprived cells). **D,** Plot of mean normalised latency and current injection demonstrating the relationship between current injection size and latency time. Latency at each current injection is normalised to the latency value at the first current injection (100 pA) within a cell. Error bars indicate s.e.m.

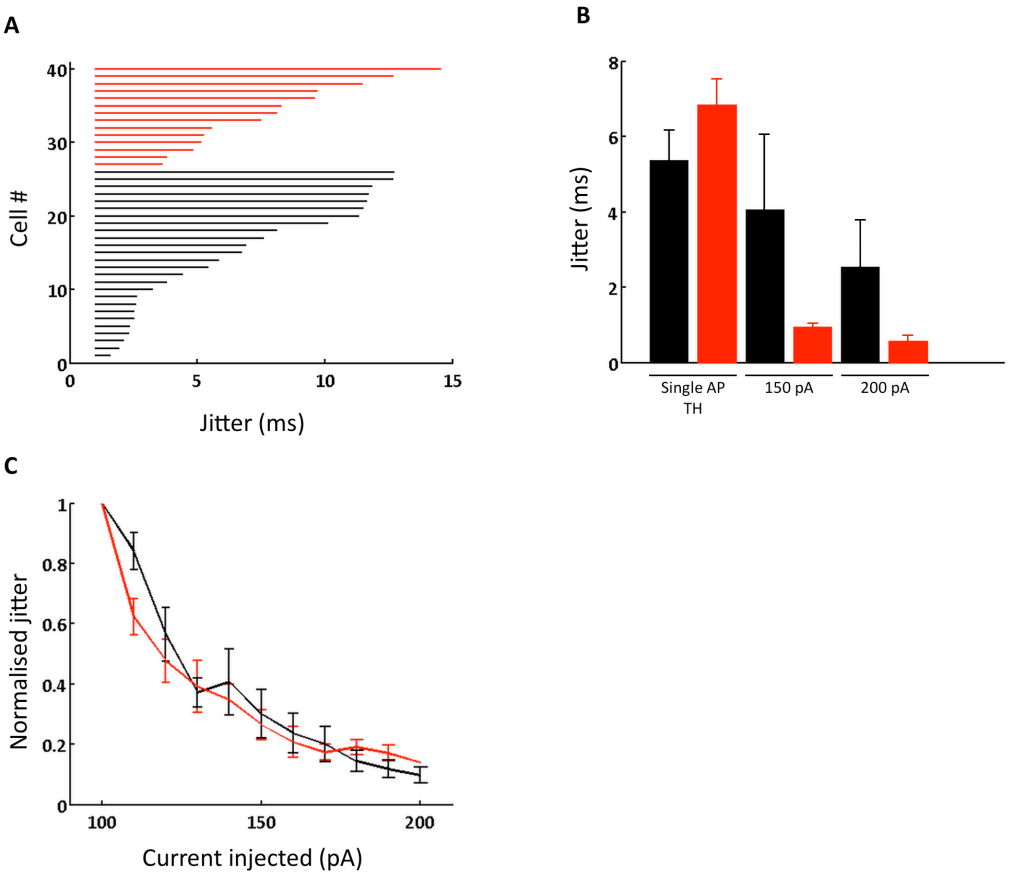

Figure 3.14 Deprivation does not affect the precision of spike timing

A, Line plot of jitter times for individual cells at single AP threshold. Each line represents the jitter across three trials in a cell where a single AP was elicited, with control in black, and deprived in red. **B,** Mean jitter at different current injections in control (black) and deprived (red) neurons. Mean jitter for single AP: control, 5 ± 1 ms; deprived, 7 ± 1 ms; p = 0.197, n = 26 control cells and 14 deprived cells; at 150 pA: control, 4 ± 2 ms; deprived, 1 ± 0.1 ms; p = 0.067, n = 6 control cells, n = 4 deprived cells; at 200 pA: control, 3 ± 1 ms; deprived, 1 ± 0.2 ms; p = 0.412, n = 7 control cells, 4 deprived cells. All p values were determined using a Mann-Whitney rank sum. **C,** Normalised jitter value at each current injection demonstrating relationship between injected current and jitter in control (black) and deprived (red) conditions. Error bars indicate s.e.m.

Table 3.2 Animal numbers for each experiment and condition in Chapter 3

	Number of animals					
	Control (Time/hours)			Deprived (Time/hours)		
Experiment	24	48	72	24	48	72
Fixed AIS staining	4	3	2	2	3	3
Electrophysiology		13			7	
Electrophysiology (with synaptic blockers)		7			5	

Summary

In this chapter I have described two types of intrinsic plasticity observed in layer 2/3 pyramidal neurons following monocular enucleation. First, I described a structural change to the AIS, where following deprivation this structure underwent a decrease in length. Secondly, I looked at functional measures of excitability and found that following deprivation, these measures changed such that cells were more excitable. There was a mismatch in these two observed forms of plasticity, since previous studies into AIS plasticity suggest that a decrease in length would translate to a decrease in excitability (Grubb and Burrone, 2010; Kuba et al., 2010). I then go on to address this mismatch by relating the length of AIS in an individual neuron to that neuron's excitability, and find that in this present study there is no direct relationship between the AIS and the neuronal excitability either under control conditions, or following deprivation. There are several potential explanations for this mismatch. Firstly, I was not successfully able to label sodium channels at the AIS, and thus, am not able to confirm that the shortening of the AIS seen using the AnkG label corresponds to a decrease in sodium channels at the AIS. Therefore, it is possible that despite the decreased AnkG label there has not been a change in the number of sodium channels at this location, and thus, the changes to AnkG may not reflect any functional change in excitability. The increase in excitability observed at 48 hours post deprivation corroborates with previous work by Desai et al (1999), who find the same result in cultured visual cortex neurons treated for two days with TTX to abolish activity. They found that this TTX treatment led to an increase in the amplitude of sodium currents, likely caused by a change in channel density. This would if anything, predict that AIS length should be longer than control. However, it is possible that in the present experiments, deprivation has caused changes to the voltage-dependence and kinetics of sodium channels at the AIS, rather than density. However, I also did not observe any differences in AP waveforms between control and deprived conditions, or spike timing and precision. These are all factors that are influenced by sodium currents. Thus, it is also possible that in the present preparation, deprivation does not alter sodium channel currents, but rather

alters a different current instead, such as potassium, and that this current is responsible for the increase in excitability.

Chapter 4: Interactions between homeostatic mechanisms in individual layer 2/3 pyramidal neurons

Introduction

In the previous chapter I have shown that following deprivation, excitatory neurons in layer 2/3 of the monocular visual cortex undergo an increase in intrinsic excitability. Whether or not this intrinsic plasticity is occurring alongside other forms of homeostatic plasticity, such as synaptic scaling or changes to the EI balance was not addressed, however. It has previously been shown that layer 2/3 pyramidal neurons are able to undergo multiple forms of plasticity (Maffei and Turrigiano, 2008), depending on the form of deprivation. This work has always addressed plasticity on a population level, and does not reveal if individual neurons are undergoing multiple forms of plasticity, or, whether subpopulations of neurons are undergoing separate forms of plasticity. Moreover, recent work has shown that, in the adult, following deprivation there is a recovery of a subset of pyramidal neurons after the initial decrease in activity. This recovery occurs in just over half of neurons that were active before deprivation, while the remainder of neurons stay silent and do not contribute to overall activity following deprivation (Barnes et al., 2015a). In this study, in the adult, recovery was aided by subnetwork interactions in addition to homeostatic plasticity mechanisms. While a shift in the E/I balance, caused by a reduction in inhibition, was seen across all neurons, whether a cell recovered its activity or not was dependent on its local network correlations. During development it is unclear if the same lack of specificity of homeostatic mechanisms exists. Previous work in juvenile rats has shown that in response to eyelid suture, changes in mEPSC amplitude correlate with changes to *in vivo* firing rate of neurons indicating this to be the potential mechanism of recovery (Hengen et al., 2013). However, as the two measures were recorded from separate populations of neurons there is no way to directly determine how an individual cell is responding to deprivation.

Recovery of activity has been demonstrated using a variety of techniques. Some studies have used microelectrode recordings to monitor neuronal firing activity (Chino et al., 1995; Darian-Smith and Gilbert, 1995; Giannikopoulos and Eysel, 2006; Hengen et al., 2013). Improvements to the performance of calcium indicators have enabled the use of genetically encoded calcium indicators, such as GCAMP, to measure intracellular levels of calcium chronically across several days (Barnes et al., 2015a; Keck et al., 2013). Other studies have used the expression of activity-regulated genes, such the early immediate genes *c-Fos* and *zif-268* as indicators of neuronal activity (Arckens et al., 2000; Hu et al., 2009; Zhang et al., 1995). In particular, the expression of c-Fos is particularly favourable thanks to its rapid half-life kinetics for both protein and mRNA expression, low levels of basal expression, and, broad dynamic range of mRNA and protein expression. The expression of c-Fos is known to peak within an hour of increased neuronal firing, and following this, expression levels decline over the subsequent 4 hours (Sagar et al., 1988; Yassin et al., 2010). Recently, we (Barnes et al., 2015a) demonstrated that post-hoc immunolabelling of c-Fos could be used as a reliable indicator of a neurons *in vivo* activity status. Reconstructing regions of the visual cortex that had been imaged previously *in vivo,* c-Fos labelling of neurons was able to be matched to the same neurons' *in vivo* activity, measured via changes in fluorescence of GCAMP5. We found that all c-Fos labelled cells had been active *in vivo*, and, that only a small fraction of cells that had been active *in vivo* were not labelled with c-Fos in the post-hoc preparation. Furthermore, these false negative cells were shown to have low levels of GCAMP5 activity during the *in vivo* recordings. Thus, the presence of c-Fos labelling in slice preparations may be a useful tool to determine a cells *in vivo* activity status. In this chapter, I shall use this approach in attempt to address two issues raised by recent work: first, I shall examine whether or not individual neurons are engaging in multiple mechanisms of homeostatic plasticity, and secondly, I shall determine whether there are differences in the homeostatic mechanisms employed by active and inactive neurons in the developing rodent, following deprivation.

Results

To determine whether individual neurons undergo multiple plasticity mechanisms following activity deprivation, I took a two-step approach. First, I recorded from layer 2/3 pyramidal neurons in acute slices of monocular visual cortex. Initially upon breaking into a cell, I recorded the current action potential threshold, injecting just enough current to elicit one single action potential. A hyperpolarising current injection was also applied to allow calculation of passive membrane properties. Next, TTX was washed onto slices and recording was switched to voltage-clamp mode to record mini postsynaptic currents incoming onto the cell (Fig. 4.1a). Recordings were carried out at a holding potential of -65 mV. Since only TTX was present in the bath ACSF, both excitatory and inhibitory receptors were non-inhibited and the below analysis did not separate the two types of events. At a holding potential of -65 mV, however, close to the reversal potential for chloride ions it is likely that the majority of events are excitatory. Thus, these experiments provide insight into the excitability of the neuron and additionally a rough gauge of incoming synaptic activity, using the frequency and amplitude of mini events as an indicator of synaptic number and strength respectively (although see chapter summary). At the end of recordings, the patch pipette, which contained fluorescent dye (AF 488) added to its internal solution, was carefully reversed out of the cell and the slice was fixed immediately in 1% PFA. Slices were fixed overnight at 4°C and staining was performed the following day, to label for AnkG and c-Fos (Fig. 4.1b-d). Thus, this approach enabled direct functional measures of both intrinsic and synaptic properties, as well as structural information regarding the AIS, dendritic spine size and density and the activity status of the neuron, all in the same cell.

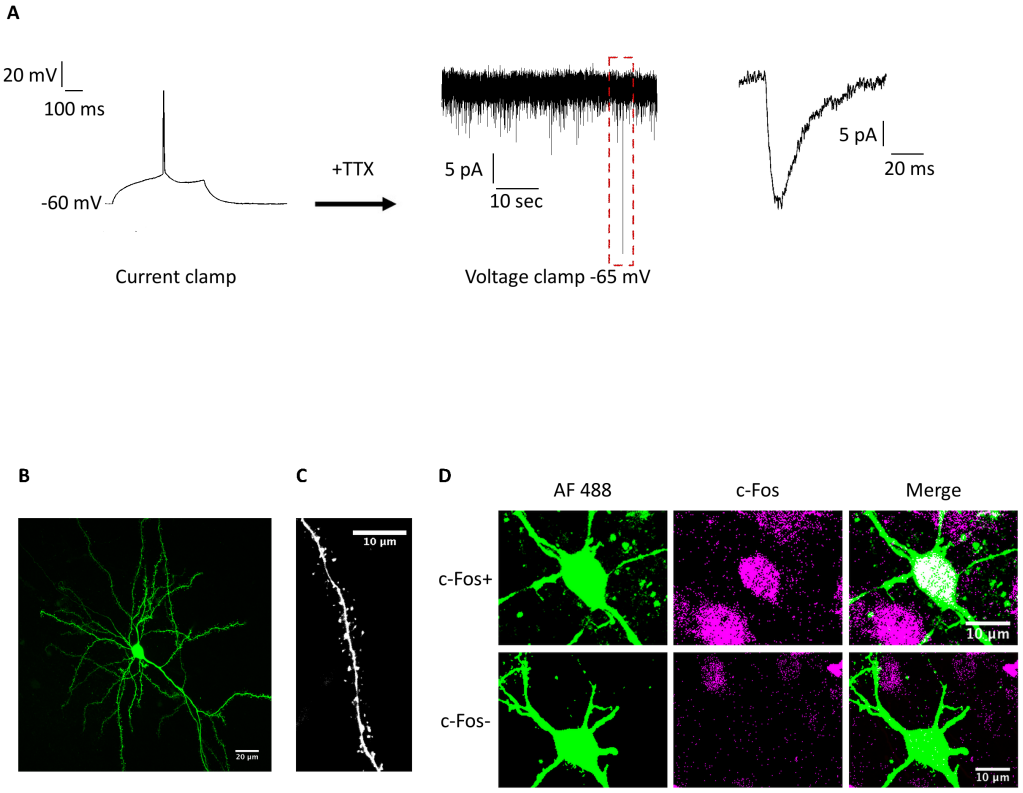

Figure 4.1 Experimental techniques.

A, Experimental paradigm: a single AP is elicited in current clamp mode, before TTX is perfused into the recording chamber and mPSCs are recorded in voltage clamp mode. Right, a zoom in of the event in red box in voltage clamp trace. **B,** Example image of a layer 2/3 cell filled with AF 488. **C,** Zoomed image of a dendritic stretch from cell in (**b**). **D,** Example images of two recorded neurons, immunostained to label for c-Fos. Top, c-Fos positive; bottom, c-Fos negative; left, AF 488; middle, c-Fos; right, merge.

Following deprivation there is a decrease in activity

There is an extensive literature showing that following the loss of input there is a rapid decrease in activity levels (Barnes et al., 2015a; Calford et al., 2000; Darian-Smith and Gilbert, 1995, 1995; Hengen et al., 2013; Keck et al., 2013). Studies have also shown that in the following hours and days there is a recovery of this reduced activity (Barnes et al., 2015a; Hengen et al., 2013; Keck et al., 2013). Recently, Barnes et al., showed that antibody labelling of the early immediate gene c-Fos could reliably report the *in vivo* status of a cell after acute slices had been prepared for electrophysiology (Fig. 4.2). All cells that were labelled positively with c-Fos antibody showed *in vivo* activity, and only a minority of cells not positively labelled for c-Fos showed *in vivo* activity (Fig. 4.2a-c). Moreover, these active but not c-Fos labelled cells showed significantly lower levels of *in vivo* activity than positively c-Fos labelled cells (Fig. 4.2d). Thus, I used this approach to first check how the present deprivation paradigm affected the levels of active and inactive neurons in juvenile mice. The density of c-Fos positive cells did not vary across the three ages used in control (Fig. 4.3b), thus, for comparison to deprived conditions all three control time points were pooled to create one control group. At 24 hours post deprivation, the density of c-Fos positive cells was significantly decreased compared to control. By 48 and 72 hours post deprivation, c-Fos density levels were in line with control (Fig. 4.3a,c). These results, in juvenile mice, fall in line with activity levels reported *in vivo* in adult mice following the same monocular enucleation deprivation paradigm (Barnes et al., 2015a). This is in contrast, however, to previous reports of activity levels in juvenile rats following deprivation by Hengen et al.,(2015), who do not report a decrease in activity until 48 hours post deprivation. However, this difference is likely due to the differing method of deprivation used. Of cells that were patched and then post-hoc stained for c-Fos, there was no statistical difference between proportions of c-Fos positive cells in control and deprived conditions. However, fewer c-Fos positive cells were seen at 24 hours post deprivation than any other time point (Fig. 4.3d).

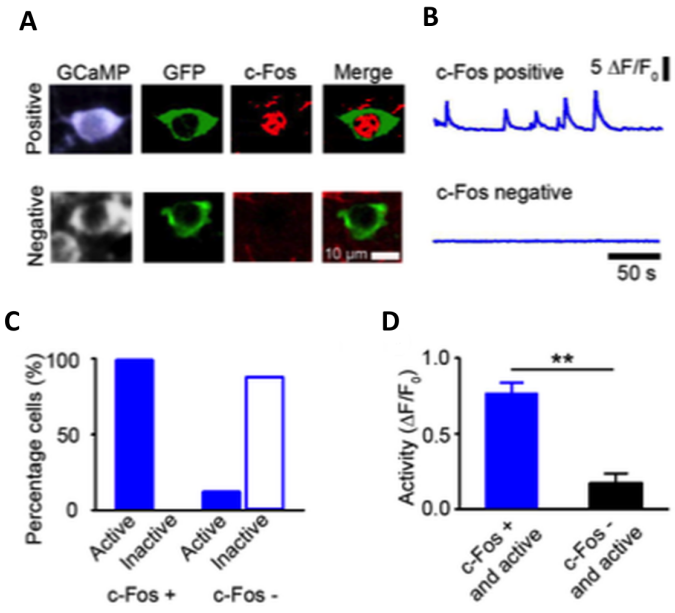

Figure 4.2 c-Fos reliably labels neurons that were active *in vivo*

These figures are taken, with permission, from Barnes et al., (2015). Work for these data was carried out by Samuel Barnes, Tara Keck, Georg Keller, David Elliott and myself.

A, Example images of two neurons, one positively labelled with c-Fos and one showing no c-Fos immunoreactivity. Left, raw GCAMP signal showing cells *in vivo*. Second left, boosted GFP signal from slice after *ex vivo* reconstruction. Third left, c-Fos immunoreactivity. Right, merge of GFP and c-Fos labelling. **B,** *In vivo* activity traces (ΔF/F GCAMP signal) of the same active and inactive cells as shown in (**a**). **C,** Percentage of neurons that show c-Fos labelling and are active or inactive *in vivo*, and cells that are not immunolabelled with c-Fos and active or inactive *in vivo* (n = 157 reconstructed cells). **D,** Average *in vivo* activity of cells either c-Fos positive and active *in vivo* or c-Fos negative and active *in vivo* ($p = 0.003$, t-test). ** $p < 0.01$

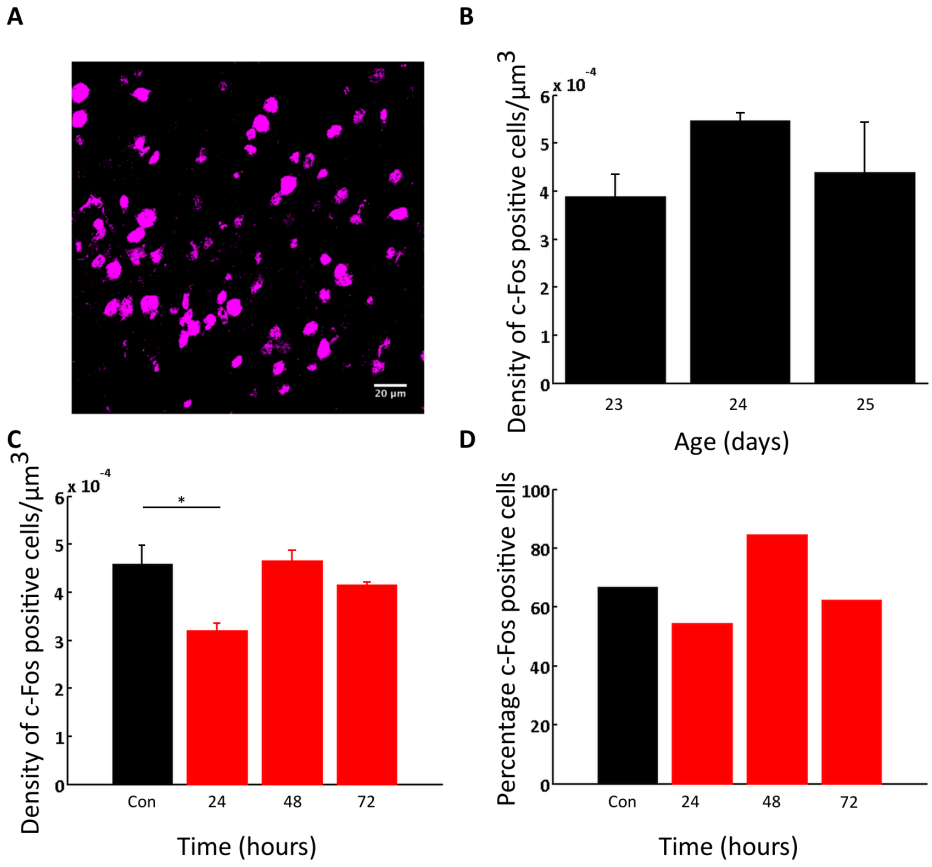

Figure 4.3 Density of c-Fos positive cells decreases following deprivation.

A, Example image of c-Fos stain in a cortical slice. **B,** Mean c-Fos density in control cells at the three ages used in the time course of study, p = 0.093, Kruskal-Wallis ANOVA on ranks. **C,** Mean c-Fos density in control (black) and at 24, 48 and 72 hours following deprivation (red). Kruskal-Wallis ANOVA on ranks, with Dunn's post hoc test compared to control (24hr) p = 0.023; (48hr) p = 0.999; (72hr) p = 0.999; control = 14 slices; 24hr = 6 slices; 48hr = 12 slices; 72hr = 4 slices. **D,** Proportion of cells in electrophysiology experiments that stained positive for c-Fos, in control and deprived. Control, n = 27 cells; deprived (24hr) n = 11 cells, (48hr) n = 13 cells, (72hr) n = 8 cells. *p < 0.05. Error bars indicate s.e.m.

In control conditions cells with greater inputs are less excitable

To examine interactions between different homeostatic mechanisms, I first looked in control cells to see if there were any relationships between excitability and synaptic properties measured through mPSCs. Control neurons were recorded from across the same developmental age course as the post-deprivation time course (i.e. p24 – 26). No differences in passive or active membrane properties (Table 4.1), or mPSC properties (Table 4.2), were observed between cells at different ages in control, and thus, all control neurons were pooled together to create a single control group. To examine how the level of synaptic input might be related to the intrinsic excitability of a cell, I then looked at correlations between mPSC properties and the current density. The current density was chosen because it is a good measure of overall excitability, taking into account both the passive and active properties of the cell that contribute towards its excitability. Firstly, I looked at mPSC frequency, which is generally regarded to give an estimation of the number of synapses present at the given cell (Turrigiano et al., 1998). Here, I find there is a positive correlation between mPSC frequency and current density (Fig. 4.4a). Since a larger current density means that more current is required to excite a given unit area of cell, there is an inverse relationship between how much putative synaptic input a cell receives and how excitable the cell is. Thus, cells with potentially more inputs are less excitable. Furthermore, the amplitude of mPSCs, thought to approximate the strength of synapses, also showed a significant correlation with current density (Fig. 4.4b). Neurons with higher amplitude mPSC events tend to have a higher current density, indicating reduced excitability. Taken together, these results suggest that cells with more and stronger synaptic input are less excitable. While in the previous chapter I have shown that AIS length does not correlate with measures of excitability, I find here that in addition to a correlation between mPSC frequency and current density, there are also significant correlations between AIS length and synaptic properties (Fig. 4.5a,b). Just as cells with a fewer potential synapses (lower mPSC frequency) have a lower current density, indicating heightened excitability, these cells also tend to have longer AISs. AIS length correlates with both mPSC frequency and amplitude, suggesting that cells with more numerous and stronger inputs will

Table 4.1 Passive membrane properties and excitability of control cells does not change over the developmental time course of this study

	Age (post-natal days)			P-value
	24 (n = 8)	25 (n = 12)	26 (n = 9)	
Vm (mV)	-74 ± 1	-71 ± 1	-73 ± 1	0.176
Input resistance (MΩ)	129 (119 – 176)	149 (102 – 204)	123 (98 – 168)	0.612
Membrane capacitance (pF)	446 ± 28	366 ± 23	398 ± 27	0.098
Membrane time constant (ms)	65 ± 6	53 ± 5	53 ± 6	0.270
Current density (pA/pF)	0.27 ± 0.02	0.27 ± 0.03	0.30 ± 0.03	0.804
AP voltage threshold (mV)	-37 (-40 – -32)	-38 (-40 – -36)	-38 (-40 – -32)	0.701

Reported values are mean ± s.e.m. where a one-way ANOVA was used for comparison, and median and interquartile range where a Kruskal-Wallis one-way ANOVA on ranks was used for comparison.

Table 4.2 Synaptic input measures are not altered in control neurons during the developmental time course of this study

	Age (post-natal days)			P-value
	24 (n = 6)	25 (n = 9)	26 (n = 8)	
mPSC frequency (Hz)	0.6 (0.4 – 1.4)	0.3 (0.2 – 0.9)	0.5 (0.3 – 1.5)	0.383
mPSC amplitude (pA)	8 ± 1	7 ± 1	8 ± 1	0.777

Reported values are mean ± s.e.m. where a one-way ANOVA was used for comparison, and median and interquartile range where a Kruskal-Wallis one-way ANOVA on ranks was used for comparison.

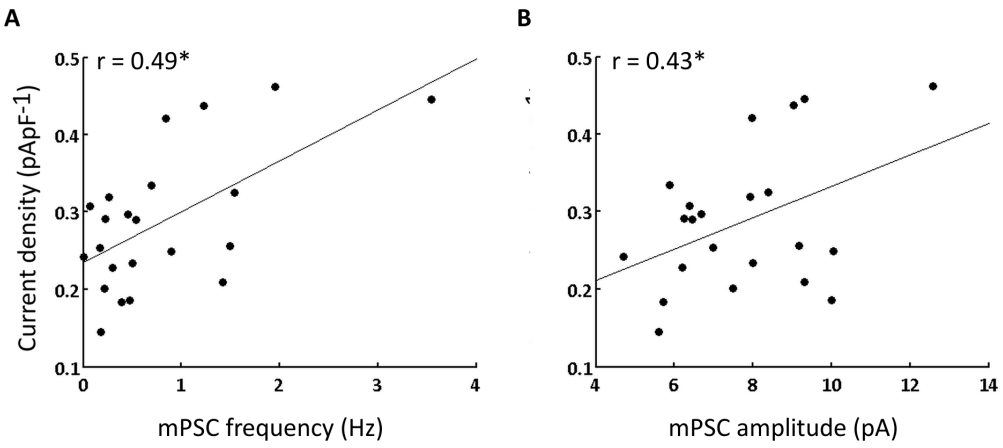

Figure 4.4 Frequency and amplitude of synaptic events and excitability are correlated under control conditions.

A, Scatter plot showing relationship between mPSC frequency and current density; p = 0.020, Spearman's rank order correlation. **B,** Scatter plot of mPSC amplitude and current density, p = 0.047, Pearson Product Moment Correlation. Correlation coefficients are indicated in the top left corner of each plot; significant correlations are fitted with a least squares regression line. *p < 0.05; CD, current density.

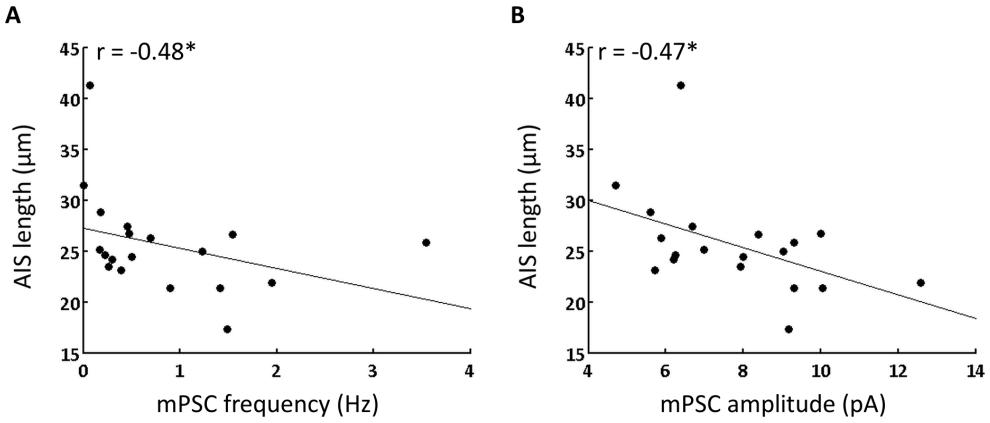

Figure 4.5 AIS length is inversely correlated with putative synaptic input.

A, Scatter plot of mPSC frequency and AIS length; p = 0.038, Spearman's rank order correlation. **B,** Scatter plot of mPSC amplitude and AIS length; p = 0.044, Spearman's rank order correlation. Correlations are fitted with a least squares regression line. *p < 0.05.

tend to have shorter AISs. This indicates that there may be an indirect relationship linking AIS length to excitability, involving synaptic input.

Under control conditions, c-Fos positive and negative neurons are not distinguishable from each other, based on the synaptic or intrinsic properties measured

Previous research using a transgenic mouse line to label recently active cells with GFP has shown that there are differences in synaptic drive and excitability between recently active and inactive cells (Yassin et al., 2010). In this study, cells that were recently active, and therefore, expressing c-Fos received greater excitatory drive and were less excitable. Given the above results, that cells with potentially more synaptic input are less excitable, I hypothesised that I might see a clear separation of c-Fos positive and negative cells within this correlation, such that the cells with higher mPSC frequency and current density would be c-Fos positive, and, the cells with lower mPSC frequencies and current densities would be c-Fos negative. Thus, I examined how the populations of putatively active and inactive neurons differed in their synaptic and intrinsic properties in the present experiment. In contrast to the findings of Yassin et al (2010), I did not find differences between c-Fos positive and negative neurons in either the synaptic (Fig. 4.6; Fig. 4.7) or intrinsic properties (Fig. 4.8) of the neurons. Upon examination of the correlations between mPSC frequency and amplitude, and current density, there is no clear separation of c-Fos positive and c-Fos negative neurons (Fig. 4.6c,d). Furthermore, I did not see any difference between mPSC frequency or amplitude in c-Fos positive and negative cells (Fig. 4.6a,b). Additionally, I looked at spine density and spine size as a structural proxy for synaptic number and strength, respectively (Keck et al., 2013), and again, saw no difference between c-Fos positive and negative neurons (Fig. 4.7a,b). While similarly to Yassin et al., I did not find any difference in passive membrane properties between c-Fos positive and negative cells (Table 4.3), I also saw no differences in excitability measures, unlike Yassin et al. Both current (rheobase) and voltage action potential threshold was the same in c-Fos positive and negative neurons, and, current density did also not differ between cells (Fig. 4.8).

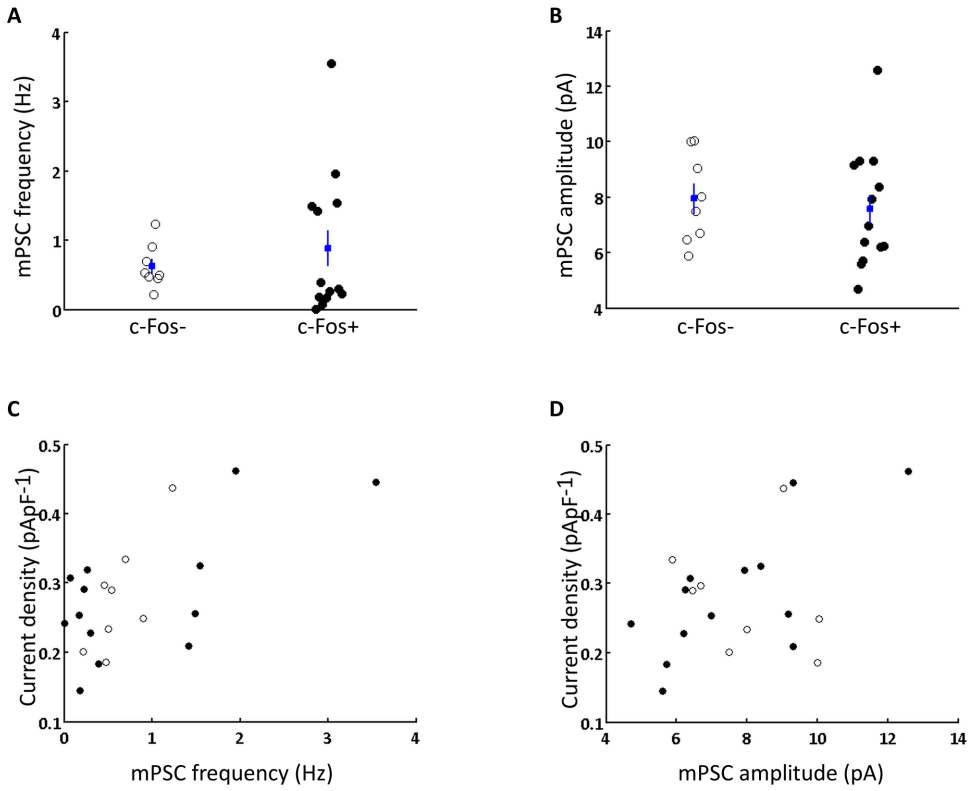

Figure 4.6 Putatively active and inactive neurons do not show differences in synaptic events under control conditions.

A, Mean mPSC frequency: c-Fos negative, 0.6 ± 0.1 Hz; c-Fos positive, 0.9 ± 0.3 Hz, p = 0.587, Mann-Whitney rank sum. **B,** Mean mPSC amplitude; c-Fos negative, 8 ± 1 pA; c-Fos positive, 8 ± 1 pA; p = 0.376, t-test. **C,** Scatter plot of mPSC frequency and current density (as in Fig. 4.4a) coloured to indicate c-Fos positive cells (filled circles) and c-Fos negative cells (open circles). **D,** Scatter plot of mPSC amplitude and current density (as in Fig. 4.4b) coloured to indicate c-Fos positive cells (filled circles) and c-Fos negative cells (open circles). For all, filled circles represent a single c-Fos positive cell and open circles represent a single c-Fos negative cell. Blue box and lines indicate mean ± s.e.m.

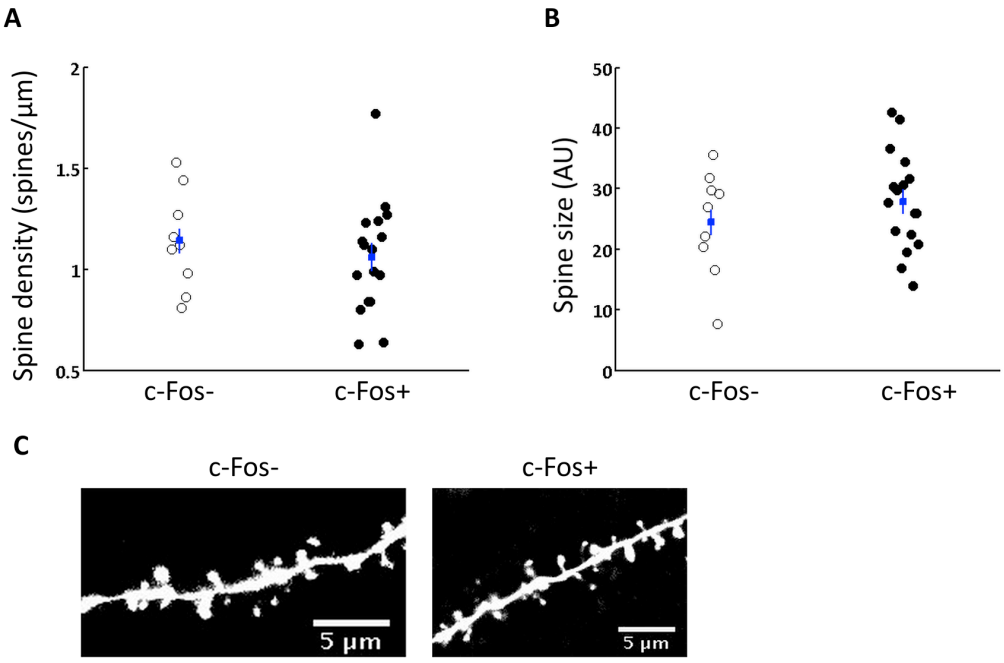

Figure 4.7 Spine density and size is similar in c-Fos positive and negative neurons.

A, Spine density: c-Fos negative 1.1 ± 0.08 spines per µm; c-Fos positive, 1.1 ± 0.07 spines per µm, p = 0.469, t-test. **B,** Spine size: c-Fos negative, 24 ± 3 AU; c-Fos positive, 28 ± 2 AU; p = 0.331, t-test. Blue box and lines indicate mean ± s.e.m. **C,** Example stretches of dendrite from a c-Fos negative (left) and c-Fos positive (right) neuron.

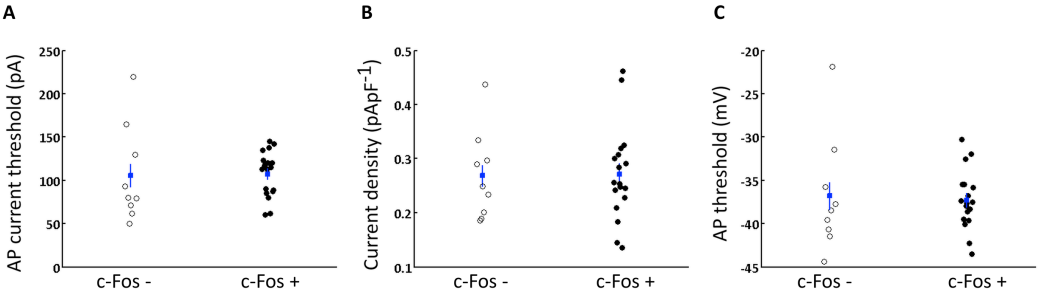

Figure 4.8 Putatively active and inactive neurons do not show differences in excitability in control conditions.

A, Current action potential threshold in c-Fos negative, 106 ± 19 pA, and c-Fos positive neurons, 107 ± 6 pA; p = 0.905, t-test. **B,** Current density in c-Fos negative, 0.27 ± 0.03 pApF^{-1}, and c-Fos positive neurons, 0.27 ± 0.2 pApF^{-1}; p = 0.939, t-test. **C,** Action potential voltage threshold in c-Fos negative, -37 ± 2 mV, and c-Fos positive neurons, -37 ± 1 mV; p = 0.589, Mann-Whitney rank sum. Blue box and lines indicates mean ± s.e.m. Each point indicates one c-Fos negative (open circles) or c-Fos positive (closed circles) neuron. N = 9 c-Fos negative cells, and 18 c-Fos positive cells.

Table 4.3 Passive membrane properties of c-Fos positive and negative cells in control

	c-Fos- (n = 9)	c-Fos+ (n = 18)	P-value
Vm (mV)	-71 (-75 – -68)	-74 (-75 – -72)	0.300
Input resistance (MΩ)	134 (104 – 168)	127 (114 – 183)	0.738
Membrane time constant (ms)	50 (44 – 56)	60 (48 – 70)	0.117
Membrane capacitance (pF)	376 ± 30	411 ± 20	0.325

All comparisons were made using a Mann-Whitney rank sum (reported values are median with interquartile range in parentheses), except for membrane capacitance which was compared using a t-test (reported values are mean ± s.e.m.).

There are several potential reasons for the differences between my observations and those of Yassin et al., including recordings being taken from different brains areas, and at different developmental ages. Overall, in the current study under control conditions, the synaptic and intrinsic properties of putatively active and inactive neurons are indistinguishable from one another, based on the expression of c-Fos.

Following deprivation, there are no changes to intrinsic or synaptic properties

In the previous chapter, I described changes to excitability following 48 hours of monocular deprivation. I have now since, determined the time course of changes to levels of activity, via changes in c-Fos density, and thus, sought to compare how both excitability and synaptic inputs might vary across this same time course. Surprisingly, and in contrast to the previous chapter, I did not observe a change in excitability at any time point post-deprivation (Fig. 4.9a-c). Similarly, there was no change in the passive membrane properties of neurons following deprivation (Table 4.4). One possibility for the discrepancy in these results is a difference in light-dark cycle that animals were kept in between the two sets of experiments; the light-dark cycle of animals used in the present experiments was reversed compared to animals used for experiments in Chapter 3 (see chapter summary). I next looked at the synaptic measurements, and again, found that there was no change in either mPSC frequency or amplitude at any time point following deprivation (Fig. 4.10). These results contrasts with studies in the literature, where following eyelid suture or TTX injection in juvenile rats changes to mEPSC amplitude and frequency are observed (Hengen et al., 2013; Maffei and Turrigiano, 2008). It is possible that the differences between this study and previous findings are due the method of activity deprivation. Previous juvenile studies have used eyelid suture and TTX injection rather than monocular enucleation, and thus, are likely to be producing different patterns of activity along the pathway of input to the visual cortex (Maffei and Turrigiano, 2008). Additionally, it is possible that by measuring only mPSCs, any potential change in mEPSCs is masked by the possible inclusion of mIPSCs in these recordings. Previous study using monocular enucleation, in adult mice, has shown that

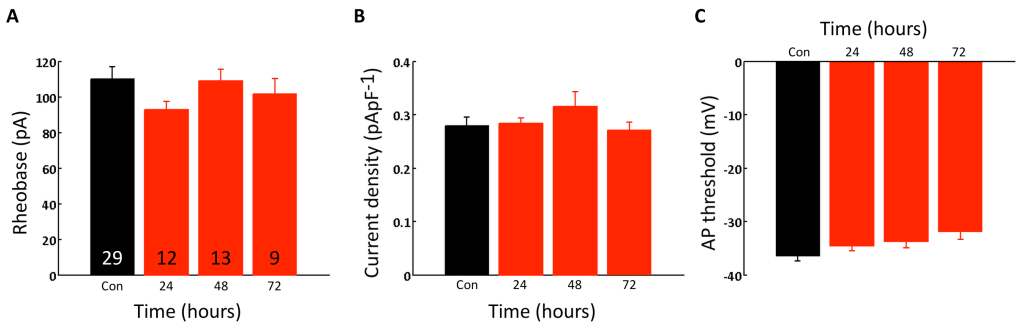

Figure 4.9 Following deprivation, there is no change in intrinsic excitability across a 72 hour time course.

A, Mean rheobase values in control and deprived time points; p = 0.507, n numbers are denoted within bars. **B,** Mean current density; p = 0.906. **C,** Mean voltage AP threshold; p = 0.197. All comparisons were made using Kruskal-Wallis one-way ANOVA on ranks. Error bars indicate s.e.m.

Table 4.4 Passive membrane properties in control and deprived neurons following monocular enucleation

	Control (n = 29)	Deprived			P-value
		24 hr (n = 12)	48 hr (n = 13)	72 hr (n = 9)	
Vm (mV)	-73 (-75 – -70)	-72 (-74 – -70)	-70 (-75 – -68)	-70 (-71 – -68)	0.099
Input resistance (MΩ)	130 (140 – 176)	154 (140 – 201)	142 (117 – 173)	166 (133 – 207)	0.196
Membrane capacitance (pF)	398 ± 15	325 ± 15	363 ± 23	371 ± 27	0.057
Membrane time constant (ms)	56 ± 3	53 ± 3	52 ± 3	61 ± 7	0.539

Comparisons were made using a Kruskal-Wallis one-way ANOVA on ranks (Vm, input resistance) or a one-way ANOVA (membrane capacitance, membrane time constant). Reported values are median, with IQR in parentheses or mean ± s.e.m.

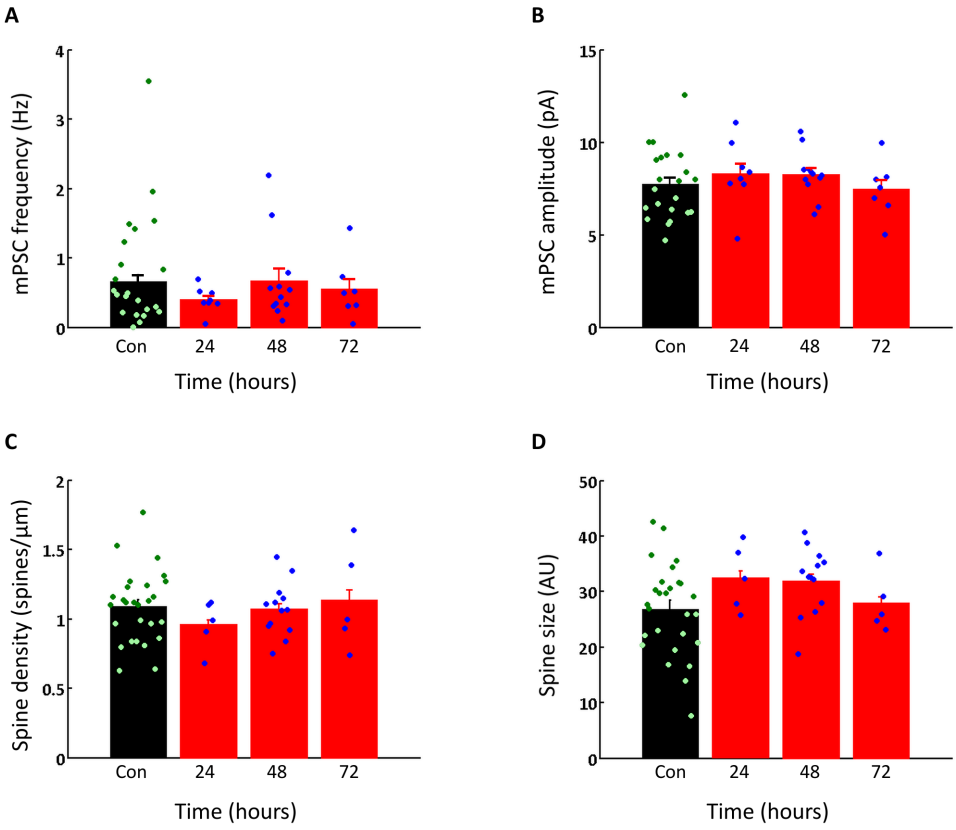

Figure 4.10 Synaptic measurements are not altered following deprivation.

A, Mean mPSC frequency in control and following deprivation; p = 0.871, Kruskal-Wallis one-way ANOVA on ranks. **B,** Mean mSPC amplitude; p = 0.642, one-way ANOVA. **C,** Mean spine density in control and following deprivation; p = 0.686, one-way ANOVA. **D,** Mean spine size (measured as a proxy) in control and following deprivation; p = 0.137, one-way ANOVA Circles represent individual cell values. Error bars indicate s.e.m.

mEPSCs are unaffected, while mIPSCs undergo a decrease in frequency (Barnes et al, 2015a). Thus, to examine the purely excitatory component, I also looked at how measures for spine density and size might be altered by deprivation, since dendritic spines are the structural site of excitatory synapses. Although there were trends towards decrease spine density at 24 hours post deprivation, and increased spine size at 24 and 48 hours post deprivation, no significant differences were observed between control and any post deprivation time point for either measure (Fig. 4.10c,d).

Deprivation alters the relationship between intrinsic excitability and synaptic input

Having established that, in the present experiments, deprivation did not cause any alterations to either the synaptic or intrinsic properties measured, I next set out to determine whether the relationships observed between synaptic and intrinsic factors in control conditions were affected by deprivation. I first looked to determine whether the relationship between synaptic input and excitability was maintained following deprivation. Here, I find that there is no longer a significant correlation between mPSC frequency and current density (Fig. 4.11a), indicating that the relationship between a cells' excitability and the number of inputs the cell receives has been lost. Furthermore, the relationship between mPSC amplitude and current density is now inverted in comparison to control (Fig. 4.11b). Following deprivation there is now a significant negative relationship between these two factors, suggesting that cells with larger synaptic events have increased excitability. Thus, in contrast to control where correlations suggested that cells with more synaptic drive were less excitable, this scenario appears to be reversed following deprivation such that cells now with higher synaptic drive are more excitable. In addition, AIS length, which in control correlated with both mSPC frequency and amplitude, no longer correlates with either synaptic measure (Fig. 4.12a,b). Thus, following deprivation there are significant changes to the relationships between synaptic input and excitability, such that now cells with stronger synaptic events are more excitable.

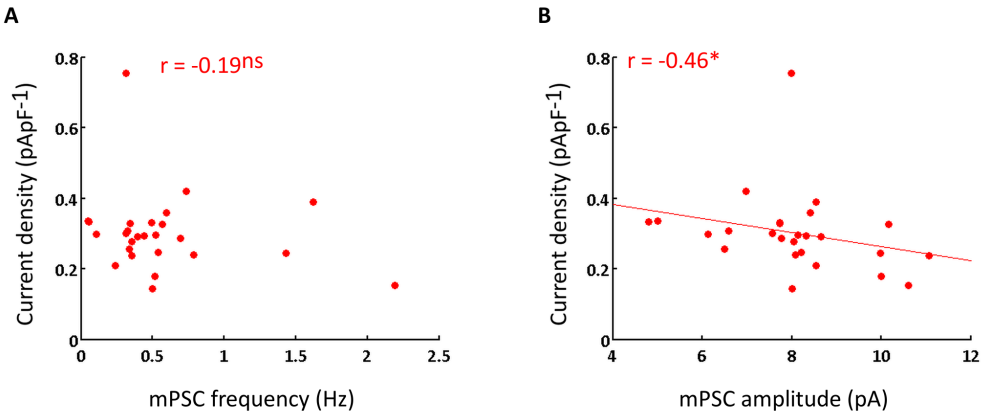

Figure 4.11 Following deprivation the relationships between synaptic and intrinsic measures are altered.

A, Scatter plot of mPSC frequency and current density in neurons following deprivation; p = 0.351, Spearman's rank order correlation. **B,** Scatter plot of mPSC amplitude and current density; p = 0.018, Spearman's rank order correlation. Significant correlations are fitted with least squares regression lines. *p < 0.05; ns, not significant.

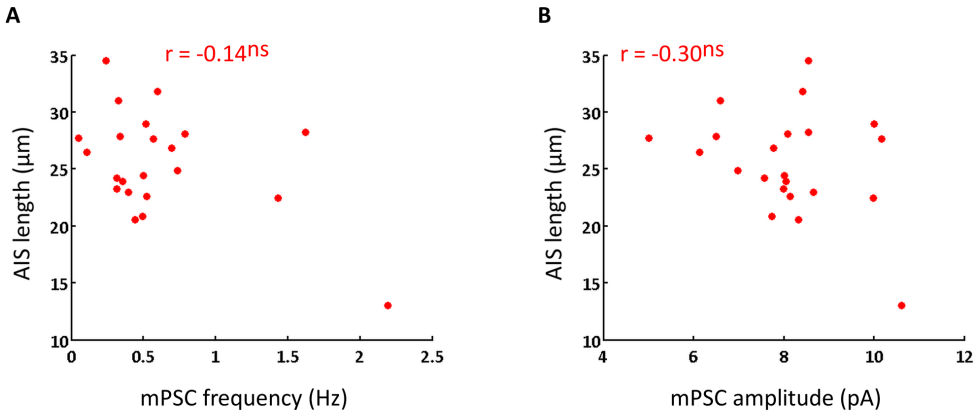

Figure 4.12 Following deprivation AIS length no longer correlates with measures of excitatory synaptic input.

A, Scatter plot of mPSC frequency and AIS length following deprivation; p = 0.524, Spearman's rank order correlation. **B,** Scatter plot of mPSC amplitude and AIS length following deprivation; p = 0.168, Pearson Product Moment Correlation. Each red point indicates one deprived neuron; ns, not significant.

Following deprivation, there are differences in intrinsic properties of c-Fos positive and negative neurons

Following deprivation, despite observing an initial decrease in density of c-Fos neurons, suggesting a reduction in activity, when examining intrinsic and synaptic properties separately, over the same time course, I did not observe any plasticity. However, looking at cells' properties on an individual basis, I did find a shift in the relationship between synaptic input measures and intrinsic excitability. While in control conditions there was no difference between putatively active or inactive cells, determined via the presence of c-Fos labelling, I hypothesised that perhaps following deprivation, when the proportions of active and inactive cells are changing, there might now be differences between these two populations of neurons, and that this might be driving the shift in relationship between synaptic and intrinsic properties. Thus, I examined how c-Fos positive and negative neurons' synaptic and intrinsic measures compared following deprivation. I found a trend towards increased mPSC frequency in c-Fos negative cells (Fig. 4.13a) and a significant increase in mPSC amplitude in c-Fos negative neurons compared to c-Fos positive cells (Fig. 4.13b). Furthermore, upon re-examination of the correlation between mPSC amplitude and current density, I found that the majority of the c-Fos negative cells were clustered towards the higher mPSC amplitude and lower current density end of the correlation (Fig. 4.14a). Comparing the intrinsic excitability of c-Fos positive and negative neurons, I also found that there was in fact a significant reduction in both current density (Fig. 4.14b), and rheobase value (Fig. 4.14c). Thus, following deprivation c-Fos negative neurons are now more excitable than c-Fos positive cells, suggesting that inactive cells are more excitable. Furthermore, while no differences were observed between passive membrane properties of c-Fos positive and negative neurons, voltage AP threshold was significantly more negative in c-Fos negative neurons (Table 4.5), further indicating their increased excitability. Thus, it appears that following deprivation it is the c-Fos negative neurons that undergo plasticity, potentially as a means to homeostatically recover their activity.

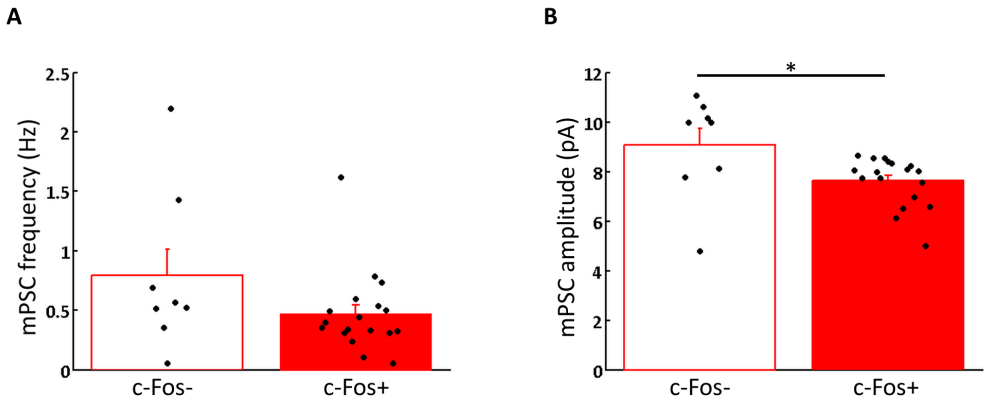

Figure 4.13 Following deprivation synaptic measures differ between c-Fos positive and negative neurons

A, Mean mPSC frequency in c-Fos negative and positive neurons after deprivation; p = 0.141, Mann-Whitney test. Median (interquartile range) in c-Fos negative: 0.6 Hz (0.4 – 1.3); c-Fos positive: 0.4 Hz (0.3 – 0.6) **B,** Mean mPSC amplitude in cells that are c-Fos negative, c-Fos positive after deprivation; p = 0.037, Mann-Whitney test. Median (interquartile range) in c-Fos negative: 10 pA (7.7 – 10.5); c-Fos positive: 8 pA (6.8 – 8.4). Error bars indicate s.e.m., c-Fos negative, open bars; c-Fos positive, filled bars. Black points indicate values for individual neurons. * $p < 0.05$.

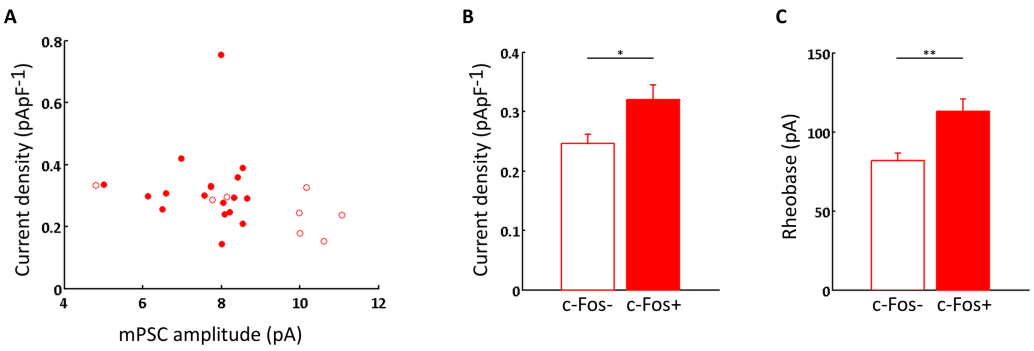

Figure 4.14 Following deprivation c-Fos negative cells are more excitable than c-Fos positive cells.

A, Scatter plot of mPSC amplitude and current density (as in Fig. 4.11b) coloured to distinguish c-Fos positive and negative cells. **B,** Mean current density in c-Fos negative (open red bar) and c-Fos positive (solid red bar) after deprivation; p = 0.044, Mann-Whitney rank sum. **C,** Mean rheobase in c-Fos negative and c-Fos positive cells after deprivation; p = 0.007, Mann-Whitney rank sum. *p < 0.05, **p < 0.01, Error bars indicate s.e.m.

Table 4.5 Membrane properties in c-Fos positive and negative cells following deprivation

	c-Fos- (n = 10)	c-Fos+ (n = 22)	P-value
Vm (mV)	-70 ± 2	-71 ± 1	0.391
Input resistance (MΩ)	164 ± 16	154 ± 7	0.519
Membrane capacitance (pF)	312 (292 – 363)	344 (309 – 407)	0.138
Membrane time constant (ms)	54 ± 4	55 ± 3	0.768
AP threshold (mV)	-38 (-41 – -35)	-34 (-36 – -26)	0.004**

Reported values are mean ± s.e.m. where a t-test was performed for comparison, or median, with interquartile range in parentheses where a Mann-Whitney rank sum was performed.

However, one caveat to the present study is that of the c-Fos negative neurons observed following deprivation, it is impossible to tell whether or not these cells were in fact active before deprivation and have fallen silent, or whether they were already silent before deprivation. Thus, the plasticity observed may also be a mechanism of recruiting new cells, that were previously inactive, into the reorganising circuit. Furthermore, rather than inactive cells undergoing plasticity to become more excitable, it may be that active cells are undergoing plasticity to become less excitable. One way to address the potential involvement of c-Fos negative cells in engaging in homeostatic plasticity to drive the recovery of activity, in the present data, is to examine the time-course of the observed intrinsic plasticity in these cells. Following deprivation, c-Fos density is reduced at 24 hours, but by 48 hours remains in line with control levels. Thus, recovery of activity appears to occur over the first 48 hours following deprivation. If recruitment or recovery of c-Fos negative cells is responsible for aiding this recovery, then we might expect to see an initial increase in excitability of c-Fos negative cells at 24 hours. As these cells become more excitable and potentially recruit or recover they will become active and thus c-Fos positive. Thus, at later stages following deprivation when recovery of activity has now occurred (48-72 hours post-deprivation), the cells that remain c-Fos negative at this later stage might not show any difference in excitability compared to c-Fos positive cells, since they are not being recruited for recovery. Thus, I sought to examine how levels of excitability across c-Fos positive and negative cells changed across the post-deprivation time course. Splitting each time point into c-Fos positive and negative results in low numbers of cells for comparison, however. Thus, since density of c-Fos positive neurons has returned to control levels by 48 hour post-deprivation (Fig. 4.3c) and remains steady at 72 hours post-deprivation, I combined these two time points to create a delayed response (48-72 hr), which can be compared to the initial response at 24 hours post-deprivation. I then also compare these changes to control cells to determine whether it is the active or inactive cells that are undergoing plasticity. Examining the rheobase value, there was a significant reduction in the rheobase values of c-Fos negative cells at 24 hours post-deprivation, compared to c-Fos positive neurons at this time point (Fig. 4.15a). This difference was not seen at

the 48-72 hour time point. While no significant differences were found between control and any group, there were strong trends towards c-Fos negative cells in deprived animals having lower rheobase values, rather than c-Fos positive neurons having greater rheobase values than control. Thus, while greater numbers of c-Fos negative neurons would be desirable to more confidently probe these results, they suggest two points. First, that it is the c-Fos negative cells undergoing plasticity to become more excitable rather than c-Fos positive cells becoming less excitable. Second, the increase in excitability in c-Fos negative cells is greatest immediately following deprivation, indicating that these cells are potentially undergoing plasticity to help homeostatic recovery of activity. Examination of current density across the same time course was less informative, with no significant differences observed between any groups (Fig. 4.15b). Again, greater numbers of inactive cells would help elucidate exactly how differences in excitability are altering across time.

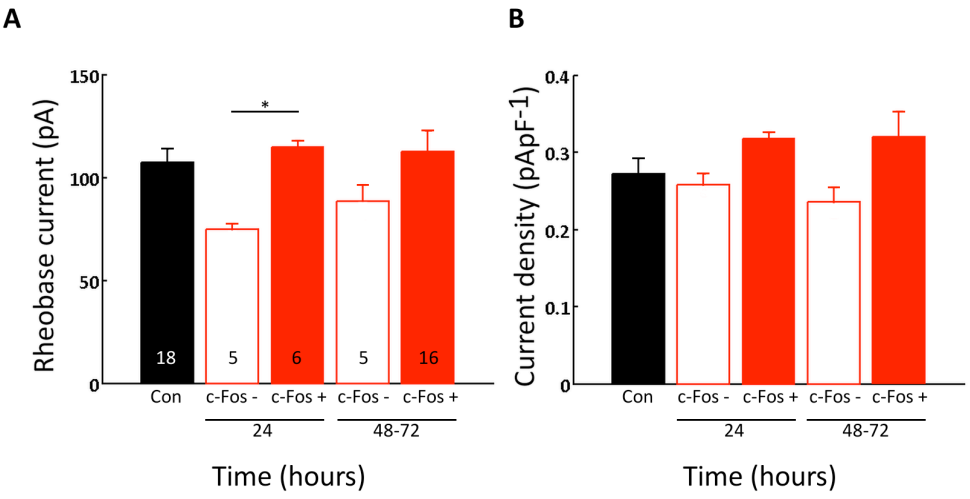

Figure 4.15 Excitability is increased in c-Fos negative neurons at 24 hours post-deprivation.

A, Mean rheobase in control (c-Fos positive, black), c-Fos positive (filled bars) and c-Fos negative neurons (open bars) at initial (24 hr) and late (48-72 hr) post deprivation stages; $p = 0.043$, Kruskal-Wallis one-way ANOVA on ranks. Pairwise comparisons with Bonferroni correction for 5x2 comparisons ($\alpha = 0.05/10 = 0.005$) between control and (24h) c-Fos-, $p = 0.014$; c-Fos+, $p = 0.537$; (48-72h) c-Fos-, $p = 0.187$; c-Fos+, $p = 0.931$; (24h) c-Fos- versus c-Fos+, $p = 0.004$. $p > 0.005$ for all other comparisons. Comparisons were performed with Mann-Whitney rank sum tests between pairs. **B,** Mean current density in control (c-Fos positive, black), c-Fos positive (filled bars) and c-Fos negative neurons (open bars) at initial (24 hr) and late (48-72 hr) post-deprivation stages; $p = 0.226$, Kruskal-Wallis one-way ANOVA on ranks.

Table 4.6 Animal numbers for each condition in experiments in Chapter 4

	Number of animals					
	Control (Time/hours)			Deprived (Time/hours)		
Experiment	24	48	72	24	48	72
Electrophysiology	4	6	4	6	6	5

Summary

In the present chapter, I have described both synaptic and intrinsic responses of layer 2/3 pyramidal neurons to monocular enucleation. Measures of intrinsic excitability and synaptic properties in individual neurons revealed that, in control conditions, there is a relationship between how much putative synaptic input a cell receives and how much current is needed to excite the cell. Cells receiving greater synaptic input require more current to elicit AP firing. To the best of my knowledge, this is the first time that this relationship has been demonstrated in individual cells in a mammalian system. While previous study has shown that active cells receive more excitatory drive, and show reduced excitability (Yassin et al., 2010), in the present experiments, I do not find differences in synaptic or intrinsic properties of putatively active and inactive neurons. This could be due to differences in the labelling methods of c-Fos, while here I used post-hoc antibody labelling, Yassin et al., use a transgenic mouse line to label c-Fos expressing cells. It is possible that there are differences in the sensitivity of c-Fos detection between the two techniques. Differences could also arise from study of different brain regions, and different developmental ages of study.

In contrast to previous studies (Maffei & Turrigiano, 2008; Maffei et al., 2004), I did not find alterations to the synaptic input measured following deprivation. Additionally, the current data does not provide information on the levels of inhibition received by the recorded neurons, thus preventing examination of the E/I ratio in these cells. Furthermore, the use of mPSCs as a proxy for synaptic number and strength should be used cautiously since the roles of presynaptic factors such as release probability and vesicle filling are unknown in the present experiments and alterations to these factors are also likely to influence mPSC parameters. While no overall changes are observed when comparing distinct synaptic and intrinsic factors in control versus deprived, there are significant alterations to the relationships between the synaptic and intrinsic factors measured. Following deprivation, cells with putatively stronger inputs (higher

mPSC amplitude), are now more excitable. Furthermore, it appears that it is c-Fos negative, putatively inactive, neurons that are undergoing plasticity, as these cells show increased excitability compared to their active counterparts. In the first 24 hours following deprivation, there is a reduction in c-Fos positive cell density. Thus, the heightened excitability in c-Fos negative cells may be a means of recruiting these cells to become active and integrate into the recovering circuit. However, further study chronically following the activity of individual neurons would be needed to confirm this. This would help to address exactly what the post-deprivation population of c-Fos negative neurons are made up of, i.e. silent pre-deprivation, or fallen silent following deprivation.

In the present experiments, following deprivation, I did not observe the same increase in excitability that was observed previously, in chapter 3. One of the possible explanations for this is the difference of light-dark cycles that animals were kept in across the two experiments. Both sets of animals were kept in 12 hour light-dark cycles. However, experiments in chapter 3 were performed during the animals' light period, while experiments in the present chapter were performed during the animals' period of darkness. Circadian rhythms in diurnal animals such as mice, are driven by pacemaker cells in the suprachiasmatic nucleus (SCN), which are in turn responsive to light exposure (Dijk and Archer, 2009). As well as regulating numerous behavioural activities, circadian rhythms have also been shown to regulate neuronal excitability (Herzog, 2007). Rhythmic cycles of intracellular Ca^{2+} have been reported in the SCN (Colwell, 2000; Ikeda et al., 2003), and exposure to light has been shown to alter the neuronal excitability of SCN neurons also (LeSauter et al., 2011). Thus, it is possible that circadian rhythms are interacting with the deprivation causing the differential results observed between the two chapters.

Chapter 5: AIS and intrinsic plasticity in regular spiking cortical inhibitory neurons

Introduction

In the field of homeostatic plasticity, there has been extensive work into the mechanisms occurring in excitatory neurons. Much less is known about homeostatic plasticity occurring within GABAergic inhibitory neurons. In particular, the regular spiking population of inhibitory neurons remain far less studied than the proportionally larger group of fast-spiking, parvalbumin expressing interneurons. Recently however, it has been shown that a subset of regular spiking GAD65-GFP inhibitory neurons carry dendritic spines, and that, following deprivation, these dendrites undergo structural remodelling (Keck et al., 2011). Whether or not this is the only form of plasticity expressed by these neurons remains unclear. Thus, in this chapter of work, I examine whether GAD65-GFP inhibitory neurons undergo other forms of plasticity following activity deprivation.

In this chapter, I shall examine two forms of plasticity in the regular spiking population of layer 2/3 inhibitory neurons. I shall first determine whether these neurons undergo AIS plasticity. Earlier in this thesis, I examined AIS plasticity in layer 2/3 pyramidal neurons, and found a mismatch between the structural and functional changes observed. I shall examine if the GAD65-GFP inhibitory neurons also show this mismatch between structure and function, or whether in these neurons, the AIS might be more reflective of intrinsic excitability. Thus, I shall also explore the functional consequences that deprivation may have on the excitability of the regular spiking inhibitory neurons. Little is known about the AIS of inhibitory neurons and only a single study has described AIS plasticity in inhibitory neurons (Chand et al., 2015). This study examined dopaminergic neurons in dissociated cultures of the olfactory bulb, and observed both lengthening and a proximal relocation of the AIS in response to chronic

depolarisation. However, high variability in both structural and functional parameters meant that a definitive connection between the two could not be made. Whether or not cortical inhibitory neurons might undergo AIS plasticity is unknown, and is thus, what I shall address in the following chapter of work.

Results

To examine plasticity in cortical GABAergic neurons, I used a transgenic mouse line, GAD65-GFP, where a subset of regular spiking inhibitory neurons express GFP under the GAD65 promoter. Plasticity was induced during the critical period (for full details see methods, enucleation or control anaesthesia occurred at p23) via monocular enucleation. Animals were sacrificed at three time points (24, 48 and 72 hours) following deprivation and brains were removed and fixed in 1% PFA overnight. Coronal slices containing the monocular visual cortex of the contralateral hemisphere to enucleation were taken and immunostained with an antibody against AnkG to label the AIS. Since this study was performed during the critical period, and there has been evidence that AIS length is altered during development (Gutzmann et al., 2014), I first checked to see if the length and position of the AIS in GAD65-GFP neurons varied across the three ages used in the time course of this study. Thus, I compared the length and position of the AIS in control conditions at 24, 48 and 72 hours after control anaesthesia to see if developmental age had any effect on the AIS. Both length and starting position were consistent across the three different ages used as 24, 48 and 72 hour time points (Fig. 5.1a). Thus, data from the three time points were pooled to create one control group for subsequent comparisons with the deprived condition. There was no correlation between the length of the AIS and its starting position along the axon (Fig. 5.1b).

Following deprivation AIS length but not position of the AIS in GAD65-GFP neurons is altered

I looked to see how AIS length and position of GAD65-GFP neurons might be affected by activity deprivation. At 24 hours post deprivation, the AIS was significantly longer than in control, by approximately 20% (Fig. 5.2a,b). In contrast, at 48 hours post deprivation, mean AIS length was approximately 15% shorter than in control. At 72 hours post deprivation, AIS length was equivalent to control length. No significant change in AIS position was seen at any time point.

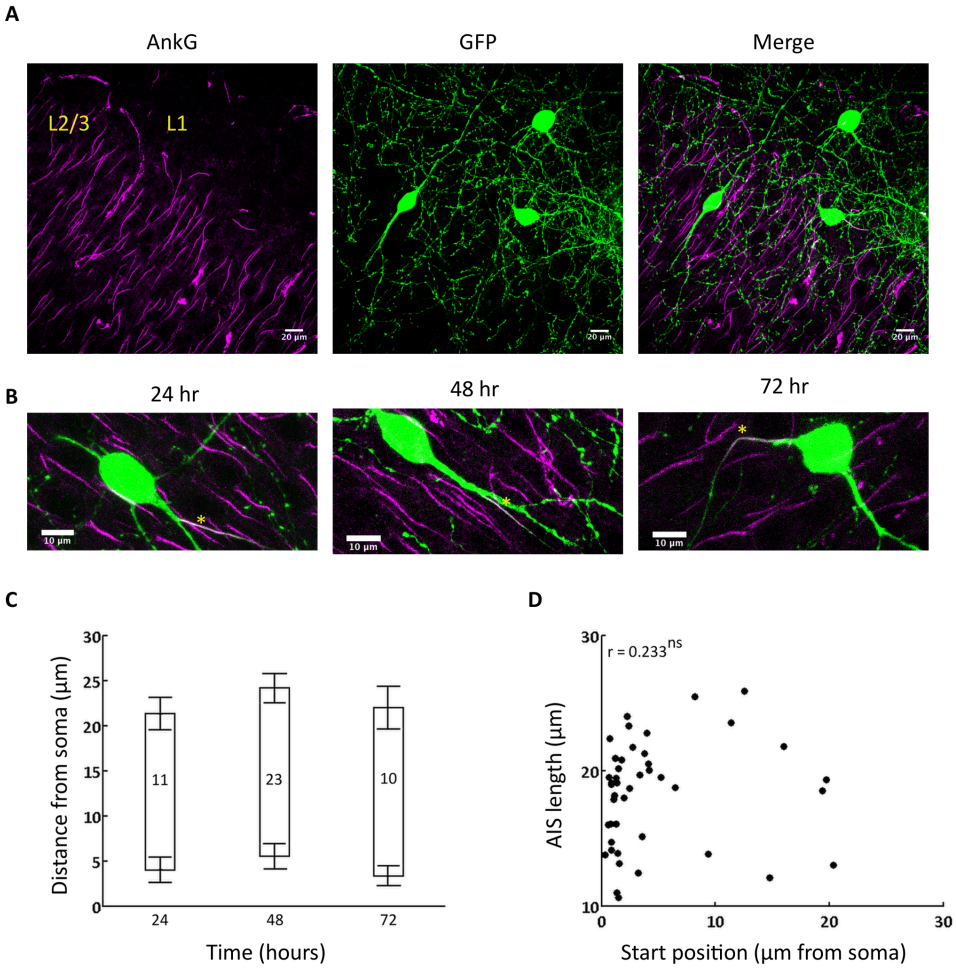

Figure 5.1 The AIS of GAD65-GFP neurons does not alter over the developmental time course of this study.

A, Example images of a portion of monocular visual cortex taken from a GAD65-GFP slice and stained for AnkG. The clear separation between layer 1 and layers 2/3 can be observed by the lack of parallel AISs visible in layer 1. **B,** Example images of three control GAD65-GFP neurons and their labelled AISs, indicated by yellow asterisks, at the different time points in control. **C,** AIS length and positions of GAD65-GFP neurons at three time points following control anaesthesia. Bottom and top edges of bar indicate mean start and end position of the AIS in relation to cell soma respectively. Mean start position: 24 hr, 4 ± 1.5µm; 48 hr, 5.5 ± 1.4µm; 72 hr, 3.3 ± 1.2µm, p = 0.981, Kruskal-Wallis ANOVA on ranks. Mean AIS length: 24 hr, 17.3 ± 1.2µm; 48 hr, 18.6 ± 0.8µm; 72 hr, 18.6

± 1.5; p = 0.634, one-way ANOVA. Numbers in bars indicate the number of AISs measured. **D,** Scatter plot of AIS start position and length; p = 0.127, Spearman's rank order correlation, n = 44. Error bars indicate s.e.m.

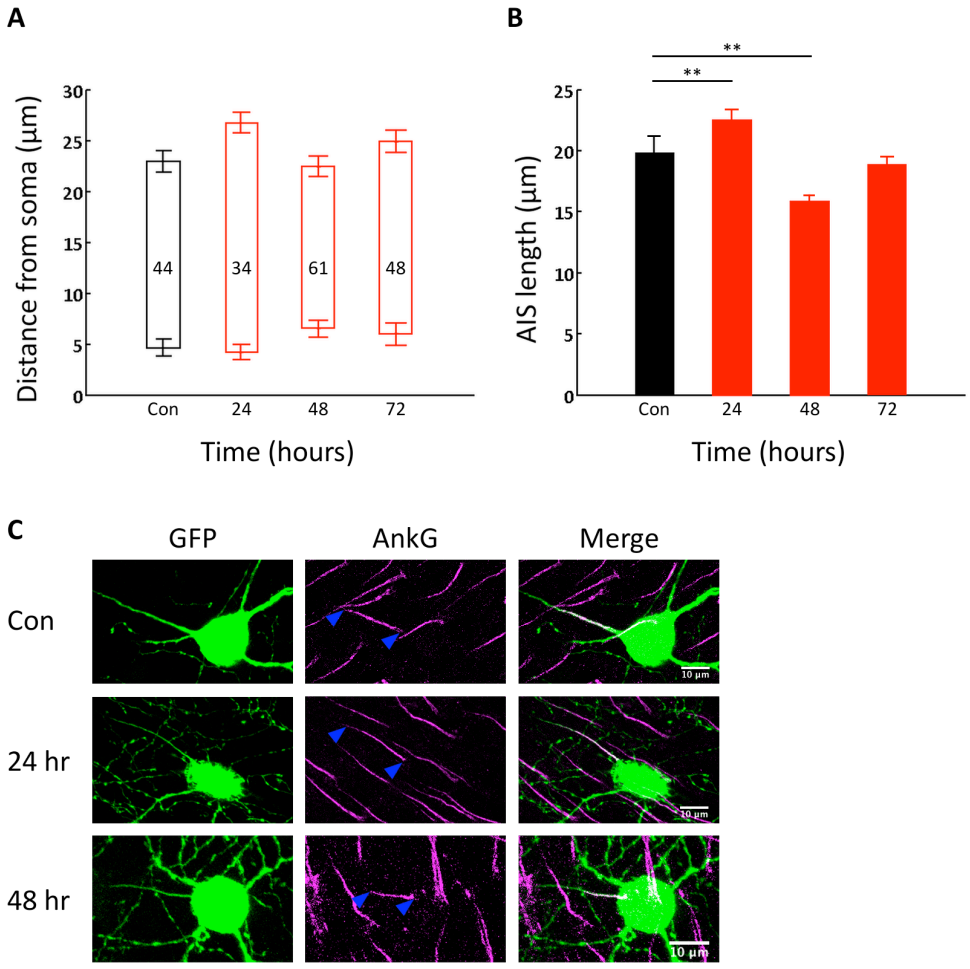

Figure 5.2 Following deprivation the AIS of GAD65-GFP neurons undergoes plasticity.

A. AIS length and position in GAD65-GFP neurons in control and deprived conditions. Mean start position: control, 4.6 ± 0.9 µm; deprived (24 hr) 4.7 ± 1 µm, (48 hr) 6.5 ± 0.8 µm, (72 hr) 6 ± 1.1 µm. p = 0.124, Kruskal-Wallis one-way ANOVA on ranks. **B,** Mean AIS length in control, 18.3 ± 0.6 µm, and deprived, (24 hr) 21.8 ± 1 µm, p = 0.002, (48 hr) 15.9 ± 0.5 µm, p = 0.009, (72 hr) 18.9 ± 0.6 µm, p = 0.999, Kruskal-Wallis one way ANOVA on ranks, with Dunn's post hoc test (versus control). **C,** Example images of GAD65-GFP AIS in control (top), and 24 (middle) and 48 (bottom) hours post deprivation. Blue arrowheads indicate start and end of AIS. **p < 0.01. Error bars indicate s.e.m.

Compared to the AIS plasticity observed in pyramidal neurons across this same developmental window, the AIS appears to be much more dynamic in the inhibitory population, with first lengthening and then shortening occurring in response to activity deprivation. This may reflect either a different mechanism of plasticity between inhibitory and excitatory neurons, or it possible that the inhibitory plasticity observed is from a mixture of inhibitory subtypes undergoing different responses. While the GAD65-GFP transgenic line labels regular-spiking inhibitory neurons, there are several different molecular subtypes of neurons labelled in this line (López-Bendito et al., 2004).

Deprivation does not alter the intrinsic excitability of GAD65-GFP neurons

To determine whether these structural alterations might have any functional effect on the neurons I targeted whole-cell patch clamp recordings to GAD65-GFP positive cells and recorded measures of excitability in these neurons. Although plasticity was observed at both 24 and 48 hours post deprivation, I decided to focus on the 48 hour time-point where the observed plasticity matched what was first observed in pyramidal neurons at the same time. Thus, the effects of having a shortened AIS on the two different neuron types could be compared. Acute slices were prepared from juvenile mice that had undergone either enucleation or control anaesthesia 48 hours prior (see methods). GAD65-GFP neurons in layer 2/3 of the monocular visual cortex were targeted using LED fluorescence to identify GFP expressing neurons (Fig. 5.3a). Somatic current injections were applied to determine the action potential threshold and to measure passive membrane properties (Fig. 5.3). In contrast to what was seen in excitatory neurons, the GAD65-GFP inhibitory neurons did not show an increase in excitability at 48 hours post deprivation. Although there was an increase in input resistance (Fig. 5.3c), this did not translate to increase excitability via rheobase (current necessary to elicit a single AP; Fig. 5.3d) or current density measure (Fig. 5.3e). Furthermore, AP voltage threshold and AP height were not different in deprived neurons compared to control. Maximum rate of rise (dV/dt) was not different in the two conditions, and neither was membrane time constant (Table 5.1).

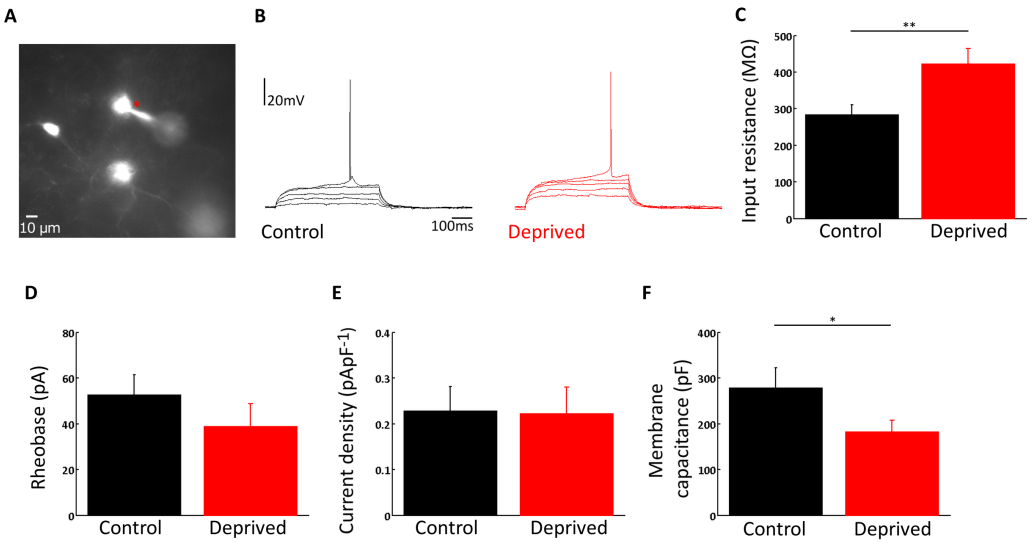

Figure 5.3 Intrinsic excitability does not change in GAD65-GFP neurons after monocular deprivation.

A, Image of GAD65-GFP neurons in a slice. Red asterisk indicates neuron with pipette attached. **B,** Example traces of increasing somatic current injections (0-50pA) in a control (black) and deprived (red) neuron. **C,** Mean input resistance in control, 285 ± 25 MΩ and deprived, 424 ± 39 MΩ; p = 0.008, two-sample t-test. **D,** Mean rheobase in control, 53 ± 8 pA and deprived, 39 ± 10 pA; p = 0.157, Mann-Whitney rank sum. **E,** Mean current density in control, 0.23 ± 0.05 $pApF^{-1}$, and deprived, 0.22 ± 0.05 $pApF^{-1}$, Mann-Whitney rank sum. **F,** Mean membrane capacitance in control, 279 ± 41 pF, and deprived, 183 ± 24 pF; p = 0.046, Mann-Whitney rank sum. *p < 0.05, **p < 0.01. Error bars indicate s.e.m.

Table 5.1 Membrane properties of GAD65-GFP neurons

	Control (n = 11)	Deprived (n = 12)	P-value
Vm (mV)	-62 ± 1	-62 ± 1	0.797
Membrane time constant (ms)	77 ± 8	70 ± 6	0.474
Max dV/dt (V/s)	10 ± 1	11 ± 2	0.455
AP threshold (mV)	-40 (-42 – -37)	-42 (-45 – -36)	0.340
AP height (mV)	58 ± 3	62 ± 5	0.500

Reported values are mean ± s.e.m. where a t-test was used for comparison, or median, with interquartile range in parentheses where a Mann-Whitney rank sum was used.

There was a significant decrease in membrane capacitance, in deprived neurons, (Fig. 5.3e), which is a potential cause for the increased input resistance. Unfortunately, recovery of the GAD65-GFP neurons that were recorded from was often unsuccessful, with the process of removing the pipette disrupting the membrane enough to cause loss of GFP. Of all the GAD65-GFP neurons recorded, only 3 were successfully recovered. Therefore, analysis of structural and functional data from individual neurons was not possible.

Heterogeneity within the GAD65-GFP population

One observation made during electrophysiological recordings was that, although all regular spiking neurons, there was significant variation in the spiking patterns of different GAD65-GFP neurons (Fig. 5.4). It is known that the GAD65-GFP transgenic line labels several different molecular subclasses of inhibitory neurons, including VIP, NPY and somatostatin expressing neurons (Keck et al., 2011; López-Bendito et al., 2004; Wierenga et al., 2010). With different pre- and post-synaptic partners, and different subcellular targets it is entirely plausible that different subgroups of GAD65-GFP inhibitory neurons undergo varying degrees and mechanisms of plasticity following activity deprivation. Given the high degree of plasticity seen in AIS lengths across 72 hours after deprivation, I decided to look at a single molecular population of GAD65-GFP neurons to see if their plasticity followed that of the general GAD65-GFP population. The subset of spiny neurons previously shown to undergo synaptic plasticity after activity deprivation is known to express the neuropeptide Y (NPY) (Keck et al., 2011). Therefore I chose to examine this subgroup of the GAD65-GFP population in more depth, to determine whether they also undergo AIS plasticity.

NPY expressing GAD65-GPF neurons have distinct AIS properties

In control mice, 42.5% of GAD65-GFP neurons expressed NPY (41 cells, 5 animals), and of these NPY positive neurons, 80% of neurons were spiny (Fig. 5.5).

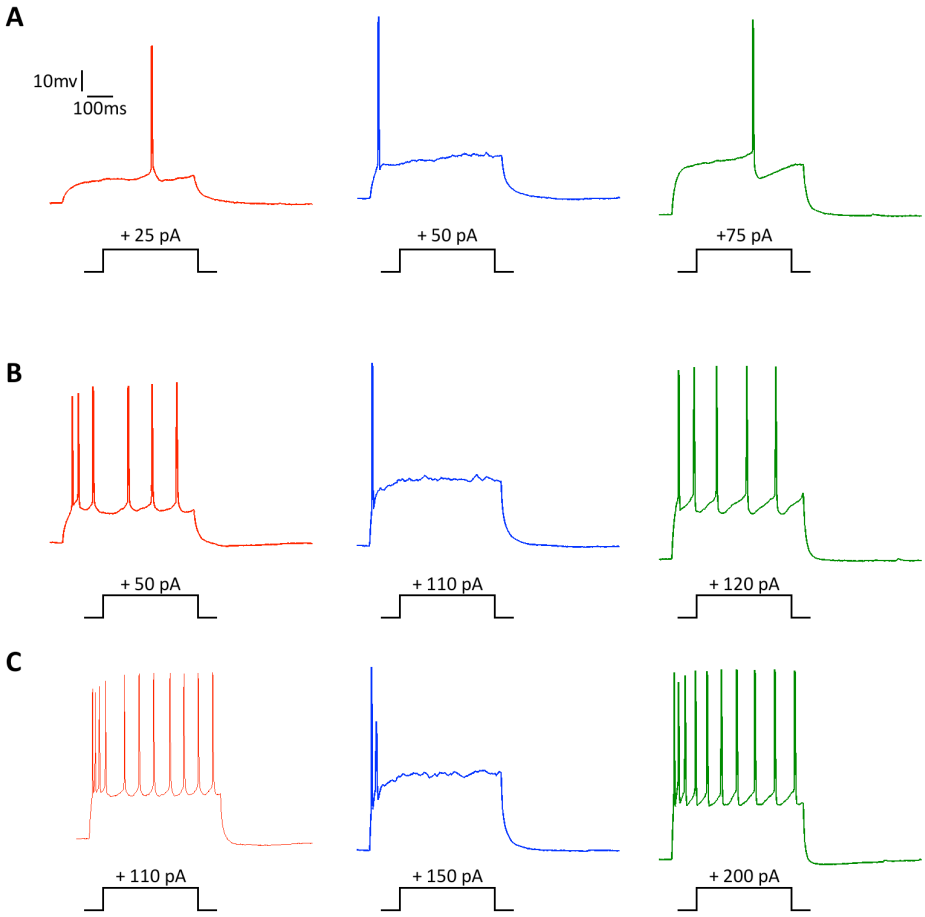

Figure 5.4 Heterogeneity in spiking properties of GAD65-GFP neurons.

Example traces from three different GAD65-GFP neurons, with each colour corresponding to a single neuron. **A,** Single spikes elicited by somatic injection of current close to AP threshold. **B,** Train of APs fired in response to medium stimulation by somatic current injection. **C,** High frequency train of APs in response to high somatic current injection.

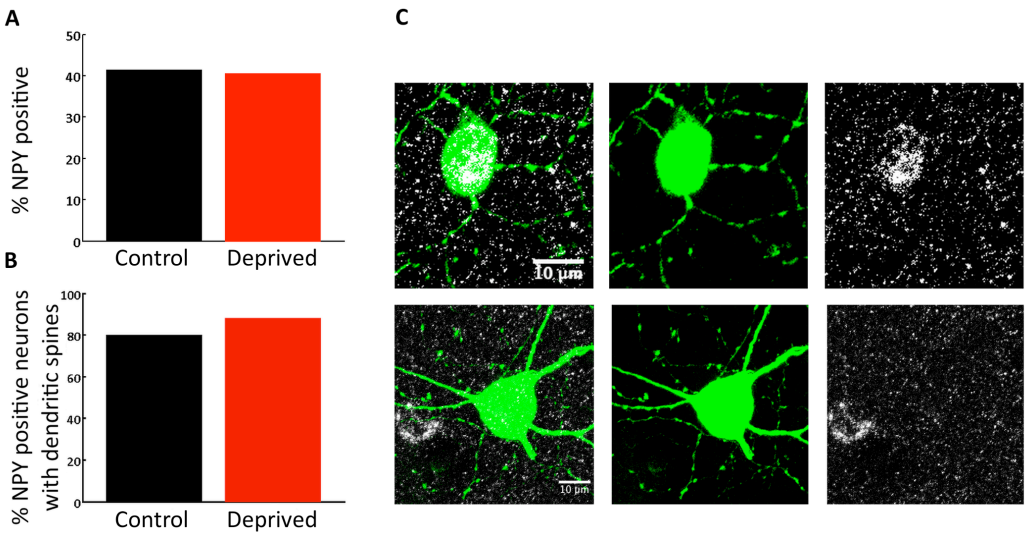

Figure 5.5 NPY expression in GAD65-GFP neurons.

A, Proportion of GAD65-GFP neurons showing NPY immunostaining presence. **B,** Proportion of NPY positive neurons with dendritic spines. **C,** Example images of an NPY positive (top row) and an NPY negative (bottom row) GAD65-GFP neuron.

The fraction of NPY positive neurons was similar following deprivation (40%), and here 88% of NPY expressing neurons also carried dendritic spines (n = 106 cells, 9 animals). I first looked to identify any NPY-subtype specific characteristics within the control GAD65-GFP expressing group of neurons. NPY positive neurons had a significantly more proximal AIS compared to NPY negative neurons (Fig. 5.6a-c). Meanwhile, the overall AIS length did not differ between NPY positive and NPY negative GAD65-GFP neurons. Although no difference in length, the more proximal start position indicates that there are subtype-specific features to the AIS, which may affect results when pooling all subgroups together.

Now that the specific characteristics of the AIS in the NPY subgroup had been defined, the effect of deprivation on these neurons was examined. The first time point after deprivation, 24 hours, suffered from low numbers of both NPY positive and negative cells, and thus, despite seeing a significantly more distal start position in NPY positive neurons at this time-point (Fig. 5.7a,b), compared to the control NPY positive neurons, this result should be treated with caution since this data is quite variable. Despite this, at 48 hours there is a trend towards a more distally located AIS. At 72 hours post-deprivation AIS position is comparable to control once again (Fig. 5.7b). Thus, these results suggest that there may be an initial AIS relocation, which then reverses over a period of 48-72 hours following deprivation. AIS length in the NPY positive GAD65-GFP neurons does not differ from control NPY positive neurons at any time point following deprivation. This contrasts with early examination of the general GAD65-GFP population, where a decrease in length was observed at 48 hours post-deprivation (Fig. 5.2a,b). Looking at the non-NPY GAD65-GFP neurons however, these still show a decrease in AIS length at this time-point, compared to the non-NPY controls (Fig. 5.8a). While there is a trend towards a longer AIS in the NPY negative neurons at 24 hours post-deprivation, as seen in the general population, this is not statistically significant. Similar to NPY positive neurons, at 72 hours post-deprivation, NPY negative neurons do not differ in AIS position or length from controls. It is possible that within the population of non-NPY

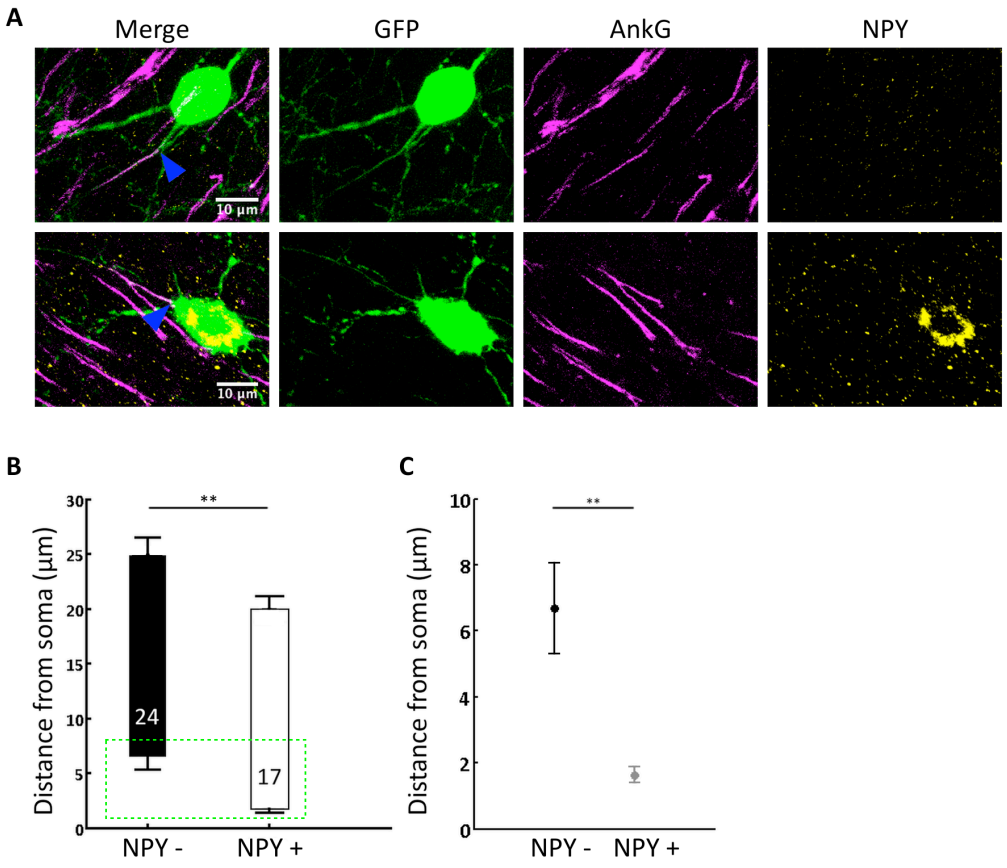

Figure 5.6 Distinct characteristics of NPY expressing GAD65-GFP neurons.

A, Example images of an NPY negative (top row) and an NPY positive (bottom row) GAD65-GFP neuron. Blue arrowhead indicates start of AIS. **B,** AIS length and position of NPY negative (filled) and NPY positive (unfilled) GAD65-GFP neurons. Bottom and top edges of bar indicate mean start and end position of AIS, respectively, in relation to the cell soma. Numbers in bar indicate the number of AISs measured. Mean AIS length in cells that are NPY negative, 18.3 ± 0.8 µm, and NPY positive, 18.3 ± 1 µm, p = 0.781, Mann-Whitney rank sum. **C**, Zoom of boxed region in **b**, showing mean AIS start position in NPY negative (black) and NPY positive (grey) neurons. Mean start position in cells that are NPY negative, 6.7 ± 1.4 µm, and NPY positive, 1.6 ± 0.3 µm, p = 0.004, Mann-Whitney rank sum. ** $p < 0.01$. Error bars indicate s.e.m.

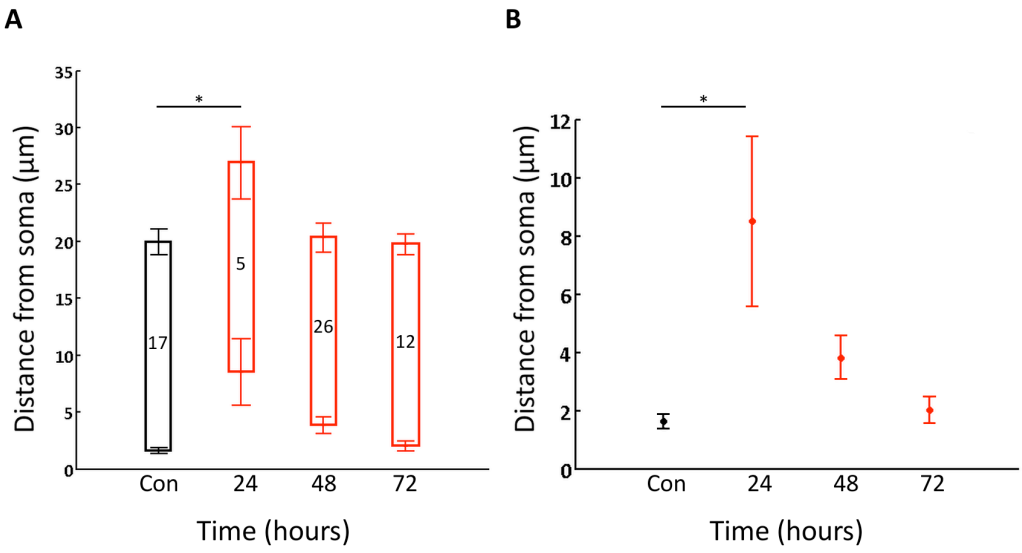

Figure 5.7 Deprivation causes a distal shift in the AIS, but does not affect length in NPY expressing GAD65-GFP neurons.

A, AIS length and position in control and following 24, 48 and 72 hours deprivation in NPY expressing GAD65-GFP inhibitory neurons. Bottom and top edges of bars indicate mean start and end AIS position respectively, in relation to the soma. N numbers within bars indicate number of AISs measured for each group. Mean AIS length in control, 18.3 ± 1 µm, and deprived (24 hr) 18.4 ± 0.9 µm, (48 hr) 16.5 ± 0.8 µm, (72 hr) 17.7 ± 0.9, p = 0.442 Kruskal-Wallis one-way ANOVA. **B,** Zoom in of AIS start position in NPY positive neurons. Mean start position in control, 1.6 ± 0.3 µm, and deprived, (24 hr) 8.5 ± 4.3 µm, p = 0.045, (48 hr) 3.8 ± 0.8 µm, p = 0.101, (72 hr) 2 ± 0.5 µm, p = 0.999, Kruskal-Wallis one-way ANOVA with Dunn's post hoc test. Error bars indicate s.e.m.

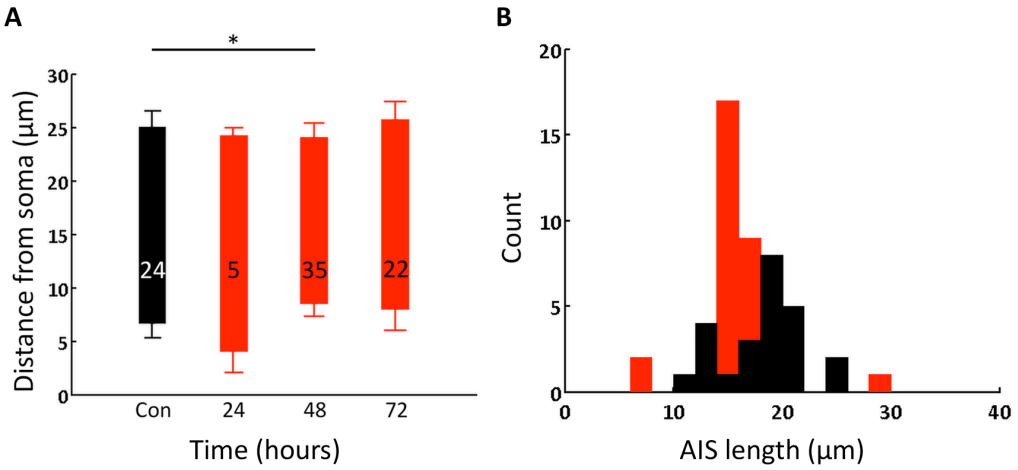

Figure 5.8 Deprivation causes a decrease in AIS length in non-NPY expressing GAD65-GFP neurons.

A, AIS length and position in control and following 24, 48 and 72 hours deprivation in non-NPY expressing GAD65-GFP inhibitory neurons. Mean start position in control, 6.7 ± 1.4 µm, and deprived (24 hr) 4.1 ± 2.2 µm, (48 hr) 8.5 ± 1.2 µm, (72 hr) 8 ± 2 µm, p = 0.430 Kruskal-Wallis ANOVA. Mean AIS length in control, 18.3 ± 0.8 µm, and deprived (24 hr) 22.5 ± 0.9 µm, p = 0.712, (48 hr) 15.9 ± 0.5 µm, p = 0.025, (72 hr) 18.9 ± 0.6 µm, p = 0.999, Kruskal-Wallis one-way ANOVA with Dunn's post hoc test, control versus enucleated. **B,** Histogram showing distribution of AIS lengths in NPY negative GAD65-GPF neurons in control (black), and at 48 hours post-deprivation (red). Error bars indicate s.e.m.

GAD65-GFP neurons there are further subgroups of inhibitory neurons that have specific AIS characteristics. Thus, the difference observed at 48 hours post-deprivation may be the result of plasticity, or it may be a result of further heterogeneity within the remaining GAD65-GFP population. In attempt to address this, I examined the distribution of lengths in control and at this deprived time point (Fig. 5.8b). While it is not possible to definitively rule out the possibility of having different subtypes of neurons showing different AIS characteristics, the deprived distribution does appear to be shifted towards the left, indicating that AIS shortening does generally occur in the non-NPY subset of GAD65-GFP inhibitory neurons.

Table 5.2 Animal numbers for conditions and experiments in Chapter 5

	Number of animals					
	Control (Time/hours)			Deprived (Time/hours)		
Experiment	24	48	72	24	48	72
Fixed AIS staining	3	2	2	5	4	5
Electrophysiology		5			8	

Summary

Here, I have shown that specific subtypes of cortical inhibitory neurons exhibit characteristic AIS features. In the regular-spiking population of GAD65-GFP neurons, NPY positive neurons, which largely expressed dendritic spines as previously reported (Keck et al., 2011), were found to have more proximally located AISs in comparison to the rest of the GAD65-GFP population. Previous work has demonstrated that the composition of channels at the AIS in cortical inhibitory neurons is different from cortical pyramidal neurons (Lorincz and Nusser, 2008). However, the AIS of distinct cortical subtypes of inhibitory neurons has not been studied before. Cortical inhibitory neurons have very diverse firing patterns, as demonstrated here and by others (Butt et al., 2005; Kawaguchi and Kubota, 1996; Miyoshi et al., 2007). The AIS is the site of AP generation in cortical inhibitory neurons (Li et al., 2014), and thus, the position of the AIS in different subtypes may be linked to their firing patterns. In the present study, I was unable to obtain direct measures of function and structure in individual neurons, however, to examine this.

Following activity deprivation via monocular enucleation, I found that inhibitory neurons underwent AIS plasticity in a subtype-specific manner. While NPY expressing GAD65-GFP neurons appeared to undergo a distal relocation of the AIS, followed by a subsequent relocation back to a control position, non-NPY GAD65-GFP neurons underwent a change in AIS length instead. Furthermore, the time course of changes were different between the two groups of neurons. AIS movement in the NPY positive neurons was observed at 24 hours post-deprivation. Meanwhile, non-NPY GAD65-GFP neurons underwent a transient decrease in AIS length at 48 hours post-deprivation, and AIS length had returned to the same length as control by the following 24 hours. Functional recordings from GAD65-GFP neurons did not show any change in excitability following deprivation. However, these recordings were collected from a mixed population of inhibitory neurons, and as demonstrated by the structural data, different subpopulations appear to be undergoing different forms of plasticity, and at different time points. Thus, a single subtype of inhibitory neurons should

be targeted in the future, when examining the effects of activity deprivation on inhibitory cell plasticity.

Chapter 6: Discussion

In this thesis, I have explored mechanisms of homeostatic plasticity, in both excitatory and inhibitory neurons in layers 2/3 of the mouse visual cortex. Despite heterogeneity hindering work in inhibitory neurons, a number of key findings were made exploring plasticity in pyramidal neurons. The aims of this thesis were first, to address AIS plasticity within the visual cortex, and secondly to address the employment and interactions of multiple homeostatic plasticity mechanisms. While AIS plasticity was observed, its functional implications were less clear, and questions remain as to exactly what role this form of plasticity might have in the regulation of activity levels following the loss of input in the present preparation. Investigation into different homeostatic plasticity mechanisms in individual neurons revealed a number of interesting correlations, both before and after the induction of plasticity.

Relationship between intrinsic excitability and synaptic inputs

In Chapter 4, I described a relationship between the amount of estimated synaptic input (mPSC frequency and amplitude), and the intrinsic excitability (current density) of pyramidal neurons in layer 2/3 of the juvenile mouse visual cortex (Fig. 6.1). This relationship suggests that cells receiving greater synaptic input would require more current to elicit an action potential. While such a relationship has been described before in the developing tectum of xenopus tadpoles (Pratt and Aizenman, 2007), it is the first time, to my knowledge, that this relationship has been shown in individual neurons in the mammalian cortex. Previous work in mammalian systems has been suggestive of such a relationship, for example Yassin et al., (2010) find a subset of cells with higher activity show both more synaptic input and reduced excitability in comparison to their lesser active counterparts. However, it has not been directly demonstrated at the level of the individual cell. In the present work, under normal control conditions, I do not find the activity status of a neuron to have

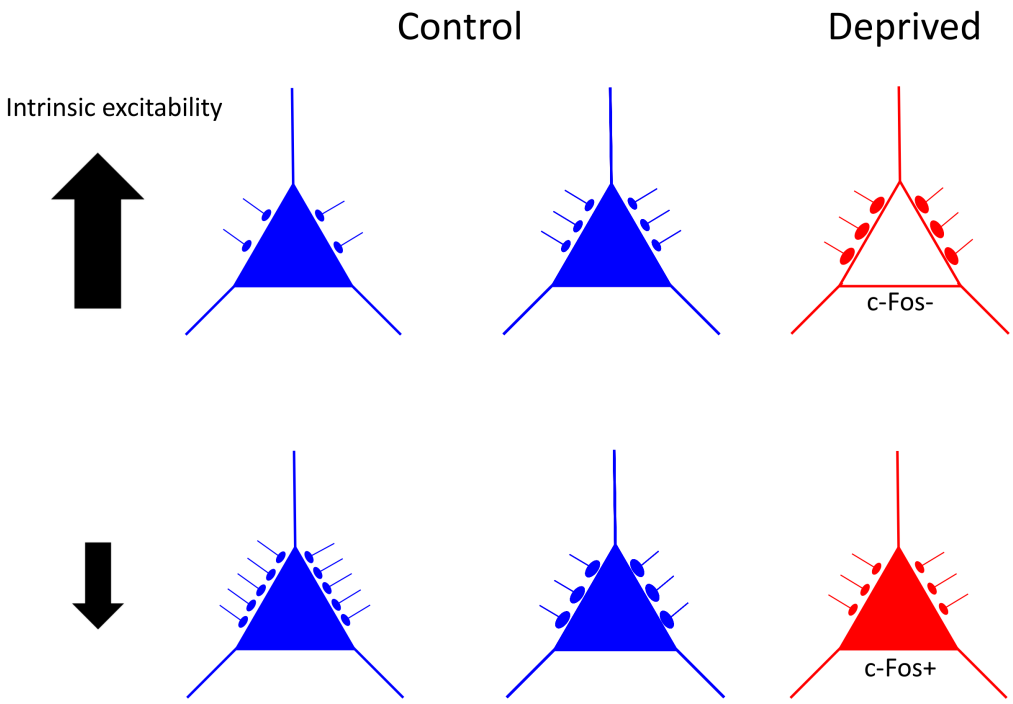

Figure 6.1 Schematic of the relationship between synaptic inputs and intrinsic excitability in control and deprived conditions.

Control neurons, in blue, with either putatively fewer synaptic inputs, or weaker synaptic inputs will have increased intrinsic excitability (top row, blue neurons), while neurons with more, or stronger inputs will have a reduced intrinsic excitability (bottom row, blue neurons). The activity status of the neuron in control does not have any effect on which of these scenarios applies. In contrast, following deprivation, neurons, in red, that are c-Fos negative tend to have stronger inputs, and a higher intrinsic excitability (top, red neuron). Meanwhile, c-Fos positive neurons have weaker synaptic inputs and a lower intrinsic excitability (bottom, red neuron).

any relationship to neuronal input or output. However, I do provide a direct demonstration that in individual neurons the level of synaptic input a cell receives is inversely associated with its level of intrinsic excitability. It is not known whether this relationship also exists in adulthood. However, as a developmental characteristic, this relationship may serve as a way to maintain stable activity levels within neurons, during a time of intense synaptic growth and organisation. In the adult following a large perturbation in activity, synaptic scaling is proposed as a way to regulate activity (Keck et al., 2013). However, during normal developmental conditions there may be smaller, transient imbalances of activity, caused by the dynamic refinement of synapses and circuits during the critical period. Altering the weight of all of a cells synapses in response to these changes in activity may disturb the on-going establishment of these synaptic connections, and as further new connections change and cause potentially more small imbalances, synaptic weights would need to change again. Thus, altering the intrinsic excitability of the neuron instead, may provide a more central, and effective way to regulate the activity of the cell that is less disruptive to the on-going synaptic organisation that is taking place during this window of development.

Following deprivation, I observed a number of different events. While not always manifested in the same way, it was apparent that there were changes to the intrinsic excitability of cells following enucleation. In the first set of experiments, in Chapter 3, I observed a decrease in intrinsic excitability following 2 days of deprivation, consistent with previous work (Desai et al., 1999; Lambo and Turrigiano, 2013; Maffei and Turrigiano, 2008). In the second set of experiments (Chapter 4), however, when simply comparing control and deprived neurons, no change in excitability was observed at any of the three time points studied post-deprivation. Breaking deprived neurons down into c-Fos positive and negative, however, revealed that c-Fos negative cells were more excitable than the c-Fos positive population of cells. This divergence between c-Fos positive and negative cells was a result of deprivation, as in control conditions, cells showed the same synaptic and intrinsic properties regardless of c-Fos presence. One explanation for the discrepancy in excitability

results is that, it is possible that the deprived dataset in the first set experiments contained an unusually high proportion of inactive neurons (cells in these experiments were not stained for c-Fos), which would bring up the average excitability of the group of neurons, or vice versa in the second experiments. However, given that at 48 hours following deprivation, when the first set of experiments was conducted, c-Fos levels have returned to control levels, this scenario is perhaps unlikely. The second possibility for the discrepancies between experiments is the switching of light-dark cycles between the two sets of experiments. The intrinsic excitability of neurons has been shown to be regulated by the circadian rhythm, as has the expression of numerous genes involved in neuronal function (Feng et al., 2007; Herzog, 2007; LeSauter et al., 2011). Thus, it is possible that this may have played a role in the differences observed between the two experiments.

Despite not seeing a direct increase in excitability following deprivation in the second series of experiments, I did find a complete reversal of the relationship between synaptic input and intrinsic excitability. Thus, there was a change in excitability in relation to the cells' inputs. Cells now with higher amplitude mPSC events, and thus putatively stronger synaptic inputs, were now more likely to fire APs, as reflected in their lower current density, than cells with weak inputs (Fig. 6.1). Coinciding with this change in relationship between synaptic inputs and excitability is a divergence of properties between putatively active and inactive neurons (determined by presence of c-Fos immunoreactivity). Inactive neurons become more excitable than active cells, and have increased mPSC amplitudes, indicating potentially stronger synapses. These properties reflect a potential employment of multiple homeostatic mechanisms in inactive neurons to restore their activity. While provisional, the time course of excitability changes between c-Fos positive and negative neurons showed the greatest difference to be at 24 hours post-deprivation, supporting the idea that an increase in excitability might drive the switch from inactive to active in cells, since c-Fos density returns to baseline at 48 hours post-deprivation. However, it should also be considered that, unless accompanied by synaptic changes, any increase in excitability might need to be retained in order to maintain elevated activity within a recovered cell. Owing to small numbers of cells in each group,

once the time course had been split up into active and inactive cells, changes in synaptic inputs across different times following deprivation were not well resolved. Further experiments to increase this dataset would no doubt enhance understanding of exactly how recovery might take shape.

Specificity of homeostatic response to deprivation paradigm

A number of differences were observed in the work of this thesis in comparison to previous work in the field of homeostatic plasticity. Firstly, several studies have reported synaptic scaling (Keck et al., 2013; Hengen et al., 2013; Desai et al., 2002; Lambo and Turrigiano, 2013) and alterations to mESPC frequency (Maffei and Turrigiano, 2008) following monocular deprivation. In the present work, following deprivation and comparing all neurons in a condition (i.e. regardless of activity status) I saw no changes to functional indicators of synaptic input in my mPSC recordings, and although these recordings do not conclusively target excitatory input alone, using a structural marker to address exclusively excitatory input, again I saw no change in dendritic spine density or size following deprivation, as has been previously described (Keck et al., 2008; Keck et al., 2013). Thus, overall following deprivation there does not appear to be a general population-wide alteration to the synaptic factors measured in the present work, contrasting with many literature reports (Keck et al., 2008; Keck et al., 2013; Hengen et al., 2013; Desai et al., 2002; Lambo and Turrigiano, 2013; Maffei and Turrigiano, 2008). Secondly, the timing of activity reduction following monocular deprivation contrasts with previous reports of study in juvenile rodents (Hengen et al., 2013). While in the present study c-Fos measurements suggest a reduction in activity after 24 hours of monocular deprivation, Hengen et al., (2013) report pyramidal cell activity to be reduced at 48 hours post deprivation. There are two factors that likely explain the contrast in results observed in this thesis, compared to previous literature; these are the age at which the study is carried out, and the activity deprivation paradigm used to induce plasticity. Differences between adult and juvenile studies may be the result of changing inhibition over the course of the critical period, when the present study was carried out. During the critical period, GABAergic circuitry is still forming and GABA concentrations are increasing (Huang et al., 1999; Wolff

et al., 1984). Thus, the influence of differential levels of inhibition at different stages of development may alter the outcome of synaptic homeostatic plasticity between adult and juvenile animals.

Several studies in juvenile rodents have reported changes to synaptic homeostatic changes following deprivation (Desai et al., 2002; Lambo and Turrigiano, 2013; Maffei and Turrigiano, 2008). While not all experiments have been carried out at exactly the same age during development, minor differences in the age of deprivation onset during the critical period have been shown to not exert differences on observed effects (Lambo and Turrigiano, 2013). However, the specific deprivation paradigm used, as highlighted by Maffei and Turrigiano (2008), has been shown to lead to different homeostatic responses taking place. This effect is almost certainly due to how different forms of deprivation affect activity patterns along the visual pathway. For example, eyelid suture, commonly used in monocular deprivation studies, (Hengen et al., 2013; Lambo and Turrigiano, 2013; Maffei and Turrigiano, 2008; Maffei et al., 2006) leaves the retina anatomically in tact. In this scenario, light is still able to pass through the eyelid and onto the retina, and thus, though objects will not be defined, the retina will still receive low contrast inputs. This form of deprivation does not result in a complete loss of activity, but rather, reduces visual drive and leads to uncorrelated activity at the level of the cortex (Frenkel and Bear, 2004; Wiesel and Hubel, 1965). In contrast, a second form of deprivation, intraocular TTX injection (Desai et al., 2002; Frenkel and Bear, 2004; Maffei and Turrigiano, 2008), reflects a more similar scenario to the monocular enucleation used in the present experiments. TTX injection strongly reduces visual drive onto LGN neurons (Rittenhouse et al., 1999; Stryker and Harris, 1986) by blocking any retinal discharge. One possible difference between intraocular injections and monocular enucleation is the immunological response that might be produced. However, Smith and Trachtenberg showed that pharmacological blockage of retinal transmission and monocular enucleation led to similar levels of activity in the cortex, and no pronounced injury artefact was observed more greatly in one technique over the other (Smith and Trachtenberg, 2007). Monocular enucleation completely removes all retinal input, either light-driven, or spontaneous, while TTX injection leaves both the retina and optic nerve

anatomically in tact. Thus, it is possible that following TTX injection, there may be some spontaneous release from the retina, although this would not be enough to produce an AP and further transmission along the visual pathway. In spite of this, monocular enucleation has been reported to be the most robust method for downregulation of activity dependent genes such as BDNF and c-Fos (Majdan and Shatz, 2006; Nys et al., 2015). Thus, while TTX injection and monocular enucleation are similar in their modes of action in reducing activity, there may be subtle differences in resultant activity levels or patterns between the two deprivation paradigms. Cortical activity is a dynamic process, influenced by intracortical interactions between excitation and inhibition (Isaacson and Scanziani, 2011), as well as thalamo-cortical communication, which in turn is influenced itself by the timing of cortical oscillatory phases (Briggs and Usrey, 2007). Thus, through manipulations that cause differential changes in activity at multiple targets along the visual pathway, a whole myriad of activity patterns can ultimately be produced by the time information reaches layer 2/3 of the cortex.

But how might different afferent activities lead to different homeostatic responses? First, the pattern of remaining activity is likely to affect exactly how the neuron responds to its loss of input. Following eyelid suture, the LGN and cortex still receive inputs from the occluded eye (Wiesel and Hubel, 1965). However, these inputs are now ill-defined patterns of light rather than structured, high contrast inputs. This decorrelated activity leads to LTD between LGN and cortical synapses (Heynen et al., 2003; Rittenhouse et al., 1999). In contrast, monocular inactivation via TTX injection produces less decorrelated activity, and thus, does not promote LTD (Frenkel and Bear, 2004). Instead, following TTX injection thalamo-cortical feedback is maintained (Weliky and Katz, 1999), producing spontaneous, synchronous bursting in the LGN, and thus, preventing LTD (Linden et al., 2009). Monocular enucleation therefore, also removing all retinal input and decorrelated activity, is also less likely to promote LTD in the cortex (Nys et al., 2015). Differential engagement of LTD following activity deprivation will mean that homeostatic mechanisms being implemented following alternate deprivation paradigms could be facing different E/I ratios upon initiation. Thus, there may be greater need to implement mechanisms in

certain cells over others. For example, a cell that has undergone large amounts of LTD at glutamatergic synapses will have had its excitatory drive significantly reduced, compared to a cell having undergone little or no LTD. Thus, a stronger homeostatic response may be required to bring its activity levels back to within a normal range.

Further, the activity occurring post-deprivation will influence the unmasking and strengthening of pre-existing connections (Eysel et al., 1999). Another factor to consider are the secondary inputs into the visual cortex. As well as visually evoked activity, the mouse visual cortex also receives inputs from other sensory modalities including auditory (Iurilli et al., 2012), motor (Andermann et al., 2011; Ayaz et al., 2013; Keller et al., 2012; Niell and Stryker, 2010; Saleem et al., 2013), and somatosensory areas (Charbonneau et al., 2012). The varying contributions of each of these inputs to a cell, as well as any unmasking or strengthening that may occur following visual deprivation will influence that cells activity levels, and may alter its E/I balance. This in turn may have an impact on the homeostatic response of the neuron. For example, a cell receiving relatively more input from another sensory modality may not experience as great a decrease in activity levels following visual deprivation than a cell receiving little or no secondary input. Thus, it may not necessarily need to engage in as strong a homeostatic response than a cell receiving little secondary input. Finally, as demonstrated by the present work, and that of others (Aizenman et al., 2003; Cudmore and Turrigiano, 2004; Pratt and Aizenman, 2007), under certain conditions intrinsic excitability is associated with, and can be regulated by, synaptic input. Thus, during developmental periods when intrinsic excitability has been shown to be plastic, any synaptic modifications undergone following deprivation may also influence changes in intrinsic excitability.

Furthermore, the present experiments did not allow for investigation of the E/I balance, which has been described to alter in response to deprivation both in the adult (Barnes et al., 2015a; Keck et al., 2013) and juvenile rodent (Desai et al., 2002; Lambo and Turrigiano, 2013; Maffei and Turrigiano, 2008). Future work detailing the balance between excitation and inhibition alongside intrinsic

excitability in individual neurons will provide great value to the present investigation, determining which neurons might undergo which forms of homeostatic plasticity.

Intrinsic plasticity in adult versus juvenile mice

One of the issues raised by this study, is the ability of the juvenile system to undergo changes in intrinsic excitability following activity deprivation. Making a direct comparison to work where the same activity deprivation paradigm, monocular enucleation, is performed during adulthood (Barnes et al., 2015a), I here find that either all, or a subset of neurons undergo increased excitability, something that does not occur in the adult animal. Why might juvenile animals be more susceptible to this form of plasticity? One possibility is that differential expression of channel or channel subunit isoforms between juvenile and adult mice might alter a neurons ability to undergo intrinsic excitability. For example, during early post-natal life the composition of NMDA receptors switches from a NR1/NR2B complex, to a NR1/NR2A complex, altering the kinetics of NMDA currents as it transitions (Liu et al., 2004). Similarly, AMPA receptors undergo a subunit transition during early post-natal life, altering their permeability to calcium (Kumar et al., 2002). Also during early development, there is a switch between $Na_v1.2$ and $Na_v1.6$ expression in the nodes of Ranvier (Kaplan et al., 2001). Two things might affect different channel or receptor isoforms ability to promote changes in excitability. First, direct alterations to the channels conductance could be variable between different subunits or isoforms. Alternatively, the second messenger pathways activated by channels or receptors of different compositions might be different, and this may determine whether or not a particular plasticity mechanism is triggered.

Another possibility for why intrinsic plasticity is prominent in development but not in adulthood might be that by the time a neuron has reached its full size in adulthood, a change in excitability is harder to generate due to the neuron having a greater capacitive load. Thus, the same changes in conductance may occur in juvenile and adult animals, but in the adult it does not result in a detectable change in excitability.

Recovery of activity

In the present dataset, the precise temporal resolution of activity recovery cannot be assessed. Equally, the precise level of activity in individual cells is not determinable from this dataset. While overall density of c-Fos positive neurons, and thus putatively active neurons, returns to baseline levels following 48 hours deprivation the actual activity levels of these neurons, and ultimately the network as a whole is unknown. Furthermore, the activity profile of cells across time is unknown. Previous study in adult mice shows that following monocular enucleation, recovery of activity occurs in a subset of previously active neurons, with very little recruitment of previously inactive cells, and the cells that were recruited following deprivation contributed little to overall network activity (Barnes et al., 2015a). It is possible that during development, when circuits are less well-established, there is greater potential for recruitment of new cells to aid activity recovery. In the juvenile rat following eyelid suture, *in vivo* multielectrode recordings have indicated that the recovery of firing rates is due to the recovery of single previously active units, though this cannot be confirmed using single unit recordings alone. Furthermore, whether monocular enucleation during development also causes specific recovery of previously active neurons remains unknown. Thus, chronic monitoring of individual cell activity, for example using two-photon imaging of a genetically encoded calcium indicator such as GCAMP, would greatly enhance interpretation of the present findings.

Functional implications of AIS plasticity in the mouse visual cortex

Structural analysis of the AIS did not correlate with functional readings of neuronal output in the present experiments, as has previously been reported (Grubb and Burrone, 2010; Kuba et al., 2010). In the inhibitory neurons, this might have been caused by differences in individual interneuron subtypes. I identified specific characteristics of AISs in NPY expressing GAD65-GFP neurons. However, I was not able to isolate this population in electrophysiology recordings. Clearly though, if the AIS does relate to functional output in

interneurons, it will be important to study this relationship in a non-heterogeneous population of cells. In spite of this, in layer 2/3 pyramidal neurons I did not observe any correlation between AIS length or position and any of the measured outputs of excitability. However, I did find a correlation, in control conditions, between AIS length and synaptic input strength. A relationship between AIS length and input has been described before, in the auditory cortex, where AIS length and position is dependent on the characteristic frequencies that the neuron receives (Kuba et al., 2006). Furthermore, potassium channels at the AIS have been shown to alter AP half-width and consequently, transmitter release in cortical pyramidal neurons (Kole et al., 2007) . Evidence is building for a more multifaceted role for the AIS in addition to simply signalling neuronal output (Kole and Stuart, 2012). Thus, in the visual cortex, where thus far the AIS has been little studied, it is possible that this structure reflects more than just a neurons' intrinsic excitability, but rather represents a more complex integration of excitability and synaptic input. I found that in control conditions there was an inverse relationship between both synaptic input and excitability, and synaptic input and AIS length, yet no direct correlation between AIS length and excitability. Following deprivation, the relationship between synaptic input and excitability was reversed, so that the two factors were positively correlated, and the association between synaptic input and AIS length was lost. What might cause the loss of relationship between synaptic input and AIS length? One hypothesis is that, the AIS is correlated to the specific balance of excitation and inhibition in a neuron, and that following deprivation this balance is altered. Alternatively, the AIS may be tuned specifically to local levels of synaptic input. Different subgroups of inhibitory neurons are known to target different compartments of the neuron. For example, PV basket cells target the soma of pyramidal neurons (Marin-Padilla, 1969), while axo-axonic chandelier cells form cartridges of boutons synapsing onto the AIS (Somogyi, 1977). Thus, it is also possible that overall levels of inhibition may remain balanced with excitation, but there may be a shift from one type of inhibition to another causing a spatial mismatch between the two. For example if inhibition shifted from being predominantly at the AIS, to now more heavily targeted at the soma instead, this might create a local imbalance of excitation and inhibition at the AIS. The AIS might respond to this by shortening,

in spite of the overall cell E/I remaining balanced, and thus, disrupting the relationship between synaptic inputs and AIS length.

Further speculations

The present work has provided further evidence that the engagement of homeostatic plasticity mechanisms is highly dependent on both the age at which activity manipulation occurs, and the specific paradigm of activity manipulation. In this particular study, I find that different cells may undergo differential responses to activity deprivation, with some cells engaging in a greater homeostatic response than others, suggesting a tailored homeostatic response for individual neurons. This contrasts with work in the adult, where all cells are seen to undergo a homeostatic decrease in inhibition, but the recovery of cells is thought to be dependent on the specific subnetwork within which a cell resides (Barnes et al., 2015a). While the present results suggest that neurons might be responding to their own individual activity levels, these individual responses could also have implications for the wider network. For example, perhaps certain cells are part of, or are recruited into a circuit involved in reorganisation. These cells might be triggered to undergo a greater homeostatic response, in order to drive this circuit more strongly, or be selected for recruitment into this circuit following the implementation of a certain level of homeostatic plasticity. Homeostatic plasticity, such as synaptic scaling in these neurons, may also make them more likely to undergo subsequent activity-dependent forms of plasticity that would further strengthen and consolidate these neurons into a new circuit. Meanwhile, cells not integrating into a reorganising circuit might undergo little or no homeostatic plasticity, and instead provide low-level basal activity to the general network. Thus, during development, the initial homeostatic plasticity response of a neuron, may determine its selection for the involvement of the future reorganised network. This hypothesis reflects a greater flexibility of the system during development. While in the adult, activity recovery is reliant on previously existing subnetworks, in development it is possible that due to the immature nature of cortical circuits there is greater scope for incorporating previously unrelated neurons into functional circuits.

References

Aizenman, C.D., Akerman, C.J., Jensen, K.R., and Cline, H.T. (2003). Visually Driven Regulation of Intrinsic Neuronal Excitability Improves Stimulus Detection In Vivo. Neuron *39*, 831–842.

Andermann, M.L., Kerlin, A.M., Roumis, D.K., Glickfeld, L.L., and Reid, R.C. (2011). Functional Specialization of Mouse Higher Visual Cortical Areas. Neuron *72*, 1025–1039.

Arckens, L., Van Der Gucht, E., Eysel, U.T., Orban, G.A., and Vandesande, F. (2000). Investigation of Cortical Reorganization in Area 17 and Nine Extrastriate Visual Areas through the Detection of changes in Immediate Early Gene expression as induced by retinal lesions. J. Comp. Neurol. *425*, 531–544.

Ascoli, G.A., Alonso-Nanclares, L., Anderson, S.A., Barrionuevo, G., Benavides-Piccione, R., Burkhalter, A., Buzsáki, G., Cauli, B., DeFelipe, J., Fairén, A., et al. (2008). Petilla Terminology: Nomenclature of Features of GABAergic Interneurons of the Cerebral Cortex. Nat. Rev. Neurosci. *9*, 557–568.

Ayaz, A., Saleem, A.B., Schölvinck, M.L., and Carandini, M. (2013). Locomotion Controls Spatial Integration in Mouse Visual Cortex. Curr. Biol. *23*, 890–894.

Baalman, K.L., Cotton, R.J., Rasband, S.N., and Rasband, M.N. (2013). Blast Wave Exposure Impairs Memory and Decreases Axon Initial Segment Length. J. Neurotrauma *30*, 741–751.

Barnes, S.J., Sammons, R.P., Jacobsen, R.I., Mackie, J., Keller, G.B., and Keck, T. (2015a). Subnetwork-Specific Homeostatic Plasticity in Mouse Visual Cortex In Vivo. Neuron *86*, 1290–1303.

Barnes, S.J., Cheetham, C.E., Liu, Y., Bennett, S.H., Albieri, G., Jorstad, A.A., Knott, G.W., and Finnerty, G.T. (2015b). Delayed and Temporally Imprecise Neurotransmission in Reorganizing Cortical Microcircuits. J. Neurosci. *35*, 9024–9037.

Bartley, A.F., Huang, Z.J., Huber, K.M., and Gibson, J.R. (2008). Differential Activity-Dependent, Homeostatic Plasticity of Two Neocortical Inhibitory Circuits. J. Neurophysiol. *100*, 1983–1994.

Bean, B.P. (2007). The Action Potential in Mammalian Central Neurons. Nat. Rev. Neurosci. *8*, 451–465.

Béïque, J.-C., Lin, D.-T., Kang, M.-G., Aizawa, H., Takamiya, K., and Huganir, R.L. (2006). Synapse-Specific Regulation of AMPA Receptor Function by PSD-95. Proc. Natl. Acad. Sci. *103*, 19535–19540.

Ben-Ari, Y. (2002). Excitatory Actions of Gaba During development: the Nature of the Nurture. Nat. Rev. Neurosci. *3*, 728–739.

Bliss, T.V., and Lomo, T. (1973). Long-Lasting Potentiation of Synaptic Transmission in the Dentate Area of the Anaesthetized Rabbit Following Stimulation of the Perforant Path. J. Physiol. *232*, 331–356.

Bliss, T.V.P., and Collingridge, G.L. (1993). A Synaptic Model of Memory: Long-Term Potentiation in the Hippocampus. Nature *361*, 31–39.

Branco, T., Staras, K., Darcy, K.J., and Goda, Y. (2008). Local Dendritic Activity Sets Release Probability at Hippocampal Synapses. Neuron *59*, 475–485.

Breton, J.-D., and Stuart, G.J. (2009). Loss of Sensory Input Increases the Intrinsic Excitability of Layer 5 Pyramidal Neurons in Rat Barrel Cortex. J. Physiol. *587*, 5107–5119.

Briggs, F., and Usrey, W.M. (2007). Cortical Activity Influences Geniculocortical Spike Efficacy in the Macaque Monkey. Front. Integr. Neurosci. *1*.

Burrone, J., O'Byrne, M., and Murthy, V.N. (2002). Multiple Forms of Synaptic Plasticity Triggered by Selective Suppression of Activity in Individual Neurons. Nature *420*, 414–418.

Butt, S.J.B., Fuccillo, M., Nery, S., Noctor, S., Kriegstein, A., Corbin, J.G., and Fishell, G. (2005). The Temporal and Spatial Origins of Cortical Interneurons Predict Their Physiological Subtype. Neuron *48*, 591–604.

Calford, M.B., Wang, C., Taglianetti, V., Waleszczyk, W.J., Burke, W., and Dreher, B. (2000). Plasticity in Adult Cat Visual Cortex (Area 17) Following Circumscribed Monocular Lesions of all Retinal Layers. J. Physiol. *524*, 587–602.

Chand, A.N., Galliano, E., Chesters, R.A., and Grubb, M.S. (2015). A Distinct Subtype of Dopaminergic Interneuron Displays Inverted Structural Plasticity at the Axon Initial Segment. J. Neurosci. *35*, 1573–1590.

Charbonneau, V., Laramée, M.-E., Boucher, V., Bronchti, G., and Boire, D. (2012). Cortical and Subcortical Projections to Primary Visual Cortex in Anophthalmic, Enucleated and Sighted Mice. Eur. J. Neurosci. *36*, 2949–2963.

Chino, Y.M., Smith, E.L., Kaas, J.H., Sasaki, Y., and Cheng, H. (1995). Receptive-Field Properties of Deafferentated Visual Cortical Neurons after Topographic Map Reorganization in Adult Cats. J. Neurosci. *15*, 2417–2433.

Clark, B.A., Monsivais, P., Branco, T., London, M., and Häusser, M. (2005). The Site of Action Potential Initiation in Cerebellar Purkinje Neurons. Nat. Neurosci. *8*, 137–139.

Collingridge, G.L., Peineau, S., Howland, J.G., and Wang, Y.T. (2010). Long-Term Depression in the CNS. Nat. Rev. Neurosci. *11*, 459–473.

Colwell, C.S. (2000). Circadian Modulation of Calcium Levels in Cells in the Suprachiasmatic Nucleus. Eur. J. Neurosci. *12*, 571–576.

Coombs, J.S., Curtis, D.R., and Eccles, J.C. (1957). The Interpretation of Spike Potentials of Motoneurones. J. Physiol. *139*, 198–231.

Cragg, B.G. (1967). The Density of Synapses and Neurones in the Motor and Visual Areas of the Cerebral Cortex. J. Anat. *101*, 639–654.

Cudmore, R.H., and Turrigiano, G.G. (2004). Long-Term Potentiation of Intrinsic Excitability in LV Visual Cortical Neurons. J. Neurophysiol. *92*, 341–348.

Darian-Smith, C., and Gilbert, C.D. (1995). Topographic Reorganization in the Striate Cortex of the Adult Cat and Monkey is Cortically Mediated. J. Neurosci. *15*, 1631–1647.

DeFelipe, J., López-Cruz, P.L., Benavides-Piccione, R., Bielza, C., Larrañaga, P., Anderson, S., Burkhalter, A., Cauli, B., Fairén, A., Feldmeyer, D., et al. (2013). New Insights into the Classification and Nomenclature of Cortical GABAergic Interneurons. Nat. Rev. Neurosci. *14*, 202–216.

Desai, N.S., Rutherford, L.C., and Turrigiano, G.G. (1999). Plasticity in the Intrinsic Excitability of Cortical Pyramidal Neurons. Nat. Neurosci. *2*, 515–520.

Desai, N.S., Cudmore, R.H., Nelson, S.B., and Turrigiano, G.G. (2002). Critical Periods for Experience-Dependent Synaptic Scaling in Visual Cortex. Nat. Neurosci. *5*, 783–789.

Dijk, D.-J., and Archer, S.N. (2009). Light, Sleep, and Circadian Rhythms: Together Again. PLoS Biol *7*, e1000145.

Evans, M.D., Sammons, R.P., Lebron, S., Dumitrescu, A.S., Watkins, T.B.K., Uebele, V.N., Renger, J.J., and Grubb, M.S. (2013). Calcineurin Signaling Mediates Activity-Dependent Relocation of the Axon Initial Segment. J. Neurosci. *33*, 6950–6963.

Eysel, U.T., Schweigart, G., Mittmann, T., Eyding, D., Qu, Y., Vandesande, F., Orban, G., and Arckens, L. (1999). Reorganization in the Visual Cortex after Retinal and Cortical Damage. Restor. Neurol. Neurosci. *15*, 153–164.

Fagiolini, M., and Hensch, T.K. (2000). Inhibitory Threshold for Critical-Period Activation in Primary Visual Cortex. Nature *404*, 183–186.

Fatt, P. (1957). Sequence of Events in Synaptic Activation of a Motoneurone. J. Neurophysiol. *20*, 61–80.

Feng, J., Fouse, S., and Fan, G. (2007). Epigenetic Regulation of Neural Gene Expression and Neuronal Function. Pediatr. Res. *61*, 58R – 63R.

Fong, M., Newman, J.P., Potter, S.M., and Wenner, P. (2015). Upward Synaptic Scaling is Dependent on Neurotransmission rather than Spiking. Nat. Commun. *6*.

Frenkel, M.Y., and Bear, M.F. (2004). How Monocular Deprivation Shifts Ocular Dominance in Visual Cortex of Young Mice. Neuron *44*, 917–923.

Fuortes, M.G.F., Frank, K., and Becker, M.C. (1957). Steps in the Production of Motoneuron Spikes. J. Gen. Physiol. *40*, 735–752.

Gainey, M.A., Hurvitz-Wolff, J.R., Lambo, M.E., and Turrigiano, G.G. (2009). Synaptic Scaling Requires the GluR2 Subunit of the AMPA Receptor. J. Neurosci. *29*, 6479–6489.

Giannikopoulos, D.V., and Eysel, U.T. (2006). Dynamics and Specificity of Cortical Map Reorganization after Retinal Lesions. Proc. Natl. Acad. Sci. *103*, 10805–10810.

Goel, A., and Lee, H.-K. (2007). Persistence of Experience-Induced Homeostatic Synaptic Plasticity through Adulthood in Superficial Layers of Mouse Visual Cortex. J. Neurosci. Off. J. Soc. Neurosci. *27*, 6692–6700.

Golowasch, J., Casey, M., Abbott, L.F., and Marder, E. (1999a). Network Stability from Activity-Dependent Regulation of Neuronal Conductances. Neural Comput. *11*, 1079–1096.

Golowasch, J., Abbott, L.F., and Marder, E. (1999b). Activity-Dependent Regulation of Potassium Currents in an Identified Neuron of the Stomatogastric Ganglion of the Crab Cancer Borealis. J. Neurosci. Off. J. Soc. Neurosci. *19*, RC33.

Goold, C.P., and Nicoll, R.A. (2010). Single-Cell Optogenetic Excitation Drives Homeostatic Synaptic Depression. Neuron *68*, 512–528.

Grubb, M.S., and Burrone, J. (2010). Activity-Dependent Relocation of the Axon Initial Segment Fine-Tunes Neuronal Excitability. Nature *465*, 1070–1074.

Gutzmann, A., Ergül, N., Grossmann, R., Schultz, C., Wahle, P., and Engelhardt, M. (2014). A Period of Structural Plasticity at the Axon Initial Segment in Developing Visual Cortex. Front. Neuroanat. *8*.

Hanover, J.L., Huang, Z.J., Tonegawa, S., and Stryker, M.P. (1999). Brain-Derived Neurotrophic Factor Overexpression Induces Precocious Critical Period in Mouse Visual Cortex. J. Neurosci. Off. J. Soc. Neurosci. *19*, RC40.

Hartman, K.N., Pal, S.K., Burrone, J., and Murthy, V.N. (2006). Activity-Dependent Regulation of Inhibitory Synaptic Transmission in Hippocampal Neurons. Nat. Neurosci. *9*, 642–649.

Harty, R.C., Kim, T.H., Thomas, E.A., Cardamone, L., Jones, N.C., Petrou, S., and Wimmer, V.C. (2013). Axon Initial Segment Structural Plasticity in Animal Models of Genetic and Acquired Epilepsy. Epilepsy Res. *105*, 272–279.

Hedstrom, K.L., Ogawa, Y., and Rasband, M.N. (2008). AnkyrinG is Required for Maintenance of the Axon Initial Segment and Neuronal Polarity. J. Cell Biol. *183*, 635–640.

Hendry, S.H., and Jones, E.G. (1986). Reduction in Number of Immunostained GABAergic Neurones in Deprived-Eye Dominance Columns of Monkey Area 17. Nature *320*, 750–753.

Hendry, S.H., Huntsman, M.M., Vinuela, A., Mohler, H., Blas, A. de, and Jones, E.G. (1994). GABAA Receptor Subunit Immunoreactivity in Primate Visual Cortex:

Distribution in Macaques and Humans and Regulation by Visual Input in Adulthood. J. Neurosci. *14*, 2383–2401.

Hengen, K.B., Lambo, M.E., Van Hooser, S.D., Katz, D.B., and Turrigiano, G.G. (2013). Firing Rate Homeostasis in Visual Cortex of Freely Behaving Rodents. Neuron *80*, 335–342.

Hensch, T.K. (2005). Critical Period Plasticity in Local Cortical Circuits. Nat. Rev. Neurosci. *6*, 877–888.

Hensch, T.K., Fagiolini, M., Mataga, N., Stryker, M.P., Baekkeskov, S., and Kash, S.F. (1998). Local GABA Circuit Control of Experience-Dependent Plasticity in Developing Visual Cortex. Science *282*, 1504–1508.

Herzog, E.D. (2007). Neurons and Networks in Daily Rhythms. Nat. Rev. Neurosci. *8*, 790–802.

Heynen, A.J., Yoon, B.-J., Liu, C.-H., Chung, H.J., Huganir, R.L., and Bear, M.F. (2003). Molecular Mechanism for Loss of Visual Cortical Responsiveness following brief Monocular Deprivation. Nat. Neurosci. *6*, 854–862.

Hou, Q., Zhang, D., Jarzylo, L., Huganir, R.L., and Man, H.-Y. (2008). Homeostatic Regulation of AMPA Receptor Expression at Single Hippocampal Synapses. Proc. Natl. Acad. Sci. *105*, 775–780.

Hu, T.-T., Laeremans, A., Eysel, U.T., Cnops, L., and Arckens, L. (2009). Analysis of c-fos and zif268 Expression Reveals Time-Dependent Changes in Activity Inside and Outside the Lesion Projection Zone in Adult Cat Area 17 after Retinal Lesions. Cereb. Cortex *19*, 2982–2992.

Huang, Z.J., Kirkwood, A., Pizzorusso, T., Porciatti, V., Morales, B., Bear, M.F., Maffei, L., and Tonegawa, S. (1999). BDNF Regulates the Maturation of Inhibition and the Critical Period of Plasticity in Mouse Visual Cortex. Cell *98*, 739–755.

Ibata, K., Sun, Q., and Turrigiano, G.G. (2008). Rapid Synaptic Scaling Induced by Changes in Postsynaptic Firing. Neuron *57*, 819–826.

Ikeda, M., Sugiyama, T., Wallace, C.S., Gompf, H.S., Yoshioka, T., Miyawaki, A., and Allen, C.N. (2003). Circadian Dynamics of Cytosolic and Nuclear Ca2+ in Single Suprachiasmatic Nucleus Neurons. Neuron *38*, 253–263.

Isaacson, J.S., and Scanziani, M. (2011). How Inhibition Shapes Cortical Activity. Neuron *72*, 231–243.

Iurilli, G., Ghezzi, D., Olcese, U., Lassi, G., Nazzaro, C., Tonini, R., Tucci, V., Benfenati, F., and Medini, P. (2012). Sound-Driven Synaptic Inhibition in Primary Visual Cortex. Neuron *73*, 814–828.

Jakawich, S.K., Nasser, H.B., Strong, M.J., McCartney, A.J., Perez, A.S., Rakesh, N., Carruthers, C.J.L., and Sutton, M.A. (2010). Local Presynaptic Activity Gates Homeostatic Changes in Presynaptic Function driven by Dendritic BDNF Synthesis. Neuron *68*, 1143–1158.

Jung, S.-C., and Hoffman, D.A. (2009). Biphasic Somatic A-Type K+ Channel Downregulation Mediates Intrinsic Plasticity in Hippocampal CA1 Pyramidal Neurons. PLoS ONE *4*, e6549.

Kaplan, M.R., Cho, M.-H., Ullian, E.M., Isom, L.L., Levinson, S.R., and Barres, B.A. (2001). Differential Control of Clustering of the Sodium Channels Nav1.2 and Nav1.6 at Developing CNS Nodes of Ranvier. Neuron *30*, 105–119.

Kawaguchi, Y., and Kondo, S. (2002). Parvalbumin, Somatostatin and Cholecystokinin as Chemical Markers for Specific GABAergic Interneuron Types in the Rat Frontal Cortex. J. Neurocytol. *31*, 277–287.

Kawaguchi, Y., and Kubota, Y. (1996). Physiological and Morphological Identification of Somatostatin- or Vasoactive Intestinal Polypeptide-Containing Cells among GABAergic Cell Subtypes in Rat Frontal Cortex. J. Neurosci. *16*, 2701–2715.

Keck, T., Scheuss, V., Jacobsen, R.I., Wierenga, C.J., Eysel, U.T., Bonhoeffer, T., and Hübener, M. (2011). Loss of Sensory Input Causes Rapid Structural Changes of Inhibitory Neurons in Adult Mouse Visual Cortex. Neuron *71*, 869–882.

Keck, T., Keller, G.B., Jacobsen, R.I., Eysel, U.T., Bonhoeffer, T., and Hübener, M. (2013). Synaptic Scaling and Homeostatic Plasticity in the Mouse Visual Cortex In Vivo. Neuron *80*, 327–334.

Keller, G.B., Bonhoeffer, T., and Hübener, M. (2012). Sensorimotor Mismatch Signals in Primary Visual Cortex of the Behaving Mouse. Neuron *74*, 809–815.

Kilman, V., van Rossum, M.C.W., and Turrigiano, G.G. (2002). Activity Deprivation Reduces Miniature IPSC Amplitude by Decreasing the Number of Postsynaptic GABAA Receptors Clustered at Neocortical Synapses. J. Neurosci. *22*, 1328–1337.

Kim, J., and Tsien, R.W. (2008). Synapse-Specific Adaptations to Inactivity in Hippocampal Circuits Achieve Homeostatic Gain Control while Dampening Network Reverberation. Neuron *58*, 925–937.

Knogler, L.D., Liao, M., and Drapeau, P. (2010). Synaptic Scaling and the Development of a Motor Network. J. Neurosci. Off. J. Soc. Neurosci. *30*, 8871–8881.

Kole, M.H.P., and Stuart, G.J. (2012). Signal Processing in the Axon Initial Segment. Neuron *73*, 235–247.

Kole, M.H.P., Letzkus, J.J., and Stuart, G.J. (2007). Axon Initial Segment Kv1 Channels Control Axonal Action Potential Waveform and Synaptic Efficacy. Neuron *55*, 633–647.

Kole, M.H.P., Ilschner, S.U., Kampa, B.M., Williams, S.R., Ruben, P.C., and Stuart, G.J. (2008). Action Potential Generation Requires a High Sodium Channel Density in the Axon Initial Segment. Nat. Neurosci. *11*, 178–186.

Kuba, H., Ishii, T.M., and Ohmori, H. (2006). Axonal Site of Spike Initiation Enhances Auditory Coincidence Detection. Nature *444*, 1069–1072.

Kuba, H., Oichi, Y., and Ohmori, H. (2010). Presynaptic Activity Regulates Na+ Channel Distribution at the Axon Initial Segment. Nature *465*, 1075–1078.

Kumar, S.S., Bacci, A., Kharazia, V., and Huguenard, J.R. (2002). A Developmental Switch of AMPA Receptor Subunits in Neocortical Pyramidal Neurons. J. Neurosci. *22*, 3005–3015.

Lambo, M.E., and Turrigiano, G.G. (2013). Synaptic and Intrinsic Homeostatic Mechanisms Cooperate to Increase L2/3 Pyramidal Neuron Excitability During a Late Phase of Critical Period Plasticity. J. Neurosci. Off. J. Soc. Neurosci. *33*, 8810–8819.

Lau, C.G., and Murthy, V.N. (2012). Activity-Dependent Regulation of Inhibition via GAD67. J. Neurosci. Off. J. Soc. Neurosci. *32*, 8521–8531.

LeMasson, G., Marder, E., and Abbott, L.F. (1993). Activity-Dependent Regulation of Conductances in Model Neurons. Science *259*, 1915–1917.

LeSauter, J., Silver, R., Cloues, R., and Witkovsky, P. (2011). Light Exposure Induces Short- and Long-Term changes in the Excitability of Retinorecipient Neurons in Suprachiasmatic Nucleus. J. Neurophysiol. *106*, 576–588.

Li, M., Jia, M., Fields, R.D., and Nelson, P.G. (1996). Modulation of Calcium Currents by Electrical Activity. J. Neurophysiol. *76*, 2595–2607.

Li, T., Tian, C., Scalmani, P., Frassoni, C., Mantegazza, M., Wang, Y., Yang, M., Wu, S., and Shu, Y. (2014). Action Potential Initiation in Neocortical Inhibitory Interneurons. PLoS Biol *12*, e1001944.

Linden, M.L., Heynen, A.J., Haslinger, R.H., and Bear, M.F. (2009). Thalamic Activity that Drives Visual Cortical Plasticity. Nat. Neurosci. *12*, 390–392.

Lissin, D.V., Gomperts, S.N., Carroll, R.C., Christine, C.W., Kalman, D., Kitamura, M., Hardy, S., Nicoll, R.A., Malenka, R.C., and Zastrow, M. von (1998). Activity Differentially Regulates the Surface Expression of Synaptic AMPA and NMDA Glutamate Receptors. Proc. Natl. Acad. Sci. U. S. A. *95*, 7097–7102.

Liu, X.-B., Murray, K.D., and Jones, E.G. (2004). Switching of NMDA Receptor 2A and 2B Subunits at Thalamic and Cortical Synapses during Early Postnatal Development. J. Neurosci. Off. J. Soc. Neurosci. *24*, 8885–8895.

López-Bendito, G., Sturgess, K., Erdélyi, F., Szabó, G., Molnár, Z., and Paulsen, O. (2004). Preferential Origin and Layer Destination of GAD65-GFP Cortical Interneurons. Cereb. Cortex *14*, 1122–1133.

Lorincz, A., and Nusser, Z. (2008). Cell-Type-Dependent Molecular Composition of the Axon Initial Segment. J. Neurosci. *28*, 14329–14340.

LoTurco, J.J., Owens, D.F., Heath, M.J.S., Davis, M.B.E., and Kriegstein, A.R. (1995). GABA and Glutamate Depolarize Cortical Progenitor Cells and Inhibit DNA Synthesis. Neuron *15*, 1287–1298.

Maffei, A., and Turrigiano, G.G. (2008). Multiple Modes of Network Homeostasis in Visual Cortical Layer 2/3. J. Neurosci. *28*, 4377–4384.

Maffei, A., Nelson, S.B., and Turrigiano, G.G. (2004). Selective Reconfiguration of Layer 4 Visual Cortical Circuitry by Visual Deprivation. Nat. Neurosci. *7*, 1353–1359.

Maffei, A., Nataraj, K., Nelson, S.B., and Turrigiano, G.G. (2006). Potentiation of Cortical Inhibition by Visual Deprivation. Nature *443*, 81–84.

Magee, J.C., and Johnston, D. (1997). A Synaptically Controlled, Associative Signal for Hebbian Plasticity in Hippocampal Neurons. Science *275*, 209–213.

Majdan, M., and Shatz, C.J. (2006). Effects of Visual Experience on Activity-Dependent Gene Regulation in Cortex. Nat. Neurosci. *9*, 650–659.

Marik, S.A., Yamahachi, H., Meyer zum Alten Borgloh, S., and Gilbert, C.D. (2014). Large-Scale Axonal Reorganization of Inhibitory Neurons following Retinal Lesions. J. Neurosci. *34*, 1625–1632.

Marin-Padilla, M. (1969). Origin of the Pericellular Baskets of the Pyramidal Cells of the Human Motor Cortex: a Golgi Study. Brain Res. *14*, 633–646.

Markram, H., Lübke, J., Frotscher, M., and Sakmann, B. (1997). Regulation of Synaptic Efficacy by Coincidence of Postsynaptic APs and EPSPs. Science *275*, 213–215.

Matsuzaki, M., Ellis-Davies, G.C.R., Nemoto, T., Miyashita, Y., Iino, M., and Kasai, H. (2001). Dendritic Spine Geometry is Critical for AMPA Receptor Expression in Hippocampal CA1 Pyramidal Neurons. Nat. Neurosci. *4*, 1086–1092.

Meeks, J.P., and Mennerick, S. (2007). Action Potential Initiation and Propagation in CA3 Pyramidal Axons. J. Neurophysiol. *97*, 3460–3472.

Miyoshi, G., Butt, S.J.B., Takebayashi, H., and Fishell, G. (2007). Physiologically Distinct Temporal Cohorts of Cortical Interneurons Arise from Telencephalic Olig2-Expressing Precursors. J. Neurosci. *27*, 7786–7798.

Niell, C.M., and Stryker, M.P. (2010). Modulation of Visual Responses by Behavioral State in Mouse Visual Cortex. Neuron *65*, 472–479.

Nys, J., Scheyltjens, I., and Arckens, L. (2015). Visual System Plasticity in Mammals: the Story of Monocular Enucleation-Induced Vision Loss. Front. Syst. Neurosci. *9*.

O'Brien, R.J., Kamboj, S., Ehlers, M.D., Rosen, K.R., Fischbach, G.D., and Huganir, R.L. (1998). Activity-Dependent Modulation of Synaptic AMPA Receptor Accumulation. Neuron *21*, 1067–1078.

O'Leary, T., van Rossum, M.C.W., and Wyllie, D.J.A. (2010). Homeostasis of Intrinsic Excitability in Hippocampal Neurones: Dynamics and Mechanism of the Response to Chronic Depolarization. J. Physiol. *588*, 157–170.

Owens, D.F., Boyce, L.H., Davis, M.B.E., and Kriegstein, A.R. (1996). Excitatory GABA Responses in Embryonic and Neonatal Cortical Slices Demonstrated by Gramicidin Perforated-Patch Recordings and Calcium Imaging. J. Neurosci. *16*, 6414–6423.

Palmer, L.M., and Stuart, G.J. (2006). Site of Action Potential Initiation in Layer 5 Pyramidal Neurons. J. Neurosci. *26*, 1854–1863.

Pratt, K.G., and Aizenman, C.D. (2007). Homeostatic Regulation of Intrinsic Excitability and Synaptic Transmission in a Developing Visual Circuit. J. Neurosci. *27*, 8268–8277.

Rannals, M.D., and Kapur, J. (2011). Homeostatic Strengthening of Inhibitory Synapses is Mediated by the Accumulation of GABA(A) Receptors. J. Neurosci. Off. J. Soc. Neurosci. *31*, 17701–17712.

Rasband, M.N. (2010). The Axon Initial Segment and the Maintenance of Neuronal Polarity. Nat. Rev. Neurosci. *11*, 552–562.

Rial Verde, E.M., Lee-Osbourne, J., Worley, P.F., Malinow, R., and Cline, H.T. (2006). Increased Expression of the Immediate-Early Gene arc/arg3.1 Reduces AMPA Receptor-Mediated Synaptic Transmission. Neuron *52*, 461–474.

Rittenhouse, C.D., Shouval, H.Z., Paradiso, M.A., and Bear, M.F. (1999). Monocular Deprivation Induces Homosynaptic Long-Term Depression in Visual Cortex. Nature *397*, 347–350.

Rivera, C., Voipio, J., Payne, J.A., Ruusuvuori, E., Lahtinen, H., Lamsa, K., Pirvola, U., Saarma, M., and Kaila, K. (1999). The K^+/Cl^- Co-Transporter KCC2 Renders GABA Hyperpolarizing during Neuronal Maturation. Nature *397*, 251–255.

Rudy, B., Fishell, G., Lee, S., and Hjerling-Leffler, J. (2011). Three Groups of Interneurons Account for nearly 100% of Neocortical GABAergic Neurons. Dev. Neurobiol. *71*, 45–61.

Rutherford, L.C., Nelson, S.B., and Turrigiano, G.G. (1998). BDNF Has Opposite Effects on the Quantal Amplitude of Pyramidal Neuron and Interneuron Excitatory Synapses. Neuron *21*, 521–530.

Sagar, S.M., Sharp, F.R., and Curran, T. (1988). Expression of c-fos Protein in Brain: Metabolic Mapping at the Cellular Level. Science *240*, 1328–1331.

Saleem, A.B., Ayaz, A., Jeffery, K.J., Harris, K.D., and Carandini, M. (2013). Integration of Visual Motion and Locomotion in Mouse Visual Cortex. Nat. Neurosci. *16*, 1864–1869.

Schüz, A., and Palm, G. (1989). Density of Neurons and Synapses in the Cerebral Cortex of the Mouse. J. Comp. Neurol. *286*, 442–455.

Shepherd, J.D., Rumbaugh, G., Wu, J., Chowdhury, S., Plath, N., Kuhl, D., Huganir, R.L., and Worley, P.F. (2006). Arc/Arg3.1 Mediates Homeostatic Synaptic Scaling of AMPA Receptors. Neuron *52*, 475–484.

Smith, S.L., and Trachtenberg, J.T. (2007). Experience-Dependent Binocular Competition in the Visual Cortex Begins at Eye Opening. Nat. Neurosci. *10*, 370–375.

Somogyi, P. (1977). A Specific "Axo-Axonal" Interneuron in the Visual Cortex of the Rat. Brain Res. *136*, 345–350.

Stellwagen, D., and Malenka, R.C. (2006). Synaptic Scaling Mediated by Glial TNF-α. Nature *440*, 1054–1059.

Stryker, M.P., and Harris, W.A. (1986). Binocular Impulse Blockade Prevents the Formation of Ocular Dominance Columns in Cat Visual Cortex. J. Neurosci. *6*, 2117–2133.

Stuart, G., and Häusser, M. (1994). Initiation and Spread of Sodium Action Potentials in Cerebellar Purkinje Cells. Neuron *13*, 703–712.

Stuart, G.J., and Sakmann, B. (1994). Active Propagation of Somatic Action Potentials into Neocortical Pyramidal Cell Dendrites. Nature *367*, 69–72.

Stuart, G., Schiller, J., and Sakmann, B. (1997). Action Potential Initiation and Propagation in Rat Neocortical Pyramidal Neurons. J. Physiol. *505 (Pt 3)*, 617–632.

Swanwick, C.C., Murthy, N.R., and Kapur, J. (2006). Activity-Dependent Scaling of GABAergic Synapse Strength is Regulated by Brain-Derived Neurotrophic Factor. Mol. Cell. Neurosci. *31*, 481–492.

Thiagarajan, T.C., Piedras-Renteria, E.S., and Tsien, R.W. (2002). alpha- and betaCaMKII. Inverse Regulation by Neuronal Activity and Opposing Effects on Synaptic Strength. Neuron *36*, 1103–1114.

Turrigiano, G. (2011). Too many cooks? Intrinsic and Synaptic Homeostatic Mechanisms in Cortical Circuit Refinement. Annu. Rev. Neurosci. *34*, 89–103.

Turrigiano, G. (2012). Homeostatic Synaptic Plasticity: Local and Global Mechanisms for Stabilizing Neuronal Function. Cold Spring Harb. Perspect. Biol. *4*, a005736.

Turrigiano, G.G., and Nelson, S.B. (2000). Hebb and Homeostasis in Neuronal Plasticity. Curr. Opin. Neurobiol. *10*, 358–364.

Turrigiano, G., Abbott, L.F., and Marder, E. (1994). Activity-Dependent Changes in the Intrinsic Properties of Cultured Neurons. Science *264*, 974–977.

Turrigiano, G.G., Leslie, K.R., Desai, N.S., Rutherford, L.C., and Nelson, S.B. (1998). Activity-Dependent Scaling of Quantal Amplitude in Neocortical Neurons. Nature *391*, 892–896.

Weliky, M., and Katz, L.C. (1999). Correlational Structure of Spontaneous Neuronal Activity in the Developing Lateral Geniculate Nucleus in Vivo. Science *285*, 599–604.

Wierenga, C.J., Ibata, K., and Turrigiano, G.G. (2005). Postsynaptic Expression of Homeostatic Plasticity at Neocortical Synapses. J. Neurosci. *25*, 2895–2905.

Wierenga, C.J., Müllner, F.E., Rinke, I., Keck, T., Stein, V., and Bonhoeffer, T. (2010). Molecular and Electrophysiological Characterization of GFP-Expressing CA1 Interneurons in GAD65-GFP Mice. PLoS ONE *5*, e15915.

Wiesel, T.N., and Hubel, D.H. (1965). Comparison of the Effects of Unilateral and Bilateral Eye Closure on Cortical Unit Responses in Kittens. J. Neurophysiol. *28*, 1029–1040.

Wolff, J.R., Böttcher, H., Zetzsche, T., Oertel, W.H., and Chronwall, B.M. (1984). Development of GABAergic Neurons in Rat Visual Cortex as Identified by Glutamate Decarboxylase-like Immunoreactivity. Neurosci. Lett. *47*, 207–212.

Wonders, C.P., and Anderson, S.A. (2006). The Origin and Specification of Cortical Interneurons. Nat. Rev. Neurosci. *7*, 687–696.

Yassin, L., Benedetti, B.L., Jouhanneau, J.-S., Wen, J.A., Poulet, J.F.A., and Barth, A.L. (2010). An Embedded Subnetwork of Highly Active Neurons in the Neocortex. Neuron *68*, 1043–1050.

Zhang, F., Vanduffel, W., Schiffmann, S.N., Mailleux, P., Arckens, L., Vandesande, F., Orban, G.A., and Vanderhaeghen, J.-J. (1995). Decrease of zif-268 and c-fos and Increase of c-jun mRNA in the Cat Areas 17, 18 and 19 Following Complete Visual Deafferentation. Eur. J. Neurosci. *7*, 1292–1296.

Zhao, C., Dreosti, E., and Lagnado, L. (2011). Homeostatic Synaptic Plasticity through Changes in Presynaptic Calcium Influx. J. Neurosci. *31*, 7492–7496.

Zhou, D., Lambert, S., Malen, P.L., Carpenter, S., Boland, L.M., and Bennett, V. (1998). AnkyrinG Is Required for Clustering of Voltage-gated Na Channels at Axon Initial Segments and for Normal Action Potential Firing. J. Cell Biol. *143*, 1295–1304.

Acknowledgements

My first thanks go to my supervisor, Dr Tara Keck for allowing me to undertake this adventure in her lab. Over the last three years I have been given opportunities that I would not have received elsewhere, and for this I am grateful. I am also thankful for being granted the independence to make my own mistakes and learn from these in order to become a better scientist. Thank you also to my second supervisor Dr Matt Grubb, for his support throughout this project, and to the rest of the Grubb lab for always making me feel welcome back at KCL. I must also thank Professor Ian Thompson and Dr Esther Bell for their help and advice. I thank my family for their continued support throughout these many years of education. Next, I would like to thank all past and present members of the Keck lab for making the lab a truly memorable place. In particular, thanks to Dr Sam Barnes for teaching me to patch, the endless discussions about what it all means, and offering his borrowed words of wisdom to 'never, never, never give in' when things got tough. Also, thank you to 'Uncle' Dave Elliott, not only for help in the lab, but also for enriching my PhD experience with additional history lessons. Thank you also to Ewan and Ele for providing companionship at UCL, as well as to Ewan for dutifully fulfilling my ordering requests. There is one person who I must especially thank for putting up with the blood, sweat and tears over the last three years, for keeping me fed throughout the thesis-writing process, and for always doing his best to help me see the light at the end of the tunnel. Yet another reason to be grateful for joining the Keck lab, for without so I would not have had the privilege of spending the last three years with Anton Gauert. I would like to thank all of the MRC gang; in the early days at here I have made friendships that will last longer than a pool game between Anton and myself. I already miss the mid-week pool and darts, helping to unwind after a day in the lab. Thanks to Dr Megan 'Pastoral-Care' Calvert-O'Hare for her presence at these sessions, and for all of the advice, guidance and general wisdom you have offered me over the years. Finally, thanks to Karen Davey, Sunshine Purificacion and Oniz Suleyman for introducing me to the Miller in my first week at the Centre and thanks to the rest of the Dinks for the many entertaining occasions that followed.